# KoG

**SCIENTIFIC - PROFESSIONAL JOURNAL
OF CROATIAN SOCIETY FOR GEOMETRY AND GRAPHICS**

**KoG**

SCIENTIFIC AND PROFESSIONAL JOURNAL OF
CROATIAN SOCIETY FOR GEOMETRY AND GRAPHICS

# CONTENTS

ZNANSTVENO-STRUČNI ČASOPIS
HRVATSKOG DRUŠTVA ZA GEOMETRIJU I GRAFIKU

# SADRŽAJ

MARIJA ŠIMIĆ HORVATH



# Ksenija Horvatić-Baldasar

# (1929. - 2019.)

7. svibnja 2019., u devedesetoj godini života, napustila nas je naša draga profesorica i kolegica prof. dr. sc. Ksenija Horvatić-Baldasar. Bila je dugogodišnja nastavnica na Fakultetu strojarstva i brodogradnje Sveučilišta u Zagrebu, studentska majka kako su je mnogi zvali.

Rođena je 29. rujna 1929. u Sarajevu, gdje je pohađala i završila osnovnu školu. U Splitu je upisala realnu gimnaziju, poznatu "Realku", i maturirala 1949. godine. Maturirala je s vremenskim odmakom jer je, kao brojne izbjeglice iz Dalmacije u vremenu Drugog svjetskog rata, boravila u El Shattu u Egiptu. Sklonost matematici, posebno geometriji, razvijala je od djetinjstva odrastajući uz oca profesora statike i nacrtne geometrije u Tehničkoj školi. Time je za Kseniju prirodni put bio upis studija matematike 1949. godine na Prirodoslovno-matematičkom fakultetu u Zagrebu. Diplomirala je 1954. godine s temom "Izoperimetrijski problem u prostoru" pod mentorstvom prof. dr. sc. Stanka Bilinskog.

Nakon diplome odmah se zapošljava u II. gimnaziji u Zagrebu, da bi 1955. godine bila izabrana za asistenticu iz kolegija Nacrtna geometrija na Tehničkom fakultetu, kasnije Strojarsko-brodograđevnom fakultetu Sveučilišta u Zagrebu (danas FSB-u) kod prof. dr. sc. Juraja Justinijanovića gdje je i provela cijeli svoj radni vijek. Rado se sjećala rada s prof. Justinijanovićem, često spominjući njegovu temeljitost u radu i način kako ih je uvodio i pripremao za zahtjevnu nastavu iz nacrtne geometrije. Paralelno s obvezama u nastavi akademske godine 1962./1963. upisala je studij trećeg stupnja na PMF-u Sveučilišta u Zagrebu iz područja geometrije. Magistarsku radnju radila je s velikim geometričarem tog i današnjeg vremena, akademikom Vilkom Ničeom (1902. - 1987.). Radnju pod nazivom "Polarni prostori s naročitim obzirom na kuglu" obranila je 1966. godine.

Mi danas živimo u vremenu velike mobilnosti u znanstvenim krugovima izloženi brojnim mogućnostima. Nekad nije bilo tako, no Ksenija je već u ono vrijeme provela jednu akademsku godinu, 1967./1968., na Sveučilištu u Georgiji (Athens, SAD) gdje se usavršavala u području algebarskih struktura i njihovoj primjeni na geometriju.

Habilitacijski postupak završila je 1971. godine na Arhitektonskom fakultetu u Zagrebu i time je izabrana za predavača iz Nacrtne geometrije na Fakultetu strojarstva i brodogradnje Sveučilišta u Zagrebu (FSB). Izuzetno je voljela svoj poziv nastavnika, i uvijek se u potpunosti predavala u svom poslu. Tome svjedoče i njezini brojni angažmani u nastavi po Hrvatskoj, ali i šire, po tadašnjoj Jugoslaviji. Sudjelovala je u nastavi na sljedećim fakultetima: Elektrotehnički fakultet Sveučilišta u Zagrebu (kolegij Nacrtna geometrija), Građevinski fakultet Sveučilišta u Zagrebu (kolegiji Nacrtna geometrija i Primijenjena geometrija), Strojarski fakultet u

Slavonskom Brodu i Strojarski fakultet u Banja Luci. Uvijek je održavala svoju posebnu vezu sa Splitom pa je od ak. god. 1971./1972. Deset godina izvodila nastavu na Odjelu u Splitu (kasnije Fakultetu građevinskih znanosti) te na FESB-u Sveučilišta u Splitu.

Bila je vrlo aktivna u geometrijskim krugovima, pogotovo kao članica Hrvatskog društva za geometriju i grafiku (HDGG). Ksenija je bila dio geometrijskog tima koji je osnovao našu strukovnu udrugu 1994. godine tada pod nazivom Hrvatsko društvo za konstruktivnu geometriju i kompjutorsku grafiku. Djelovala je kao članica prvog upravnog odbora Društva i u njemu se zadržala dugi niz godina. HDGG je danas bitni dio međunarodne udruge International Society for Geometry and Graphics čiji su članovi česti sudionici poznate međunarodne konferencije za geometriju i grafiku koja se održava svake četiri godine u nekom drugom dijelu svijeta. Mora se spomenuti da je Ksenija sudjelovala na prvoj takvoj konferenciji *International Conference of Descriptive Geometry and Computer Graphics* održanoj u Vancouveru, u Kanadi, 1978. godine. Tamo je pohađala tečaj s praktičnim radom u primjeni računala na zadaće u Nacrtnoj geometriji. Odmah po povratku u Zagreb sa svojim suradnicima nastojala je to implementirati u nastavni proces s ciljem unapređenja i modernizacije nastave Nacrtne geometrije.

Njezin trud i rad su rezultirali i napredovanjem u zvanjima pa je 1985. godine izabrana za docenticu, a 1991. za izvanrednu profesoricu na Katedri za matematiku i nacrtnu geometriju na FSB-u Sveučilišta u Zagrebu.

1997. godine je u koautorstvu sa svojom dragom kolegicom dr. sc. Ivankom Babić objavila sveučilišni udžbenik "Nacrtna geometrija". U nasljeđe su nam autorice ostavile jedan lijep udžbenik, pisan jednostavnim matematičkim jezikom i prilagođen studentima tehničkih fakulteta i njihovim potrebama. U deset godina taj je udžbenik imao četiri izdanja, a i danas se rado koristi u nastavi.

Znanstveni rad paralelno je razvijala uz svoje nastavno djelovanje. U tom dijelu svog profesionalnog života surađivala je s vrlo značajnim hrvatskim matematičarem svjetskih razmjera prof. dr. sc. Zvonimirom Jankom pod čijim mentorstvom je izradila i obranila doktorsku disertaciju iz područja konačne geometrije 1983. godine. U tom području se i zadržala cijeli svoj radni vijek tijekom kojeg je objavila 13 znanstvenih radova, od čega ih je većinom publicirala u koautorstvu sa svojim suradnicama prof. dr. sc. Idom Matulić Bedenić i prof. dr. sc. Erikom Kramer. S tim radovima aktivno je sudjelovala na više znanstvenih skupova na području bivše Jugoslavije i u inozemstvu.

Bila je članica Seminara za geometriju na Prirodoslovno-matematičkom fakultetu te Seminara za konačne geometrije

na Elektrotehničkom fakultetu u Zagrebu.

1994. godine odlazi u mirovinu, ali njezin rad u nastavi ne prestaje. I dalje je honorarno sudjelovala u nastavi nacrtne geometrije izvodeći vježbe studentima FSB-a. 2003. godine ukida se kolegij Nacrtna geometrija na FSB-u, za čiji ostanak se Ksenija snažno borila, i time zauvijek odlazi iz nastave.

Rado je posjećivala tematske sastanke HDGG-a i u ugodnom društvu svojih kolegica pričala o geometriji. Njezin rad, kako nastavni, tako i znanstveni, pridonio je razvoju geometrije na tehničkim fakultetima u drugoj polovici dvadesetog stoljeća, vrlo bitnom periodu za razvoj geometrije u Hrvatskoj.

Ostvarila se i kao majka dvoje djece, sina Davora i kćeri Gordane, te je imala četvero unučadi.

Profesorica Ksenija, profesionalno angažirana, komunikativna i neposredna ostaje nam u dragom sjećanju i spominje se u našim razgovorima.

## Popis radova

[1] K. HORVATIĆ-BALDASAR, A contribution to the classification of semi-biplanes with 10 points on a line, *Rad JAZU* **4** (1985), 7–13.

[2] K. HORVATIĆ-BALDASAR, The elation semi-biplane with 26 points on a line, *Rad JAZU* **4** (1985), 15–19.

[3] K. HORVATIĆ-BALDASAR, E. KRAMER, I. MATULIĆ-BEDENIĆ, Biplanes with $k = 16$ points on a line, *Rad JAZU* **4** (1985), 125–127.

[4] K. HORVATIĆ-BALDASAR, An elation semi-biplane with 14 points on a line, *Glasnik matematički* **21** (1986), 35–39.

[5] K. HORVATIĆ-BALDASAR, E. KRAMER, I. MATULIĆ-BEDENIĆ, Projective planes of order 12 do not have an Abelian group of order 6 as a collineation group, *Punime matematike* **1** (1986), 75–81.

[6] K. HORVATIĆ-BALDASAR, E. KRAMER, I. MATULIĆ-BEDENIĆ, A contribution to the classification of biplanes of order 9, *Rad JAZU* **6** (1987), 25–29.

[7] K. HORVATIĆ-BALDASAR, E. KRAMER, I. MATULIĆ-BEDENIĆ, On full collineation group of projective planes of order 12, *Punime matematike* **2** (1987), 9–11.

[8] K. HORVATIĆ-BALDASAR, An elation semi-biplane with 34 points on a line, *Rad JAZU* **8** (1989), 47–51.

[9] K. HORVATIĆ-BALDASAR, E. KRAMER, I. MA-TULIĆ-BEDENIĆ, On a Projective plane of order 11 with Frobenius group of order 21, *Radovi matematički* **6** (1990), 71–76.

[10] K. HORVATIĆ-BALDASAR, E. KRAMER, I. MA-TULIĆ-BEDENIĆ, On $2 - (85, 28, 9)$ designs, *Punime matematike* **4** (1991), 56–60.

[11] I. MATULIĆ-BEDENIĆ, K. HORVATIĆ-BALDASAR, On infinite series of biplanes of order $n \neq 2$ prime

number with Frobenius group $F_{n(n-1)}$, *Rad HAZU* **12** (1995), 7–12.

[12] K. HORVATIĆ-BALDASAR, E. KRAMER, I. MA-TULIĆ-BEDENIĆ, Construction of New Symmetric Designs with Parameters $(66, 26, 10)$, *Journal of Combinatorial Designs* **3** (1995), 406–410.

[13] K. HORVATIĆ-BALDASAR, I. MATULIĆ-BEDENIĆ, V. MANDEKIĆ-BOTTERI, On possible Infinite Series of Symmetric Block-designs with Parameters $2 - (9\lambda + 4, 3\lambda + 1, \lambda)$, *Rad HAZU* **14** (2003), 9–16.

ANGÉLA VRÁNICS
JENŐ SZIRMAI

# Lattice Coverings by Congruent Translation Balls Using Translation-like Bisector Surfaces in Nil Geometry

**Lattice Coverings by Congruent Translation Balls Using Translation-like Bisector Surfaces in Nil Geometry**

**ABSTRACT**

In this paper we study the **Nil** geometry that is one of the eight homogeneous Thurston 3-geometries.

We determine the equation of the translation-like bisector surface of any two points. We prove, that the isosceles property of a translation triangle is not equivalent to two angles of the triangle being equal and that the triangle inequalities do not remain valid for translation triangles in general. We develop a method to determine the centre and the radius of the circumscribed translation sphere of a given *translation tetrahedron*.

A further aim of this paper is to study lattice-like coverings with congruent translation balls in **Nil** space. We introduce the notion of the density of the considered coverings and give upper estimate to it using the radius and the volume of the circumscribed translation sphere of a given *translation tetrahedron*. The found minimal upper bound density of the translation ball coverings $\Delta \approx 1.42783$. In our work we will use for computations and visualizations the projective model of **Nil** described by E. Molnár in [6].

**Key words:** Thurston geometries, **Nil** geometry, translation-like bisector surface of two points, circumscribed sphere of **Nil** tetrahedron, Dirichlet-Voronoi cell

**MSC2010:** 53A20, 52C17, 53A35, 52C35, 53B20

**Rešetkasto pokrivanje kongruentnim translacijskim kuglama pomoću simetralnih ploha u Nil geometriji**

**SAŽETAK**

U radu proučavamo jednu od osam homogenih Thurstonovih 3-geometrija, **Nil** geometriju.

Određujemo jednadžbu translacijske simetralne plohe za bilo koje dvije točke. Dokazujemo da činjenica da je trokut jednakokračan nije ekvivalentna činjenici da trokut ima dva jednaka kuta, te da općenito nejednakosti trokuta ne vrijede za translacijske trokute. Razvijamo metodu za određivanje središta i polumjera opisane translacijske sfere danog *translacijskog tetraedra*.

Daljnji je cilj ovog rada proučavanje rešetkastih pokrivanja kongruentnim translacijskim kuglama u **Nil** prostoru. Uvodimo pojam gustoće promatranog pokrivanja i dajemo njezinu gornju procjenu pomoću polumjera i obujma opisane translacijske sfere danog *translacijskog tetraedra*. Pokazujemo da je gornja granica pokrivanja translacijskim kuglama $\Delta \approx 1.42783$. U radu koristimo izračune i vizualizaciju projektivnog modela **Nil** prostora opisane u radu [6] E. Molnára.

**Ključne riječi:** Thurstonove geometrije, **Nil** geometrija, translacijska simetralna ploha dviju točaka, opisana sfera **Nil** tetraedra, Dirichlet-Voronoijeve ćelije

## 1 Introduction

The basic problems in the classical theory of packings and coverings, the development of which was strongly influenced by the geometry of numbers and by crystallography, are the determination of the densest packing and the thinnest covering with congruent copies of a given body. At present the body is a ball and now we consider the lattice-like covering problem with congruent translation balls in **Nil** space.

These questions related to the theory of the Dirichlet-Voronoi cells (brifly $D-V$ cells). In 3-dimensional spaces

of constant curvature the $D-V$ cells are widely investigated, but in the further Thurston geometries $\mathbf{S}^2 \times \mathbf{R}$, $\mathbf{H}^2 \times \mathbf{R}$, **Nil**, **Sol**, $\widetilde{\mathbf{SL}_2\mathbf{R}}$ there are few results in this topic. Let $X$ be one of the above five geometries and $\Gamma$ is one of its discrete isometry groups. Moreover, we distinguish two distance function types: $d^g$ is the usual geodesic distance function and $d^t$ is the translation distance function (see Section 3). Therefore, we obtain two types of the $D-V$ cells regarding the two distance functions.

The firs step to get the $D-V$ cell of a given point set of $X$ is the determination of the translation or geodesic-like bisector (or equidistant) surface of two arbitrary points of $X$ because these surface types contain the faces of $D-V$ cells.

In [12], [13], [14] we studied the geodesic-like equidistant surfaces in $\mathbf{S}^2 \times \mathbf{R}$, $\mathbf{H}^2 \times \mathbf{R}$ and **Nil** geometries, and in [25] we discussed the translation-like bisector surfaces in **Sol** geometry, but there are no results concerning the translation-like equidistant surfaces in **Nil** and $\widetilde{\mathbf{SL}_2\mathbf{R}}$ geometries.

In the Thurston spaces can be introduced in a natural way (see [6]) translations mapping each point to any point. Consider a unit vector at the origin. Translations, postulated at the beginning carry this vector to any point by its tangent mapping. If a curve $t \rightarrow (x(t), y(t), z(t))$ has just the translated vector as tangent vector in each point, then the curve is called a *translation curve*. This assumption leads to a system of first order differential equations, thus translation curves are simpler than geodesics and differ from them in **Nil**, $\widetilde{\mathbf{SL}_2\mathbf{R}}$ and **Sol** geometries. In $\mathbf{E}^3$, $\mathbf{S}^3$, $\mathbf{H}^3$, $\mathbf{S}^2 \times \mathbf{R}$ and $\mathbf{H}^2 \times \mathbf{R}$ geometries the translation and geodesic curves coincide with each other.

Therefore, the translation curves also play an important role in **Nil**, $\widetilde{\mathbf{SL}_2\mathbf{R}}$ and **Sol** geometries and often seem to be more natural in these geometries, than their geodesic lines.

*In this paper* we study the translation-like bisector surface of any two points in **Nil** geometry, determine its equation and visualize them. The translation-like bisector surfaces play an important role in the construction of the $D-V$ cells because their faces lie on bisector surfaces. The $D-V$-cells are relevant in the study of tilings, ball packing and ball covering. E.g. if the point set is the orbit of a point - generated by a discrete isometry group of **Nil** - then we obtain a monohedral $D-V$ cell decomposition (tiling) of the considered space and it is interesting to examine its optimal ball packing and covering (see [21], [22]).

Moreover, we prove, that the isosceles property of a translation triangle is not equivalent to two angles of the triangle being equal and that the triangle inequalities do not remain valid for translation triangles in general.

Using the above bisector surfaces we develop a procedure to determine the centre and the radius of the circumscribed translation sphere of an arbitrary **Nil** tetrahedron. This is useful to determine the least dense ball covering radius of a given periodic polyhedral **Nil** tiling because the tiling can be decomposed into tetrahedra. Applying the above procedure we determine the minimal covering density of some lattice types and thus we give an upper bound of the lattice-like covering density related to the most important lattice parameter $k = 1$.

## 2　On Nil geometry

**Nil** geometry can be derived from the famous real matrix group $\mathbf{L}(\mathbb{R})$ discovered by Werner Heisenberg. The left (row-column) multiplication of Heisenberg matrices

$$\begin{pmatrix} 1 & x & z \\ 0 & 1 & y \\ 0 & 0 & 1 \end{pmatrix} \begin{pmatrix} 1 & a & c \\ 0 & 1 & b \\ 0 & 0 & 1 \end{pmatrix} = \begin{pmatrix} 1 & a+x & c+xb+z \\ 0 & 1 & b+y \\ 0 & 0 & 1 \end{pmatrix} \quad (1)$$

defines "translations" $\mathbf{L}(\mathbb{R}) = \{(x,y,z) : x, y, z \in \mathbb{R}\}$ on the points of $\mathbf{Nil} = \{(a,b,c) : a, b, c \in \mathbb{R}\}$. These translations are not commutative in general. The matrices $\mathbf{K}(z) \lhd \mathbf{L}$ of the form

$$\mathbf{K}(z) \ni \begin{pmatrix} 1 & 0 & z \\ 0 & 1 & 0 \\ 0 & 0 & 1 \end{pmatrix} \mapsto (0,0,z) \quad (2)$$

constitute the one parametric centre, i.e. each of its elements commute with all elements of $\mathbf{L}$. The elements of $\mathbf{K}$ are called *fibre translations*. **Nil** geometry of the Heisenberg group can be projectively (affinely) interpreted by "right translations" on points as the matrix formula

$$(1; a, b, c) \rightarrow (1; a, b, c) \begin{pmatrix} 1 & x & y & z \\ 0 & 1 & 0 & 0 \\ 0 & 0 & 1 & x \\ 0 & 0 & 0 & 1 \end{pmatrix} = \quad (3)$$

$$= (1; x+a, y+b, z+bx+c)$$

shows, according to (1). Here we consider $\mathbf{L}$ as projective collineation group with right actions in homogeneous coordinates. We will use the Cartesian homogeneous coordinate simplex $E_0(\mathbf{e}_0), E_1^\infty(\mathbf{e}_1), E_2^\infty(\mathbf{e}_2), E_3^\infty(\mathbf{e}_3)$, $(\{\mathbf{e}_i\} \subset \mathbf{V}^4$ with the unit point $E(\mathbf{e} = \mathbf{e}_0 + \mathbf{e}_1 + \mathbf{e}_2 + \mathbf{e}_3))$ which is distinguished by an origin $E_0$ and by the ideal points of coordinate axes, respectively. Moreover, $\mathbf{y} = c\mathbf{x}$ with $0 < c \in \mathbb{R}$ (or $c \in \mathbb{R} \setminus \{0\}$) defines a point $(\mathbf{x}) = (\mathbf{y})$ of the projective 3-sphere $\mathcal{P}\mathcal{S}^3$ (or that of the projective space $\mathcal{P}^3$ where opposite rays $(\mathbf{x})$ and $(-\mathbf{x})$ are identified). The dual system $\{(e^i)\}$, $(\{e^i\} \subset V_4)$, with $\mathbf{e}_i e^j = \delta_i^j$ (the Kronecker symbol), describes the simplex planes, especially the plane at infinity $(e^0) = E_1^\infty E_2^\infty E_3^\infty$, and generally, $v = u\frac{1}{c}$

defines a plane $(u) = (v)$ of $\mathcal{PS}^3$ (or that of $\mathcal{P}^3$). Thus $0 = \mathbf{x}u = \mathbf{y}v$ defines the incidence of point $(\mathbf{x}) = (\mathbf{y})$ and plane $(u) = (v)$, as $(\mathbf{x})\mathrm{I}(u)$ also denotes it. Thus **Nil** can be visualized in the affine 3-space $\mathbf{A}^3$ (so in $\mathbf{E}^3$) as well [11]. In this context E. Molnár [6] has derived the well-known infinitesimal arc-length square invariant under translations **L** at any point of **Nil** as follows

$$(dx)^2 + (dy)^2 + (-xdy + dz)^2 =$$
$$= (dx)^2 + (1 + x^2)(dy)^2 - 2x(dy)(dz) + (dz)^2 =: (ds)^2 \tag{4}$$

The translation group **L** defined by formula (3) can be extended to a larger group **G** of collineations, preserving the fibres, that will be equivalent to the (orientation preserving) isometry group of **Nil**.

In [7] E. Molnár has shown that a rotation through angle $\omega$ about the $z$-axis at the origin, as isometry of **Nil**, keeping invariant the Riemann metric everywhere, will be a quadratic mapping in $x, y$ to $z$-image $\bar{z}$ as follows:

$$\mathcal{M} = \mathbf{r}(O, \omega) : (1; x, y, z) \to (1; \bar{x}, \bar{y}, \bar{z});$$
$$\bar{x} = x\cos\omega - y\sin\omega, \quad \bar{y} = x\sin\omega + y\cos\omega, \tag{5}$$
$$\bar{z} = z - \frac{1}{2}xy + \frac{1}{4}(x^2 - y^2)\sin 2\omega + \frac{1}{2}xy\cos 2\omega.$$

This rotation formula $\mathcal{M}$, however, is conjugate by the quadratic mapping $\alpha$ to the linear rotation $\Omega$ in (7) as follows

$$\alpha^{-1} : \; (1; x, y, z) \xrightarrow{\alpha^{-1}} (1; x', y', z') = (1; x, y, z - \frac{1}{2}xy) \; \text{to}$$
$$\Omega : \; (1; x', y', z') \xrightarrow{\Omega} (1; x'', y'', z'') =$$
$$(1; x', y', z') \begin{pmatrix} 1 & 0 & 0 & 0 \\ 0 & \cos\omega & \sin\omega & 0 \\ 0 & -\sin\omega & \cos\omega & 0 \\ 0 & 0 & 0 & 1 \end{pmatrix},$$
$$\text{with } \alpha : (1; x'', y'', z'') \xrightarrow{\alpha} (1; \bar{x}, \bar{y}, \bar{z}) =$$
$$= (1; x'', y'', z'' + \frac{1}{2}x''y'').$$
$$\tag{6}$$

This quadratic conjugacy modifies the **Nil** translations in (3), as well. Now a translation with $(X, Y, Z)$ in (3) instead of $(x, y, z)$ will be changed by the above conjugacy to the translation

$$(1; x, y, z) \longrightarrow (1; \bar{x}, \bar{y}, \bar{z}) =$$
$$= (1; x, y, z) \begin{pmatrix} 1 & X & Y & Z - \frac{1}{2}XY \\ 0 & 1 & 0 & -\frac{1}{2}Y \\ 0 & 0 & 1 & \frac{1}{2}X \\ 0 & 0 & 0 & 1 \end{pmatrix}, \tag{7}$$

that is again an affine collineation.

## 2.1 Translation curves and balls

We consider a **Nil** curve $(1, x(t), y(t), z(t))$ with a given starting tangent vector at the origin $O = E_0 = (1, 0, 0, 0)$

$$u = \dot{x}(0), \; v = \dot{y}(0), \; w = \dot{z}(0). \tag{8}$$

For a translation curve let its tangent vector at the point $(1, x(t), y(t), z(t))$ be defined by the matrix (3) with the following equation:

$$(0, u, v, w) \begin{pmatrix} 1 & x(t) & y(t) & z(t) \\ 0 & 1 & 0 & 0 \\ 0 & 0 & 1 & x(t) \\ 0 & 0 & 0 & 1 \end{pmatrix} = (0, \dot{x}(t), \dot{y}(t), \dot{z}(t)).$$
$$\tag{9}$$

Thus, the *translation curves* in **Nil** geometry (see [8], [10], [11]) are defined by the above first order differential equation system $\dot{x}(t) = u$, $\dot{y}(t) = v$, $\dot{z}(t) = v \cdot x(t) + w$, whose solution is the following:

$$x(t) = ut, \; y(t) = vt, \; z(t) = \frac{1}{2}uvt^2 + wt. \tag{10}$$

We assume that the starting point of a translation curve is the origin, because we can transform a curve into an arbitrary starting point by translation (3), moreover, unit initial velocity translation can be assumed by "geographic" parameters $\phi$ and $\theta$:

$$x(0) = y(0) = z(0) = 0;$$
$$u = \dot{x}(0) = \cos\theta\cos\phi,$$
$$v = \dot{y}(0) = \cos\theta\sin\phi, \tag{11}$$
$$w = \dot{z}(0) = \sin\theta;$$
$$-\pi \le \phi \le \pi, \; -\frac{\pi}{2} \le \theta \le \frac{\pi}{2}.$$

**Definition 1** *The translation distance $d^t(P_1, P_2)$ between the points $P_1$ and $P_2$ is defined by the arc length of the above translation curve from $P_1$ to $P_2$.*

**Definition 2** *The sphere of radius $r > 0$ with centre at the origin, (denoted by $S_O^t(r)$), with the usual longitude and altitude parameters $\phi$ and $\theta$, respectively by (11), is specified by the following equations:*

$$S_O^t(r) : \begin{cases} x(\phi, \theta) = r\cos\theta\cos\phi, \\ y(\phi, \theta) = r\cos\theta\sin\phi, \\ z(\phi, \theta) = \frac{r^2}{2}\cos^2\theta\cos\phi\sin\phi + r\sin\theta. \end{cases} \tag{12}$$

**Definition 3** *The body of the translation sphere of centre $O$ and of radius $r$ in the **Nil** space is called translation ball, denoted by $B_O^t(r)$, i.e. $Q \in B_O^t(r)$ iff $0 \le d^t(O, Q) \le r$.*

**Remark 1** *The translation sphere is a simply connected surface without selfintersection in **Nil** space for any radius $0 < r \in \mathbb{R}$.*

We obtained in [20] the volume formula of the translation ball $B_O^t(r)$ of radius $r$ by (4), (5) and (12):

**Theorem 1** *The volume of a translation ball of radius $r$ is the same as that of an Euclidean one:*

$$Vol(B_O^t(r)) = \frac{4}{3}r^3\pi. \tag{13}$$

The convexity of the translation ball play an important role in the discussion of the ball covering therefore we recall the following Theorem from the paper [20].

**Theorem 2** *A translation* **Nil** *ball $B^t(S^t(r))$ is convex in the affine-Euclidean sense in our model if and only if $r \in [0,2]$.*

### 2.2   The discrete translation group $L(\mathbb{Z}, k)$

We consider the **Nil** translations defined in (1) and (3) and choose first two non-commuting translations

$$\tau_1 = \begin{pmatrix} 1 & t_1^1 & t_1^2 & t_1^3 \\ 0 & 1 & 0 & 0 \\ 0 & 0 & 1 & t_1^1 \\ 0 & 0 & 0 & 1 \end{pmatrix} \text{ and } \tau_2 = \begin{pmatrix} 1 & t_2^1 & t_2^2 & t_2^3 \\ 0 & 1 & 0 & 0 \\ 0 & 0 & 1 & t_2^1 \\ 0 & 0 & 0 & 1 \end{pmatrix}, \tag{14}$$

now with upper indices for the coordinate variables. Second, we define the translation $(\tau_3)^k$, $(k \in \mathbb{N} \setminus \{0\}$ $k$ is fixed natural exponent), by the following commutator:

$$(\tau_3)^k = (\tau_2^{-1}\tau_1^{-1}\tau_2\tau_1)^k = \begin{pmatrix} 1 & 0 & 0 & -t_2^1 t_1^2 + t_1^1 t_2^2 \\ 0 & 1 & 0 & 0 \\ 0 & 0 & 1 & 0 \\ 0 & 0 & 0 & 1 \end{pmatrix}^k,$$

$$\text{and so } \tau_3 \ (k = 1) \tag{15}$$

is also defined. If we take integers as coefficients for $\tau_1, \tau_2, \tau_3$, then we generate the discrete group $\langle \tau_1, \tau_2, \tau_3 \rangle$, denoted by $\mathbf{L}(\tau_1, \tau_2, k)$ or by $\mathbf{L}(\mathbb{Z}, k)$. Here $\mathbb{Z}$ refers to the integers.

We know (see e.g. [18] and [19]) that the orbit space $\mathbf{Nil}/\mathbf{L}(\mathbb{Z}, k)$ is a compact manifold, i.e. a **Nil** space form.

**Definition 4** *The* **Nil** *point lattice $\Gamma_P(\tau_1, \tau_2, k)$ is a discrete orbit of point $P$ in the* **Nil** *space under group $\mathbf{L}(\tau_1, \tau_2, k) = \mathbf{L}(\mathbb{Z}, k)$ with an arbitrary starting point $P$ for every fixed $k \in \mathbb{N} \setminus \{0\}$.*

**Remark 2** *For simplicity we have chosen the origin as starting point, by the homogeneity of* **Nil***.*

**Remark 3** *We may assume in the following that $t_1^2 = 0$, i.e. the image of the origin by the translation $\tau_1$ lies on the plane $[x,z]$.*

We consider by (14-15) a fundamental "parallelepiped complex" (see [20])

$$\widetilde{\mathcal{F}(k)} = OT_1 T_2 T_3 T_{12} T_{21} T_{23} T_{213} T_{13}, \text{ (see Fig. 1 for } k = 1, 2)$$

in the Euclidean sense, which is determined by translations $\tau_1, \tau_2, \tau_3$. The images of $\widetilde{\mathcal{F}(k)}$ under $\mathbf{L}(\mathbb{Z}, k)$ fill **Nil** without gap. Overlaps occur only on the boundary.
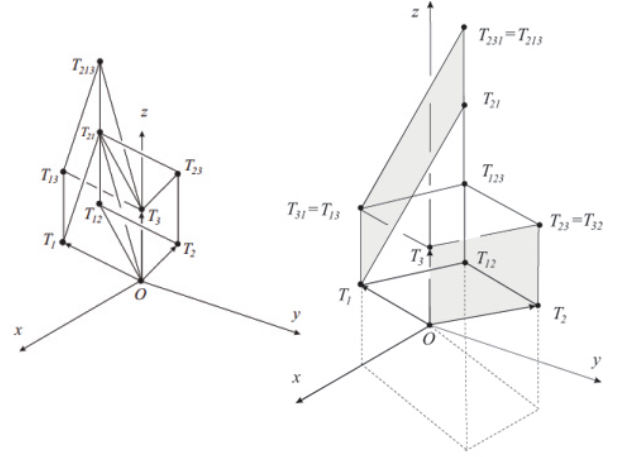


Figure 1: *The* **Nil** *parallelepipeds $\widetilde{\mathcal{F}(1)}$ (left) and $\widetilde{\mathcal{F}(2)}$ (right).*

*Analogously to the Euclidean integer lattice and parallelepiped, $\widetilde{\mathcal{F}(k)}$ $(k \in \mathbb{N} \setminus \{0\})$ can be called a* **Nil** *parallelepiped, endowed by face pairing, as the upper $\sim$ hints to it.*
$\widetilde{\mathcal{F}(k)}$ is a *fundamental domain* of $\mathbf{L}(\mathbb{Z}, k)$. We need only its interior for its volume. The homogeneous coordinates of the vertices of $\widetilde{\mathcal{F}(k)}$ can be determined in our affine model by the translations (14-15) with the parameters $t_i^j$, $i \in \{1,2\}$, $j \in \{1,2,3\}$ (see (16) and Fig. 1).

$$T_1(1, t_1^1, 0, t_1^3), \ T_2(1, t_2^1, t_2^2, t_2^3), \ T_3(1, 0, 0, \frac{t_1^1 t_2^2}{k}),$$

$$T_{13}(1, t_1^1, 0, \frac{t_1^1 t_2^2}{k} + t_1^3), \ T_{12}(1, t_1^1 + t_2^1, t_2^2, t_2^3 + t_1^3),$$

$$T_{21}(1, t_1^1 + t_2^1, t_2^2, t_1^1 t_2^2 + t_1^3 + t_2^3), \ T_{23}(1, t_2^1, t_2^2, t_2^3 + \frac{t_1^1 t_2^2}{k}),$$

$$T_{213} = T_{231}(1, t_1^1 + t_2^1, t_2^2, (k+1)\frac{t_1^1 t_2^2}{k} + t_1^3 + t_2^3). \tag{16}$$

In [19] we have determined the volume of the **Nil** parallelepiped $\widetilde{\mathcal{F}(1)}$. Analogously to that we get the volume formula of $\widetilde{\mathcal{F}(k)}$ $(k \in \mathbb{N})$ by the usual method:

$$\iiint_{\widetilde{\mathcal{F}(k)}} \sqrt{det(g_{ij})} \, \mathrm{d}x\mathrm{d}y\mathrm{d}z = Vol(\widetilde{\mathcal{F}(k)}) =$$
$$= \frac{1}{k} \int_0^{t_2^2} \int_0^{t_1^1} |t_1^1 \cdot t_2^2| \, \mathrm{d}x\mathrm{d}y = \frac{(t_1^1 \cdot t_2^2)^2}{k}. \tag{17}$$

If the parameter $k$ is given, from this formula it can be seen that the volume of a **Nil** parallelepiped depends on two parameters, i.e. on its projection into the $[x,y]$ plane.

## 3 Translation-like bisector surfaces

Our further goals are to examine and visualize the Dirichlet-Voronoi cells and the packing and covering problems of **Nil** geometry. In order to study the above questions have to determine the "faces" of the $D-V$ cells that are parts of bisector (or equidistant) surfaces of given point pairs. The definition below comes naturally:

**Definition 5** *The equidistant surface $S_{P_1P_2}$ of two arbitrary points $P_1, P_2 \in$ **Nil** consists of all points $P' \in$ **Nil**, for which $d^t(P_1,P') = d^t(P',P_2)$.*

It can be assumed by the homogeneity of **Nil** that the starting point of a given translation curve segment is $E_0 = P_1 = (1,0,0,0)$ and the other endpoint will be given by its homogeneous coordinates $P_2 = (1,a,b,c)$. We consider the translation curve segment $t_{P_1P_2}$ and determine its parameters $(\phi, \theta, r)$ expressed by the real coordinates $a$, $b$, $c$ of $P_2$. We obtain directly by equation system (12) the following:

**Lemma 1**　　*1. Let $(1,a,b,c)$ $(a,b \in \mathbb{R} \setminus \{0\}$, $c \in \mathbb{R})$ be the homogeneous coordinates of the point $P \in$ **Nil**. The parameters of the corresponding translation curve $t_{E_0P}$ are the following*

$$\phi = \text{arccot}\left(\frac{a}{b}\right), \ \theta = \text{arccot}\left(\frac{\sqrt{a^2+b^2}}{c - \frac{ab}{2}}\right), \ r = \left|\frac{c - \frac{ab}{2}}{\sin\theta}\right|. \tag{18}$$

*2. Let $(1,a,0,c)$ $(a,c \in \mathbb{R} \setminus \{0\})$ be the homogeneous coordinates of the point $P \in$ **Nil**. The parameters of the corresponding translation curve $t_{E_0P}$ are the following*

$$\phi = \pi \cdot n, \ (n \in \{0,1\}), \ \theta = \text{arccot}\left(\frac{a}{c}\right), \ r = \left|\frac{a}{\cos\theta}\right|. \tag{19}$$

*3. Let $(1,a,0,0)$ $(a \in \mathbb{R} \setminus \{0\})$ be the homogeneous coordinates of the point $P \in$ **Nil**. The parameters of the corresponding translation curve $t_{E_0P}$ are the following*

$$\phi = \pi \cdot n, \ (n \in \{0,1\}), \ \theta = \pi \cdot n, \ (n \in \{0,1\}), \ r = |a|. \tag{20}$$

*4. Let $(1,0,b,0)$ $(b \in \mathbb{R} \setminus \{0\})$ be the homogeneous coordinates of the point $P \in$ **Nil**. The parameters of the*

*corresponding translation curve $t_{E_0P}$ are the following*

$$\phi = \pm\frac{\pi}{2}, \ \theta = \pi \cdot n, \ (n \in \{0,1\}), \ r = |b|. \tag{21}$$

*5. Let $(1,0,0,c)$ $(c \in \mathbb{R} \setminus \{0\})$ be the homogeneous coordinates of the point $P \in$ **Nil**. The parameters of the corresponding translation curve $t_{E_0P}$ are the following*

$$\theta = \pm\frac{\pi}{2}, \ r = |c|. \tag{22}$$

$\square$

*In order to determine the translation-like bisector surface $S_{P_1P_2}(x,y,z)$ of two given point $E_0 = P_1 = (1,0,0,0)$ and $P_2 = (1,a,b,c)$ we define the translation $\mathbf{T}_{P_2}$ as elements of the isometry group of **Nil**, that maps the origin $E_0$ onto $P_2$ (see Fig. 2).*
This isometrie $\mathbf{T}_{P_2}$ and its inverse (up to a positive determinant factor) can be given by:

$$\mathbf{T}_{P_2} = \begin{pmatrix} 1 & a & b & c \\ 0 & 1 & 0 & 0 \\ 0 & 0 & 1 & a \\ 0 & 0 & 0 & 1 \end{pmatrix}, \ \mathbf{T}_{P_2}^{-1} = \begin{pmatrix} 1 & -a & -b & ab-c \\ 0 & 1 & 0 & 0 \\ 0 & 0 & 1 & -a \\ 0 & 0 & 0 & 1 \end{pmatrix}, \tag{23}$$

and the images $\mathbf{T}_{P_2}^{-1}(P_i)$ of points $P_i$ $(i \in \{1,2,3\})$ are the following (see also Fig. 2):

$$\mathbf{T}_{P_2}^{-1}(P_1 = E_0) = P_1^2 = (1,-a,-b,ab-c),$$
$$\mathbf{T}_{P_2}^{-1}(P_2) = E_0 = (1,0,0,0), \tag{24}$$
$$\mathbf{T}_{P_2}^{-1}(P_3) = P_3^2 = (1,(x-a),(y-b),a(b-y)-c).$$

It is clear that $P_3 = (1,x,y,z) \in S_{P_1P_2}$ iff $d^t(P_1,P_3) = d^t(P_3,P_2) \Rightarrow d^t(P_1,P_3) = d^t(E_0,P_3^2)$ where $P_3^2 = \mathbf{T}_{P_2}^{-1}(P_3)$ (see (23), (24)).
This method leads to

**Lemma 2** *The equation of the equidistant surface $S_{P_1P_2}(x,y,z)$ of two points $P_1 = (1,0,0,0)$ and $P_2 = (1,a,b,c)$ in **Nil** space (see Fig. 2, 3):*

*1. $a,b,c \neq 0$,*

$$z = \frac{1}{4}\left(\frac{8x(a^2+b^2) - 4(a^3 - ab + 4bc)}{a(b(a+x) - ay - 2c)} \right. \tag{25}$$
$$\left. - \frac{b(a(a+x)+8)}{a} + y(a+2x) + 2c\right),$$

*2. $a,b \neq 0$, $c = 0$*

$$z = -\frac{a^2(b^2 - 2by + y^2 + 4) + 2ax(b^2 - 2by + y^2 - 4)}{4(a(b-y)+bx)}$$
$$- \frac{b(x^2+4)(b-2y)}{4(a(b-y)+bx)}, \tag{26}$$

3. $a, c \neq 0$, $b = 0$

$$z = \frac{a^2 (y^2 + 4) + 2a (2cy + x (y^2 - 4)) + 4c(c + xy)}{4ay + 8c},$$

(27)

4. $b, c \neq 0$, $a = 0$

$$z = \frac{b^2 (x^2 + 4) - 2b (2cx + (x^2 + 4) y) + 4c(c + xy)}{8c - 4bx},$$

(28)

5. $b, c = 0$, $a \neq 0$

$$z = \frac{a (y^2 + 4) + 2x (y^2 - 4)}{4y}.$$

(29)

6. $a, c = 0$, $b \neq 0$

$$z = -\frac{(x^2 + 4) (b - 2y)}{4x}.$$

(30)

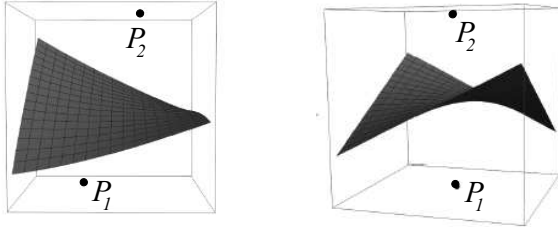7. $a, b = 0$, $c \neq 0$

$$z = \frac{1}{2} (c + xy).$$

(31)

□



Figure 2: *Translation-like bisectors (equidistant surfaces) of point pairs $(P_1, P_2)$ with coordinates $((1,0,0,0), (1,1/2,1/2,3/2))$ (left) and $((1,0,0,0), (1,0,0,2))$ (right).*

### 3.1　On isosceles and equilateral translation triangles

We consider 3 points $A_1$, $A_2$, $A_3$ in the projective model of **Nil** space. The *translation segments* connecting the points $A_i$ and $A_j$ ($i < j$, $i, j, k \in \{1,2,3\}$) are called sides of the *translation triangle* $A_1A_2A_3$. The length of its side $a_k$ ($k \in \{1,2,3\}$) is the translation distance $d^t(A_i, A_j)$ between the vertices $A_i$ and $A_j$ ($i < j$, $i, j, k \in \{1,2,3\}, k \neq i, j$). Similarly to the Euclidean geometry we can define the notions of isosceles and equilateral translation triangles.
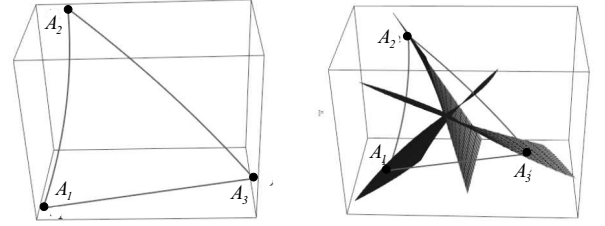


Figure 3: *Equidistant surfaces of the "edges" of the equilateral triangle $A_1A_2A_3$ where the coordinates of the vertices $A_1(1,0,0,0)$, $A_2(1,0.8,0.5,-0.131662)$, $A_3(1,0.2,-0.058102,-0.983882)$.*

An isosceles translation triangle is a triangle with (at least) two equal sides and a triangle with all sides equal is called an equilateral translation triangle (see Fig. 3) in the **Nil** space.

We note here, that if in a translation triangle $A_1A_2A_3$ e.g. $a_1 = a_2$ then the bisector surface $\mathcal{S}_{A_1A_2}$ contains the vertex $A_3$ (see Fig. 3).

In the Euclidean space the isosceles property of a triangle is equivalent to two angles of the triangle being equal therefore has both two equal sides and two equal angles. An equilateral triangle is a special case of an isosceles triangle having not just two, but all three sides and angles equal.

**Proposition 1** *The isosceles property of a translation triangle is not equivalent to two angles of the triangle being equal in the* **Nil** *space.*

**Proof.** The missing coordinates $y^3$ and $z^3$ of the vertices $A_1 = E_0 = (1,0,0,0)$, $A_2 = (1, x^2 = 1, y^2 = 1/2, z^2 = -3/4)$ and $A_3 = (1, x^3 = 0, y^3, z^3)$ can be determined by the equation system $d^t(A_1, A_2) = d^t(A_1, A_3) = d^t(A_2, A_3)$. We get the following coordinates: $y^3 \approx -0.6164636$, $z^3 \approx -1.367469$ where $(a_3 = d^t(A_1, A_2) = a_2 = d^t(A_1, A_3) = a_1 = d^t(A_2, A_3) = 1.5)$.

The *interior angles* of translation triangles are denoted at the vertex $A_i$ by $\omega_i$ ($i \in \{1,2,3\}$). We note here that the angle of two intersecting translation curves depends on the orientation of their tangent vectors.

*In order to determine the interior angles of a translation triangle $A_1A_2A_3$ and its interior angle sum $\sum_{i=1}^{3} (\omega_i)$,* we apply the method (we do not discuss here) developed in [24] using the infinitesimal arc-lenght square of **Nil** geometry (see (4)).

Our method (see [24]) provide the following results:

$$\omega_1 \approx 1.08063, \quad \omega_2 \approx 0.84167, \quad \omega_3 \approx 1.22186, \quad \sum_{i=1}^{3} (\omega_i) \approx$$

$$\approx 3.14416 > \pi \approx 3.14159.$$

From the above results follows the statement. We note here, that if the vertices of the translation triangle lie in the $[x, y]$ plane than the Euclidean isosceles property true in the **Nil** geometry, as well.                    □

Using the above methods we obtain the following

**Lemma 3** *The triangle inequalities do not remain valid for translation triangles in general.*

**Proof.** We consider the translation triangle $A_1A_2A_3$ where $A_1 = (1, 0, 0, 0)$, $A_2 = (1, -1, 3, 1)$, $A_3 = (1, 1/4, 1/2, 1/2)$. We obtain directly by equation systems (18-22) (see Lemma 1 and [24]) the lengths of the translation segments $A_iA_j$ $(i, j \in \{1, 2, 3\}, i < j)$:

$$d^t(A_1, A_2) \approx 4.03113,$$
$$d^t(A_1, A_3) \approx 0.70986,$$
$$d^t(A_2, A_3) \approx 3.14307,$$

therefore $d^t(A_2, A_3) + d^t(A_1, A_3) < d^t(A_1, A_2)$.                    □

### 3.2 The locus of all points equidistant from three given points

A point is said to be equidistant from a set of objects if the distances between that point and each object in the set are equal. Here we study that case where the objects are vertices of a **Nil** translation triangle $A_1A_2A_3$ and determine the locus of all points that are equidistant from $A_1$, $A_2$ and $A_3$.

We consider 3 points $A_1$, $A_2$, $A_3$ that do not all lie in the same translation curve in the projective model of **Nil** space. The *translation segments* connecting the points $A_i$ and $A_j$ $(i < j, \ i, j, k \in \{1, 2, 3\}, k \neq i, j)$ are called sides of the *translation triangle $A_1A_2A_3$*. The locus of all points that are equidistant from the vertices $A_1$, $A_2$ and $A_3$ is denoted by $\mathcal{C}$.

In the previous section we determined the equation of translation-like bisector (equidistant) surface to any two points in the **Nil** space. It is clear, that all points on the locus $\mathcal{C}$ must lie on the equidistant surfaces $\mathcal{S}_{A_iA_j}$, $(i < j, \ i, j \in \{1, 2, 3\})$ therefore $\mathcal{C} = \mathcal{S}_{A_1A_2} \cap \mathcal{S}_{A_1A_3}$ and the coordinates of each of the points of that locus and only those points must satisfy the corresponding equations of Lemma 2. Thus, the non-empty point set $\mathcal{C}$ can be determined and can be visualized for any given translation triangle (see Fig. 4 and 5). In the Fig. 4 we describe the translation triangle $A_1A_2A_3$ with vertices $A_1 = (1, 0, 0, 0)$, $A_2 = (1, 0, 0, 1)$, $A_3 = (1, 1, 0, 0)$ with the equidistant surfaces

$$\mathcal{S}_{A_1A_2} : z = \frac{1}{8}(4xy + 4), \quad \mathcal{S}_{A_2A_3} : z = \frac{2xy^2 - 8x + y^2 + 4y + 4}{4y}$$

of edges $A_1A_2$ and $A_2A_3$ and their intersection $\mathcal{C} = \mathcal{S}_{A_1A_2} \cap \mathcal{S}_{A_2A_3}$.
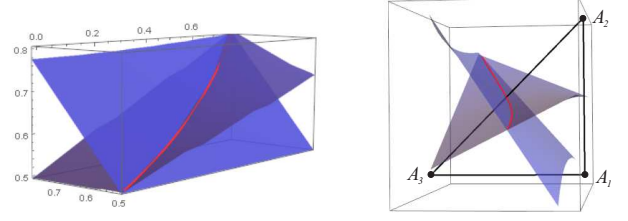


Figure 4: *Translation triangle with vertices $A_1 = (1, 0, 0, 0)$, $A_2 = (1, 0, 0, 1)$, $A_3 = (1, 1, 0, 0)$ with translation-like bisector surfaces $\mathcal{S}_{A_1A_2}$ and $\mathcal{S}_{A_2A_3}$ and a part of the locus $\mathcal{C} = \mathcal{S}_{A_1A_2} \cap \mathcal{S}_{A_1A_3}$ of all points equidistant from three given points $A_1$, $A_2$, $A_3$.*

If the vertices of the translation triangle $A_1A_2A_3$ lie in e.g. coordinate plane $[y, z]$ or $[x, z]$ we obtain the following lemmas:

**Lemma 4** *If the vertices of a translation triangle $A_1A_2A_3$ lie on the $[y, z]$ plane $A_1 = (1, 0, 0, 0)$, $A_2 = (1, 0, b_2, b_3)$, $A_3 = (1, 0, c_2, c_3)$ $(b_2 \neq 0, \ b_3 \neq 0, \ c_2 \neq 0, \ c_3 \neq 0)$ then the parametric equation $(x \in \mathbb{R})$ of $\mathcal{C}$ is the following (see Lemma 2 and Fig. 5):*

$$\mathcal{C}(x) : \left\{ x, \frac{f}{16(b_2c_3 - b_3c_2)}, \frac{g}{32(b_3c_2 - b_2c_3)} \right\}$$

*where*

$$f = -2b_3 \left( -2c_2x(b_2x + 2c_3) + 4c_3(b_2x + c_3) + c_2^2 \left( x^2 + 4 \right) \right)$$
$$+ b_2 \left( b_2 \left( x^2 + 4 \right)(2c_3 - c_2x) + x \left( c_2^2 \left( x^2 + 4 \right) - 4c_2c_3x + 4c_3^2 \right) \right)$$
$$+ b_3^2(8c_3 - 4c_2x),$$

*and*

$$g = b_2^2(x^2 + 4)(c_2(x^2 + 4) - 2c_3x)$$
$$- b_2(4c_2x(x^2 + 4)(b_3 - c_3) + 4c_3(c_3(x^2 + 4) - 2b_3x^2) + c_2^2(x^2 + 4)^2)$$
$$+ 2b_3(2b_3(c_2(x^2 + 4) - 2c_3x) + x(c_2^2(x^2 + 4) - 4c_2c_3x + 4c_3^2)).$$

**Lemma 5** *If the vertices of a translation triangle $A_1A_2A_3$ lie on the $[x, z]$ plane $A_1 = (1, 0, 0, 0)$, $A_2 = (1, b_1, 0, b_3)$, $A_3 = (1, c_1, 0, c_3)$ $(b_1 \neq 0, \ b_3 \neq 0, \ c_1 \neq 0, \ c_3 \neq 0)$ then the parametric equation $(y \in \mathbb{R})$ of $\mathcal{C}$ is the following (see Lemma 2 and Fig. 5):*

$$\mathcal{C}(y) : \left\{ \frac{f}{16(b_1c_3 - b_3c_1)}, y, \frac{g}{16(b_3c_1 - b_1c_3)} \right\}$$

*where*

$$f = -2b_3 \left( -2c_1y(b_1y - 2c_3) + 4c_3(c_3 - b_1y) + c_1^2 \left( y^2 + 4 \right) \right)$$
$$+ b_1 \left( b_1 \left( y^2 + 4 \right)(c_1y + 2c_3) - y \left( c_1^2 \left( y^2 + 4 \right) + 4c_1c_3y + 4c_3^2 \right) \right)$$
$$+ 4b_2^2(c_1y + 2c_3),$$

*and*

$$g = -b_1^2 c_1 y^3 - 4b_1^2 c_1 y - 2b_1^2 c_3 y^2 - 8b_1^2 c_3 - 4b_1 b_3 c_1 y^2$$
$$-8b_1 b_3 c_3 y + b_1 c_1^3 y^3 + 4b_1 c_1^2 y + 4b_1 c_1 c_3 y^2 + 4b_1 c_3^2 y - 4b_3^2 c_1 y$$
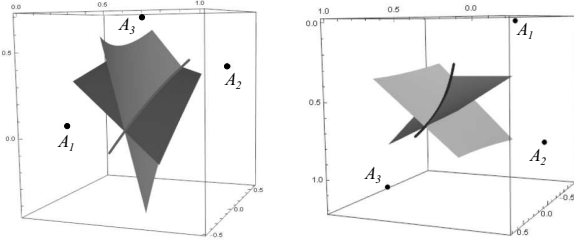$$-8b_3^2 c_3 + 2b_3 c_1^2 y^2 + 8b_3 c_1^2 + 8b_3 c_1 c_3 y + 8b_3 c_3^2.$$



Figure 5: *Translation triangle with vertices $A_1 = E_0 = (1,0,0,0)$, $A_2 = (1,1/2,0,7/10)$, $A_3 = (1,1,0,2/5)$ with translation-like bisector surfaces $\mathcal{S}_{A_1 A_2}$ and $\mathcal{S}_{A_1 A_3}$ (left) and Translation triangle with vertices $A_1 = E_0 = (1,0,0,0)$, $A_2 = (1,0,-1/5,4/5)$, $A_3 = (1,0,1,6/5)$ with translation-like bisector surfaces $\mathcal{S}_{A_1 A_2}$ and $\mathcal{S}_{A_1 A_3}$ (right).*

### 3.3 Translation tetrahedra and their circumscribed spheres

We consider 4 points $A_1$, $A_2$, $A_3$, $A_4$ in the projective model of **Nil** space (see Section 2). These points are the vertices of a *translation tetrahedron* in the **Nil** space if any two *translation segments* connecting the points $A_i$ and $A_j$ ($i < j$, $i,j \in \{1,2,3,4\}$) do not have common inner points and any three vertices do not lie in a same translation curve. Now, the translation segments $A_i A_j$ are called edges of the translation tetrahedron $A_1 A_2 A_3 A_4$.

The circumscribed sphere of a translation tetrahedron is a translation sphere (see Definition 2, (12)) that touches each of the tetrahedron's vertices. As in the Euclidean case the radius of a translation sphere circumscribed around a tetrahedron $T$ is called the circumradius of $T$, and the center point of this sphere is called the circumcenter of $T$.

**Lemma 6** *For any translation tetrahedron there exists uniquely a translation sphere (called the circumsphere) on which all four vertices lie.*

**Proof.** The Lemma follows directly from the properties of the translation distance function (see Definition 1 and (12)). The procedure to determine the radius and the circumcenter of a given translation tetrahedron is the following:

The circumcenter $C = (1,x,y,z)$ of a given translation tetrahedron $A_1 A_2 A_3 A_4$ ($A_i = (1,x^i,y^i,z^i)$, $i \in \{1,2,3,4\}$) have to hold the following system of equation:

$$d^t(A_1,C) = d^t(A_2,C) = d^t(A_3,C) = d^t(A_4,C), \qquad (32)$$

therefore it lies on the translation-like bisector surfaces $\mathcal{S}_{A_i,A_j}$ ($i < j$, $i,j \in \{1,2,3,4\}$) which equations are determined in Lemma 2. The coordinates $x,y,z$ of the circumcenter of the circumscribed sphere around the tetrahedron $A_1 A_2 A_3 A_4$ are obtained by the system of equation derived from the facts:

$$C \in \mathcal{S}_{A_1 A_2}, \mathcal{S}_{A_1 A_3}, \mathcal{S}_{A_1 A_4}. \qquad (33)$$

Finally, we get the circumradius $r$ as the translation distance e.g. $r = d^t(A_1,C)$.

We apply the above procedure to two tetrahedra determined their centres and the radii of their circumscribed balls that are displayed in Fig. 6 and 7. □



Figure 6: *Translation tetrahedron with vertices $A_1 = (1,0,0,0)$, $A_2 = (1,1.4,0,1)$, $A_3 = (1,0.5,1,1)$, $A_4 = (1,0,0,1.5)$ and its circumscibed sphere of radius $r \approx 0.92804$.*
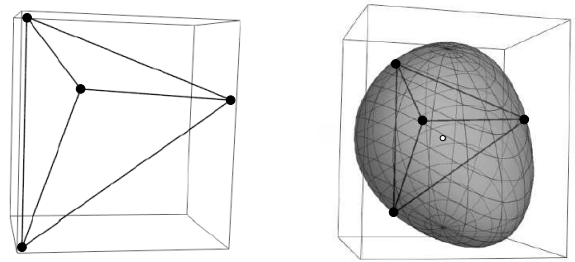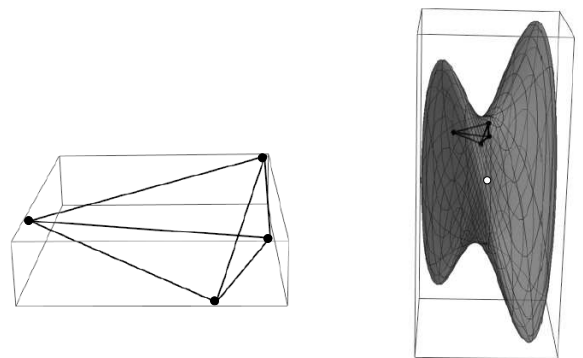


Figure 7: *Translation tetrahedron with vertices $A_1 = (1,0,0,0)$, $A_2 = (1,4,2,1)$, $A_3 = (1,1,3,0)$, $A_4 = (1,0,-2,1)$ and its circumscibed sphere of radius $r \approx 7.96825$.*

## 4 The lattice-like translation ball coverings

In [21] we investigated the lattice-like *geodesic ball coverings* with congruent geodesic balls and in this section we study the similar problem of the translation ball coverings. In the following, we shall consider lattice coverings, each of them consisting of congruent translation balls of **Nil**. Let $\mathcal{B}_\Gamma^c(R)$ denote a translation ball covering of **Nil** space with balls $B^c(R)$ of radius $R$ where their centres give rise to a **Nil** point lattice $\Gamma(\tau_1, \tau_2, k)$ ($k \in \mathbb{N}^+$). $\widetilde{\mathcal{F}(k)}$ is an arbitrary **Nil** parallelepiped of this lattice (see Section 2.2). The images of $\widetilde{\mathcal{F}(k)}$ by our discrete translation group $\mathbf{L}(\tau_1, \tau_2, k) = \mathbf{L}(\mathbb{Z}, k)$ cover the **Nil** space without gap.

**Remark 4** *In the* **Nil** *geometry, similarly to the Euclidean space* $\mathbf{E}^d$, *(*$d \geq 1$*), an arbitrary lattice* $\Gamma$ *gives a lattice-like covering of equal balls if the radius $R$ of the balls is large enough. For the geodesic ball packings it is not true because the geodesic balls should have a radius $R \in [0, 2\pi]$ (see [19]).*

If we start with a translation-like lattice covering $\mathcal{B}_\Gamma^c(R)$ and shrink the balls until they finally do not cover the space any more, then the minimal radius defines the least dense covering to a given lattice $\Gamma(\tau_1, \tau_2, k)$. The threshold value $R_\Gamma^c$ is called *the minimal covering radius* of the point lattice $\Gamma(\tau_1, \tau_2, k)$:

$$R_\Gamma^c := \min\{R : \text{where } \mathcal{B}_\Gamma^c(R) \text{ lattice covering by } \Gamma(\tau_1, \tau_2, k)\}. \tag{34}$$

For the density of the packing it is sufficient to relate the volume of the minimal covering ball to that of the solid $\widetilde{\mathcal{F}(k)}$.

Analogously to the Euclidean case it can be defined the density $\Delta(\mathcal{B}_\Gamma^c(R))$ of the lattice-like geodesic ball covering $\mathcal{B}_\Gamma^c(R)$:

**Definition 6**

$$\Delta(\mathcal{B}_\Gamma^c(R)) := \frac{Vol(B_\Gamma^c(R))}{Vol(\widetilde{\mathcal{F}(k)})}, \tag{35}$$

*and its minimum* $\Delta(\mathcal{B}_\Gamma^c(R_\Gamma^c))$ *for radius* $R_\Gamma^c$ *in (34).*

*The main problem is that to which lattice* $\Gamma(\tau_1, \tau_2, k)$ *belongs the optimal minimal density where* $k \in \mathbb{N}^+$ *is a given parameter.*

$$\Delta_{opt}(\mathcal{B}^c) = \inf_\Gamma \left\{ \Delta(\mathcal{B}_\Gamma^c(R_\Gamma^c)) \right\}. \tag{36}$$

*and* $\Gamma_{opt}^c$ *denotes any optimal lattice, if it exists at all.*

**Remark 5** *The covering radius is the radius of the circumsphere of the lattice's Dirichlet-Voronoi cell i.e. the largest distance between the midpoint and the vertices of its Dirichlet-Voronoi cell, whose description deserves separate studies (see [15]).*

In the following we study the most important case related to parameter $k = 1$.

### 4.1 Method to determination of densest lattice-like translation ball covering of a given lattice

We develop an algorithm to determine the lattice-like thinnest ball covering of a given lattice $\Gamma(\tau_1, \tau_2, 1)$.

The lattice is generated by the translations $\tau_1$ and $\tau_2$ where their coordinates in the model are $t_i^j$ ($i = 1, 2$; $j = 1, 2, 3$) (see (16)).

The **Nil** parallelepiped $\widetilde{\mathcal{F}(1)} = E_0 T_1^{opt} T_2 T_3 T_{12} T_{21} T_{23} T_{213} T_{13}$ is a *fundamental domain* of $\mathbf{L}(\mathbb{Z}, 1)$. The homogeneous coordinates of its vertices can be derived from the coordinates of $\tau_1$ and $\tau_2$ (see Fig. 1 and (3) with (16)). We examine the *minimal covering radius* $R^c$ to the given lattice $\Gamma(\tau_1, \tau_2, 1)$.

$$R_\Gamma^c := \min\{R : \text{where } \mathcal{B}_\Gamma^c(R) \text{ lattice covering by } \Gamma(\tau_1, \tau_2, 1)\}.$$

It is sufficient to investigate such ball arrangements $\mathcal{B}_\Gamma^c(R)$ where the balls cover $\widetilde{\mathcal{F}(1)}$.

From (14-16) follows, that the fundamental parallelepiped $\widetilde{\mathcal{F}(1)}$ can be decomposed into Euclidean tetrahedra $\{E_0, T_1, T_2, T_3\}$, $\{T_3, T_1, T_{23}, T_{13}\}$, $\{T_3, T_1, T_{23}, T_2\}$, $\{T_{12}, T_1, T_{23}, T_2\}$, $\{T_{12}, T_1, T_{23}, T_{13}\}$, $\{T_{12}, T_{21}, T_{23}, T_{13}\}$ which fill it just once. The radius $R_i$ ($i = 1, 2 \ldots 6$) of each circumscribed ball to the above point sets can be determined by the procedure described in the previous section. It is clear, that the lattice-like ball arrangement $\mathcal{B}_\Gamma^c(R_\Gamma^c)$ of radius $R_\Gamma^c = \max\{R_i\}$ cover the fundamental parallelepiped $\widetilde{\mathcal{F}(1)}$ and thus the **Nil** space if the translation ball of radius $R_\Gamma^c$ is convex in Euclidean sense i.e. $R_\Gamma^c \in [0, 2]$ (see Theorem 2).

#### 4.1.1 Upper bound for the covering density

To have a comparison, first we consider our optimal lattice-like arrangement $\mathcal{B}_\Gamma^p(R_p)$ for the *conjectured densest lattice-like translation ball packing* in the **Nil** space (see [24]). These balls will be blown up to a covering. This optimal lattice is given in [20] with parameters

$$t_1^{1,p} \approx 1.31225;\ t_1^{3,p} = \frac{t_3^{3,p}}{2};\ t_2^{1,p} \approx 0.65613;\ t_2^{2,p} \approx 1.13644;$$
$$t_2^{3,p} \approx 1.11847;\ r_p \approx 0.74565;\ t_3^{3,p} = 2r_p. \tag{37}$$

This packing can be generated by the translations $\Gamma^p(\tau_1^p, \tau_2^p, 1)$ where $\tau_1^p$ and $\tau_2^p$ are given by the above coordinates $t_i^{j,p}$ $i = 1, 2$; $j = 1, 2, 3$ (see (36)). Thus we obtain the neighbouring balls around an arbitrary ball of the packing $\mathcal{B}_\Gamma^p(R_{\Gamma p}^c)$ by the lattice $\Gamma^p(\tau_1^p, \tau_2^p, 1)$. We have ball

"columns" in $z$-direction and in regular hexagonal projection onto the $[x,y]$-plane. From the structure of this lattice follows that in this case the corresponding lattice point sets $\{0, T_1^p, T_2^p, T_3^p\}$, $\{T_3^p, T_1^p, T_{23}^p, T_{13}^p\}$, $\{T_1^p, T_1^p, T_{23}^p, T_2^p\}$, $\{T_{12}^p, T_1^p, T_{23}^p, T_2^p\}$, $\{T_{12}^p, T_1^p, T_{23}^p, T_{13}^p\}$, $\{T_{12}^p, T_{21}^p, T_{23}^p, T_{13}^p\}$ are congruent by **Nil** isometries. The radius $R_p$ of each circumscribed ball to the above point sets can be determined by the following system of equations:

$$d^t(O,C) = d^t(C, T_3^p) = d^t(C, T_1^p) = d^t(C, T_2^p),$$

where $C(1, c^1, c^2, c^3)$ is the center of the circumscribed ball of the point set $\{E_0, T_1^p, T_2^p, T_3^p\}$ ($d^t$ is the **Nil** translation distance, see Definition 1):

$$c^1 \approx 0.45563, c^2 \approx 0.26306, c^3 \approx 0.80558, R_{\Gamma^p}^c \approx 0.91257.$$
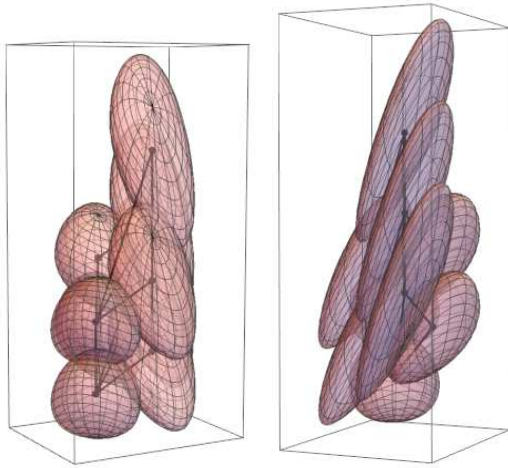


Figure 8: *Locally optimal lattice-like translation ball covering related to lattice $\Gamma^p(\tau_1^p, \tau_2^p, 1)$.*

**Remark 6** $C(1, c^1, c^2, c^3)$ *is a vertex of the Dirichlet-Voronoi domain of the centre point $E_0$.*

$R_{\Gamma^p}^c \in [0, 2]$ thus by Theorem 2 the ball of radius $R_{\Gamma^p}^c$ is convex in affin-Euclidean sense. Their circumscribed congruent **Nil** balls are convex thus they cover the tetrahedra and so the ball arrangement $\mathcal{B}_{\Gamma^p}^c(R_{\Gamma^p}^c)$ cover the **Nil** space. Thus the radius $R_{\Gamma^p}^c$ of circumscribed ball give us the covering radius to the lattice $\Gamma^p$, indeed, and we get by (13), (17) and by the Definition 6 the following results:

$$Vol(B(R_{\Gamma^p}^c)) \approx 3.18341, Vol(\widetilde{\mathcal{P}}) = Vol(\widetilde{\mathcal{F}(1)}) \approx 2.22397,$$

$$\Delta(R_{\Gamma^p}^c, \tau_1^p, \tau_2^p, 1) := \frac{Vol(\mathcal{B}_\Gamma(R_{\Gamma^p}^c))}{Vol(\widetilde{\mathcal{F}(1)})} \approx 1.43141.$$

(38)

**Remark 7** *The density of the least dense lattice-like ball covering in the the Euclidean space is*

$$\Delta_{opt}(R_{opt}^c, \tau_1^c, \tau_2^c, 1) < \Delta_E = \frac{5\sqrt{5}\pi}{24} \approx 1.46350.$$

*This $\Delta_E$ attains for the so-called inner centred cubic lattice type of $\mathbf{E}^3$. That means a **Nil**-lattice-ball-covering can be "looser" than a Euclidean one.*

Similarly to the above computations we can apply our method to any given **Nil** lattice. In the Table 1 we summarize the data of some locally optimal lattice-like translation ball coverings:

| Table 1 | | |
|---|---|---|
| Lattice parameters | $R_\Gamma^c$ | $\Delta_\Gamma^c$ |
| $t_i^j = 1$, $(i = 1, 2, \; j = 1, 2, 3)$ | $\approx 0.88666$ | $\approx 2.91980$ |
| $t_1^1 = t_1^{1,d}, \; t_1^3 = t_1^{3,d},$ $t_2^1 = t_2^{1,d}, \; t_2^2 = t_2^{2,d}, \; t_2^3 = t_2^{3,d}$ | $\approx 0.91257$ | $\approx 1.43141$ |
| $t_1^1 = 1.3, \; t_1^3 = 0.74,$ $t_2^1 = 0.65, \; t_2^2 = 1.13, \; t_2^3 = 1.12$ | $\approx 0.90406$ | $\approx 1.43429$ |
| $t_1^1 = 1.29, \; t_1^3 = 0.74,$ $t_2^1 = 0.64, \; t_2^2 = 1.13, \; t_2^3 = 1.12$ | $\approx 0.89997$ | $\approx 1.43692$ |
| $t_1^1 = 1.1, \; t_1^3 = 0.5,$ $t_2^1 = 0.5, \; t_2^2 = 1, \; t_2^3 = 1$ | $\approx 0.77177$ | $\approx 1.59134$ |
| $t_1^1 = 1.1, \; t_1^3 = 0.5,$ $t_2^1 = 0.4, \; t_2^2 = 1, \; t_2^3 = 1$ | $\approx 0.78667$ | $\approx 1.68533$ |
| $t_1^1 = 1.31, \; t_1^3 = 0.74,$ $t_2^1 = 0.65, \; t_2^2 = 1.13, \; t_2^3 = 1.12$ | $\approx 0.90732$ | $\approx 1.42783$ |

From the previous computations follows the following

**Theorem 3** *The density of the least dense lattice-like translation ball covering is less or equal than the locally thinnest covering with congruent tranlation balls related to the lattice $\Gamma^u(\tau_1^u, \tau_2^u, 1)$ where the lattice is given by the parameters $t_1^1 = 1.31$, $t_1^3 = 0.74$, $t_2^1 = 0.65$, $t_2^2 = 1.13$, $t_2^3 = 1.12$ (see Fig. 9).*

$$\Delta_{opt}(R_{opt}^c, \tau_1^c, \tau_2^c, 1) \le \Delta(R_{\Gamma^u}^c, \tau_1^u, \tau_2^u, 1) \approx 1.42783$$

*(see Table 1 and Fig. 9).*

The exact determination of the thinnest lattice-like ball covering with congruent translation balls seems to be difficult, but we are working on refining the upper bound density and determine a "good" lower bound density.

Optimal sphere packings and coverings in other homogeneous Thurston geometries represent another huge class of open mathematical problems. For **Nil**, **Sol**, $\widetilde{\mathbf{SL}_2\mathbf{R}}$, $\mathbf{H}^2 \times \mathbf{R}$, $\mathbf{S}^2 \times \mathbf{R}$ geometries only very few results are known [17], [19], [20], [21], [22], [23].

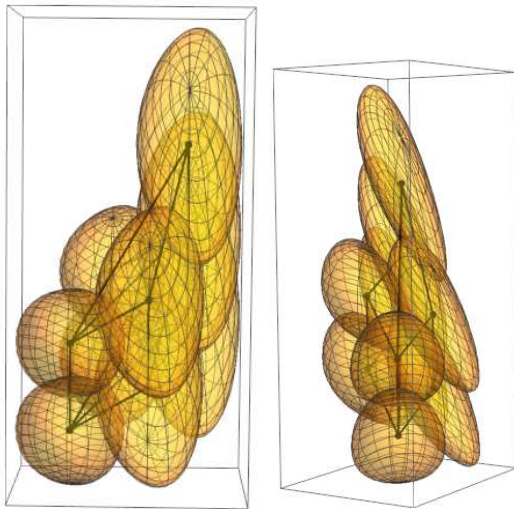Detailed studies are the objective of ongoing research.

Figure 9: *Locally optimal lattice-like translation ball covering related to lattice $\Gamma^u(\tau_1^u, \tau_2^u, 1)$ with density $\approx 1.42783$.*

## References

[1] K. BRODACZEWSKA, Elementargeometrie in **Nil**. *Dissertation (Dr. rer. nat.) Fakultät Mathematik und Naturwissenschaften der Technischen Universität Dresden*, 2014.

[2] I. CHAVEL, *Riemannian Geometry: A Modern Introduction*. Cambridge Studies in Advances Mathematics, 2006.

[3] S. KOBAYASHI, K. NOMIZU, *Fundation of differential geometry, I.*. Interscience, Wiley, New York, 1963.

[4] J. INOGUCHI, Minimal translation surfaces in the Heisenberg group **Nil**$_3$. *Geom. Dedicata* **161** (1) (2012), 221–231.

[5] J. MILNOR, Curvatures of left Invariant metrics on Lie groups. *Advances in Math.* **21** (1976), 293–329

[6] E. MOLNÁR, The projective interpretation of the eight 3-dimensional homogeneous geometries. *Beitr. Algebra Geom.* **38** (2) (1997), 261–288.

[7] E. MOLNÁR, On projective models of Thurston geometries, some relevant notes on **Nil** orbifolds and manifolds. *Sib. Electron. Math. Izv.* **7** (2010), 491–498, http://mi.mathnet.ru/semr267

[8] E. MOLNÁR, B. SZILÁGYI, Translation curves and their spheres in homogeneous geometries. *Publ. Math. Debrecen,* **78** (2) (2010), 327–346.

[9] E. MOLNÁR, J. SZIRMAI, Symmetries in the 8 homogeneous 3-geometries. *Symmetry Cult. Sci.* **21** (1-3) (2010), 87–117.

[10] E. MOLNÁR, J. SZIRMAI, A. VESNIN, Projective metric realizations of cone-manifolds with singularities along 2-bridge knots and links. *J. Geom.* **95** (2009), 91–133.

[11] E. MOLNÁR, J. SZIRMAI, On **Nil** crystallography, *Symmetry Cult. Sci.,* **17** (1-2) (2006), 55–74.

[12] J. PALLAGI, B. SCHULTZ, J. SZIRMAI, Visualization of geodesic curves, spheres and equidistant surfaces in $\mathbf{S}^2 \times \mathbf{R}$ space, *KoG* **14** (2010), 35–40.

[13] J. PALLAGI, B. SCHULTZ, J. SZIRMAI, Equidistant surfaces in **Nil** space, *Stud. Univ. Zilina. Math .Ser.* **25** (2011), 31–40.

[14] J. PALLAGI, B. SCHULTZ, J. SZIRMAI, Equidistant surfaces in $\mathbf{H}^2 \times \mathbf{R}$ space, *KoG* **15** (2011), 3–6.

[15] B. SCHULTZ, E. MOLNÁR, Geodesic lines and spheres, densest(?) geodesic ball packing in the new linear model of **Nil** geometry, *Proceedings of the Czech-Slovak Conference on Geometry and Graphics*, (2015), 177–186.

[16] B. SCHULTZ, J. SZIRMAI, On parallelohedra of **Nil**-space, *Pollack Periodica* **7. Supplement 1** (2012), 129–136.

[17] B. SCHULTZ, J. SZIRMAI, Geodesic ball packings generated by regular prism tilings in **Nil** geometry, *Miskolc Math. Notes*, (to appear), (2019), arXiv: 1607.04401.

[18] P. SCOTT, The geometries of 3-manifolds. *Bull. London Math. Soc.* **15** (1983), 401–487.

[19] J. SZIRMAI, The densest geodesic ball packing by a type of **Nil** lattices. *Beitr. Algebra Geom.* **48** (2) (2007), 383–398.

[20] J. SZIRMAI, Lattice-like translation ball packings in **Nil** space. *Publ. Math. Debrecen* **80** (3-4) (2012), 427–440.

[21] J. SZIRMAI, On lattice Coverings of **Nil** space by Congruent Geodesic Balls. *Mediterr. J. Math.* **10** (2013), 953–970.

[22] J. SZIRMAI, A candidate to the densest packing with equal balls in the Thurston geometries. *Beitr. Algebra Geom.* **55** (2) (2014), 441–452.

[23] J. SZIRMAI, The densest translation ball packing by fundamental lattices in **Sol** space. *Beitr. Algebra Geom.* **51** (2) (2010), 353–373.

[24] J. SZIRMAI, **Nil** geodesic triangles and their interior angle sums. *Bulletin of the Brazilian Mathematical Society, New Series*, **49** (2018), 761.773,

[25] J. SZIRMAI, Bisector surfaces and circumscribed spheres of tetrahedra derived by translation curves in **Sol** geometry, *New York J. Math.* **25** (2019), 107–122.

[26] W. P. THURSTON (and S. LEVY editor), *Three-Dimensional Geometry and Topology*. Princeton University Press, Princeton, New Jersey, vol. **1**, 1997.

**Angéla Vránics**
e-mail: angilord@gmail.com

**Jenő Szirmai**
orcid.org/0000-0001-9610-7993
email: szirmai@math.bme.hu

Budapest University of Technology and Economics, Institute of Mathematics, Department of Geometry

Budapest, P. O. Box: 91, H-1521

GEORG GLAESER

# Focus Stacking from a Purely Geometrical Point of View

## Focus Stacking from a Purely Geometrical Point of View

### ABSTRACT

In order to create extremely sharp photographs, focus stacking has become a widely used method nowadays, mainly in macro or micro photography. Whereas the aspect of computationally detecting sharp regions of an image has been dealt with in many publications, there is only little published about the geometric background. This paper analyzes the process from a purely geometrical point of view, revealing some non-trivial aspects that may potentially also lead to improvements in a variety of applications such as the 3D scanning of small objects. It is shown that – under calibrated conditions and with certain restrictions – focus stacking of a scene leads to arbitrarily many geometrically correct perspective images of this scene, even including normal projections. The reason for this is that the process of photography never leads to purely two-dimensional images, but collinearly distorted spatial images.

Key words: ray optics, focus stacking, Depth of Field, computational photography, image registration, light field camera

MSC2010: 51P05, 65T60, 78A05

## Podešavanje dubinske oštrine s čisto geometrijskog gledišta

### SAŽETAK

Da bi se stvorile izuzetno oštre fotografije u današnje se vrijeme često koristi metoda podešavanja dubinske oštrine. Posebno je česta njezina upotreba u makro ili mikro fotografiji. Iako je tema računalnog određivanja oštrih područja slike obrađena u mnogim publikacijama, o njegovoj je geometrijskoj pozadini objavljeno malo radova. Ovaj rad analizira spomenuti postupak s čisto geometrijskog gledišta otkrivajući neke netrivijalne aspekte koji mogu dovesti do poboljšanja u mnogim njegovim primjenama kao što je 3D skeniranje malih predmeta. Pokazano je da podešavanje dubinske oštrine scene – pod kalibriranim uvjetima i uz određena ograničenja – može proizvesti po volji mnogo geometrijski ispravnih perspektivnih slika te scene, pa čak i njezinu ortogonalnu projekciju. Razlog tome je činjenica da proces fotografiranja nikada ne rezultira čistim dvodimenzionalnim slikama, već kolinearno iskrivljenim prostornim slikama.

Ključne riječi: geometrijska optika, podešavanje dubinske oštrine, dubinska oštrina, računski rekonstruirana fotografija, registracija slike, light field kamera

## 1   Are photographs central projections?

Photography is a source of fascination for many people – especially for mathematicians and geometry enthusiasts. In geometry classes, we sometimes say (in simplified terms): photographs correspond to central projections (perspectives) of space. This means a reduction of three-dimensional space into the two-dimensional plane. This can be "proved" by the fact that it is possible to reconstruct the photographed three-dimensional scene quite accurately from a number of photographs. It is quintessential that high-quality lens systems are used that reproduce straight edges as exactly straight.

Even though this idea works quite well for scenes with larger technical objects, such as polyhedra (e.g., a furnished room or a building), it poses huge problems in the context of macro photography, meaning photographs of objects that measure just a few centimeters or even less

Figure 1: *Two flies, depicted in different ways. Left: Focus-stacked with medium aperture and without flash, right: single photo, closed aperture, twin flash. Whereas the left image is completely sharp, the image on the right illustrates the limits of macro photography, even with professional equipment.*

than that. There, the "Depth of Field" (DoF) is comparatively much smaller than in regular photography.

## 2 An impossible photograph

The flies in Figure 1, measuring about 1 cm, are fundamentally different in terms of the photographic techniques used to depict them. The picture on the left (with some disgorged digestive juice) is in sharp focus overall. An insect photographer will be puzzled: it seems impossible to take such a photograph – even if we used highly expensive equipment with special macro objectives, macro flashes and the highest aperture number possible (as in the picture on the right, where minuscule droplets of water can be seen on the complex eyes.)

This poses two questions: why can an object as small as a fly not be rendered in sharp focus overall, and how does it seem to be possible after all? This paper will explain the situation from a mathematical/geometrical point of view.

## 3 The lens formula

In physics, the method of operation of a lens (or a well-aligned lens system) is explained as follows: Let $P$ be a point in the real world. It emits (reflects) light rays in all directions. Two of them will have easily predictable properties. The *principal ray* through the lens center $C$ will not be refracted, while the ray parallel to the optical axis will

go through the focal point $F^*$ after the refraction. Behind the lens (the lens system), the two rays – and all others – meet in the pixel $P^*$.
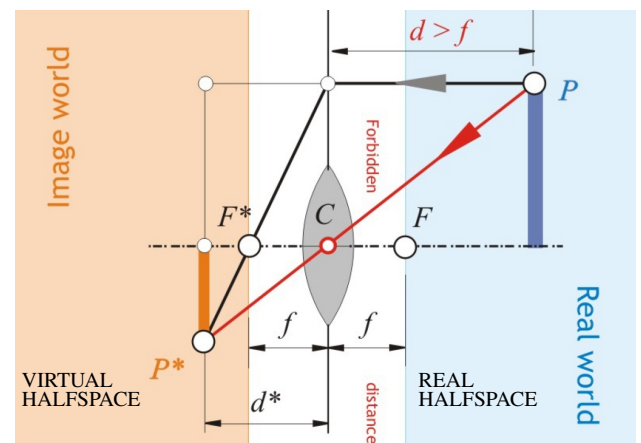


Figure 2: *The principle of geometric ray optics (simplified): From the infinitely many light rays emitted from a space point, the* principal ray *through the lens center C is not refracted, and the ray parallel to the optical axis will go through the focal point $F^*$ after the refraction.*

From Figure 2, using similar triangles, we can derive the *lens formula*:

$$\frac{1}{f} = \frac{1}{d} + \frac{1}{d^*}. \tag{1}$$

Here, $f$ denotes the focal distance and $d$ and $d^*$ the oriented distances of the point in space $P$ and the pixel $P^*$ from the symmetry plane through the lens center $C$, respectively.

Using this method, we can determine the corresponding pixel for each point in space.

## 4 The Gaussian Collineation

Let us define $d = kf$. Using the lens formula, we then get

$$d^* = \frac{k}{k-1} \cdot f = \frac{d}{k-1}. \tag{2}$$

According to the intercept theorems, we get the following simple relation between the distances of a point in space $P$ and its pixel $P^*$ from the center $C$:

$$\overline{CP^*} = \frac{1}{k-1} \cdot \overline{CP}. \tag{3}$$

Even though the geometrical mapping $P \mapsto P^*$ works in both directions, a camera will only be able to depict the half space whose points lie at a greater distance from the lens than the focal distance $f$ ($k > 1$): points in the plane through the point $F$ perpendicular to the optical axis are projected onto far points, because the denominator $k - 1$ vanishes in that case.

It is easy to show that the mapping $P \mapsto P^*$ *preserves straight lines*: Let $g$ be an arbitrary straight line in space. It can always be defined as the intersection of two special planes $\varepsilon$ and $\varphi$, with $\varepsilon$ being the connecting plane of $g$ with the center $C$ and $\varphi$ being the plane through $g$ that is parallel to the optical axis. $\varepsilon$ is transformed into itself ($\varepsilon^* = \varepsilon$) because we can think of the plane as a pencil of principal rays. The other plane, $\varphi^*$, can be conceived of as rays parallel to the optical axis that transition into a pencil through the focal point $F^*$ and the intersection line of $\varphi$ with the symmetry plane. The image $g^*$ of $g$ is the intersection of $\varepsilon^*$ and $\varphi^*$ and therefore a straight line ([1]). The mapping $P \mapsto P^*$ is thus a collineation – which is the technical term for images that preserve straight lines. This mapping is a very special form of *perspective collineation*: the center lies in the *collineation plane* (the symmetry plane). Such a collineation is called *elation*. This insight goes back to C. F. Gauss ([2]).

We briefly describe the Gaussian collineation $P(x,y,z) \mapsto P^*(x^*,y^*,z^*)$ analytically. The coordinate system shall have its origin in the camera center $C$, and the $z$-axis shall be the optical axis. Then we have

$$\begin{pmatrix} x^* \\ y^* \\ z^* \end{pmatrix} = \frac{f}{f-z} \begin{pmatrix} x \\ y \\ z \end{pmatrix}. \tag{4}$$

When we switch to homogenous coordinates

$$x = \frac{x_1}{x_0}, y = \frac{x_2}{x_0}, z = \frac{x_3}{x_0}, \text{ and } x^* = \frac{x_1^*}{x_0^*}, y^* = \frac{x_2^*}{x_0^*}, z^* = \frac{x_3^*}{x_0^*},$$

we obtain

$$\begin{pmatrix} x_0^* \\ x_1^* \\ x_2^* \\ x_3^* \end{pmatrix} = \begin{pmatrix} f x_0 - x_3 \\ f x_1 \\ f x_2 \\ f x_3 \end{pmatrix}. \tag{5}$$

From this, we can immediately read all important facts of the collineation, namely that it is an elation with center $C$. The fixpoints lie in $x_3 = 0$, i.e., the lens symmetry plane. The zero plane and the vanishing plane are parallel to the fixpoint plane at distance $\pm f$, respectively.

## 5 How does this relate to photography?

Using the simple formula (3), we can very easily transform spatial objects made of a number of points into equally *spatial* objects. How does this relate to photography, which after all produces a *two-dimensional* result?

Let us consider a point $P$ at a distance $d$ from the symmetry plane (collineation plane). If the plane $\pi$ of the sensor of our camera happens to be located at a distance $d^*$ from the collineation plane, the pixel $P^*$ will lie in $\pi$. Thus, the intersection of the object that we aim to reproduce with the "plane of sharpness" (also called focal plane), sometimes also referred as through $P$ at a distance $d$ parallel to the collineation plane is in sharp focus.[1] All other points are rendered more or less sharp.

The extent of blurring is dependent on a number of different parameters, as we shall see. One crucial parameter is the size of the distance of the photographed object proportionally to the focal length.

---

[1] Using our common sense, we may have assumed that in a photographic image, all those points would be rendered sharp that have a certain constant distance (thus lying on a sphere around $C$) from the lens center, which depends on the distance $d^*$ from the sensor plane. However, according to the lens formula, this is not the case, as all of those points lie in a plane, the *plane of sharpness*, also called focal plane, at a distance $d$.

# 6 Photographing elephants vs. flies
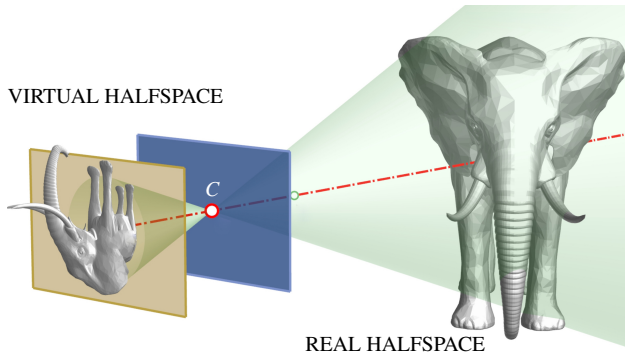


VIRTUAL HALFSPACE

REAL HALFSPACE

Figure 3: *Depicting large objects from a great distance. The corresponding virtual 3D image is "almost flat", i.e., all image points are close to the sensor plane. The image in the sensor plane is more or less "sharp".*

Let us first consider the image of a "large" object from a great distance (what we mean is the relation of the object size to the focal length $f$ (Figure 3)).

For points at a great distance $d = k \cdot f$ ($k \gg 1$), the image distance $d/(k-1)$ (formula 2) does not vary a great deal. The collinear virtual object behind the lens will thus be strongly oblate, which means that there will be minor blurring of those points that do not lie precisely in the plane of sharpness. Taking a sharp full-size photograph of an elephant thus poses no problem.

The smaller the object that we want to photograph, and the closer it is to the "forbidden" vanishing plane (Figure 4), the more the expression $f/(f-d) = 1/(1-k)$ in the transformation formula (3) will vary. This means that the points will become more blurry, which leads to a genuine problem.

A brief remark: Short focal lengths $f$ apparently have a positive effect on the focus depth, as a fly or a snail becomes larger proportionally to $f$. Cameras with small sensors have a correspondingly shorter focal length.[2]

# 7 Geometry vs. physics

In geometry, the matter seems to be trivial: Let us intersect the light ray through the lens center with the sensor plane. Seen from the perspective of physics, this, of course, does not work: a single light ray is not sufficient to expose the sensor. We will thus have to install a circle-shaped opening

in the collineation plane – the aperture. All light rays emanating from a point in space $P$ will then lie inside a skewed circular cone through the opening, which is itself refracted in a skewed circular cone (Figure 5.)

The entirety of light rays in this refracted skewed circular cone exposes the sensor plane in a dot-shaped way only if $P$ lies on the *plane of sharpness*. In all other cases, there is a so-called *circle of confusion* on the sensor (CoC for short.)

We could now assume that we only need sufficient lighting (flash) in order to keep the aperture as small as possible (we speak of a high aperture number in such cases.) However, that is only possible up to a certain limit (the aperture should be bigger than 1 mm at any rate.) If we reduce the size further, the wave properties of light further complicate the matter: this leads to diffraction on the edges of the aperture, which results in inconvenient *diffraction blurring*. Optimal results can be obtained by using the *optimum aperture* indicated by the manufacturer of the lens. Photographers know that exceeding the optimum aperture will reduce the image quality.

# 8 Focus stacking

In the picture of the elephant, we hardly ran into any problems – if a photographer targets a point that lies approximately at the end of the first third of the desired distance range, the picture will be sufficiently sharp.[3]

In macro photography, however, a lack of sharpness is a serious problem – especially if we are not dealing with artistic but scientific images.

Nowadays, a technique called *focus stacking* has been established; in essence, it works in the following way: the camera takes a number of images of a scene in as short an interval as possible, varying the distance of the focal plane. This way, we get an image series where different layers of the object are focused consecutively.

The theory of image processing is quite advanced by now, and software used for this purpose is able to distinguish sharp from blurry pixels. Here, we can only briefly mention two methods and do not go into details: One method is to use the shape of the edge gradient profile at each particular edge point to classify edge sharpness (see, e.g., [3]). The other method is to compute the fast Fourier Transform and analyze the result. The Fourier transform tells us which frequencies are present in the image. If there is a

---

[2]In technical specifications, the focal length (e.g., 100 mm) of a lens is often provided in terms of a 35 mm equivalent, which means that for a "full format sensor size" of $24\,\text{mm} \times 36\,\text{mm}$, the lens has a focal length of 100 mm.

If the sensor, however, only has a size of, for example, $6\,\text{mm} \times 9\,\text{mm}$, the same visual impression can be achieved with a focal length of just 25 mm. In this special case, we have a *crop factor* of 4. Nowadays, it is possible to take amazingly sharp macro photographs with good smartphones, owing to their extremely short focal lengths and correspondingly tiny sensors (with much larger crop factors.) However, this leads to the problem of having a large number of pixels in the tightest of spaces, which inevitably leads to a loss of quality.

[3]Artistic photographers often encounter the opposite problem: they deliberately want to work with blurred areas. In such cases, using larger focal lengths and a *wide-open aperture* is recommendable.
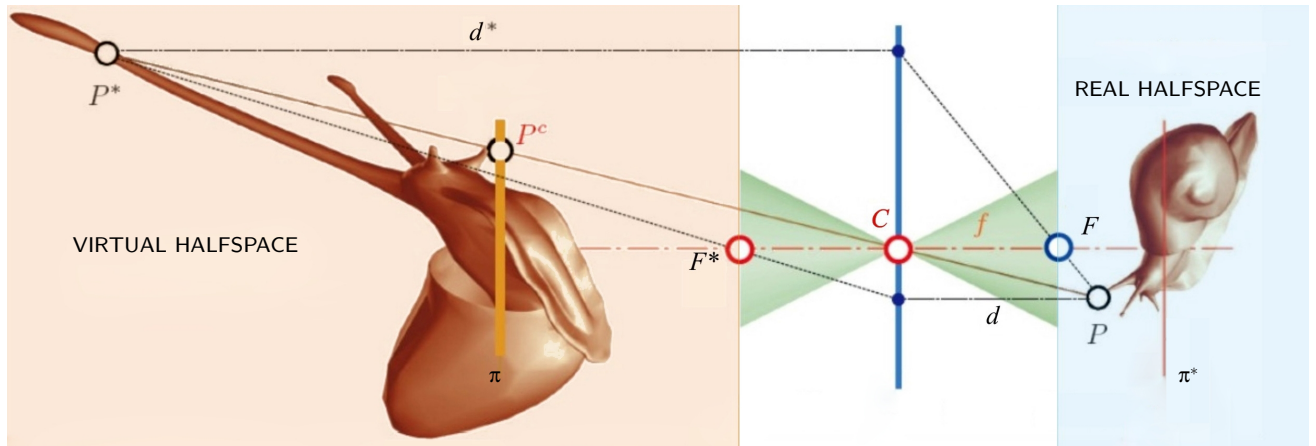
Figure 4: *When a small object close to the lens is being photographed, the 3D distortion of the corresponding virtual image is considerable. Only points in the focal plane $\pi^*$ will therefore be depicted in sharp focus.*
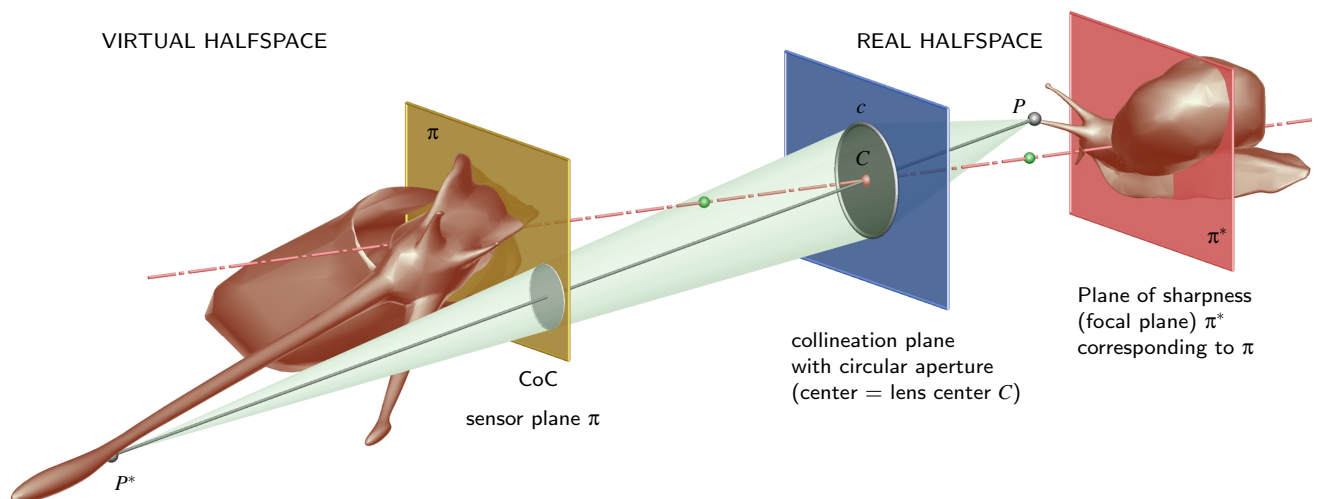


Figure 5: *The* Circle of Confusion *(CoC) in the sensor plane $\pi$ can be interpreted as the intersection of an oblique cone passing through the circular aperture opening c.*

Figure 6: *Two mating dragon flies, photographed several times with varying lens centers (and focal points). The first and the last photo of the series can be seen on the left. The focus-stacked image on the right can be considered sharp in the zone that is defined by the two animals. The background still remains blurred, which is – aesthetically speaking – a big advantage. Thus, focus stacking can also be considered as an artistic tool.*

small amount of high frequencies, then the image is blurry (e.g., [4]).

In a second step, *one* sharp image is created from this entire image series. How well this works even without a tripod is shown in Figure 6: on the left, we see the first and the last picture of such a series by way of example; on the right, we see the final product.[4]

If the photo series is done without tripod, there is of course a slight movement of the camera to be expected between the single photos. There even might be a tilt and/or motion blur. In [5], solutions for these problems are proposed that are based on affine transformations of the images.

There is an interesting connection to "light field cameras" that capture information about the light field emanating from a scene (conventional cameras only record light intensity).

One type of light field camera uses an array of micro-lenses placed in front of an otherwise conventional image sensor to sense intensity, color, and directional information. Multi-camera arrays are another type of light field camera. Holograms are a type of film-based light field image.

## 9    The focal plane sweeps through the object

For any position of the sensor plane (distance $d^*$), there is thus exactly one plane of sharpness (distance $d$) in the Gaussian collineation; its position follows from the lens formula (1):

$$d = fd^*/(d^* - f). \qquad (6)$$

### 9.1    Focus stacking with a microscope

Before we continue with "ordinary photography" (especially macro photography), let us take a quick look at "micro photography", i.e., taking pictures by means of a microscope (Figure 7). Here, the Depth of Field (DoF) is extremely shallow. When we use focus stacking, we sweep the focal plane in tiny steps. In contrast to classic photography, however, the entire lens system – including the sensor plane – is just translated. Thus, the distance of the lens center to the sensor plane stays constant during the sweeping process.

As a consequence, we do not have to care about relative scaling of the corresponding images. In principle, we get section lines of our object and we even know

---

[4]An additional advantage of this method is the fact that we usually do not get an "infinitely" sharp image, but that there is a certain layer rendered in sharp focus. Blurry backgrounds facilitate the isolation of objects from the background and prevent the viewer's gaze from getting caught in unnecessary details.

the accurate distance of these section lines: the translation of either the lens system or the object carrier respectively. Therefore, the scanned object is completely recognized three-dimensionally (see Figure 8; the microscopic photos show salt crystals and were taken by Johannes Weber, University of Applied Arts Vienna).



Figure 7: *When the focal plane of a microscope sweeps through the object, this is equivalent to a perfectly controlled translation of the object along the optical axis. The single pictures do not have to be registered – they are all scaled in the same manner.*
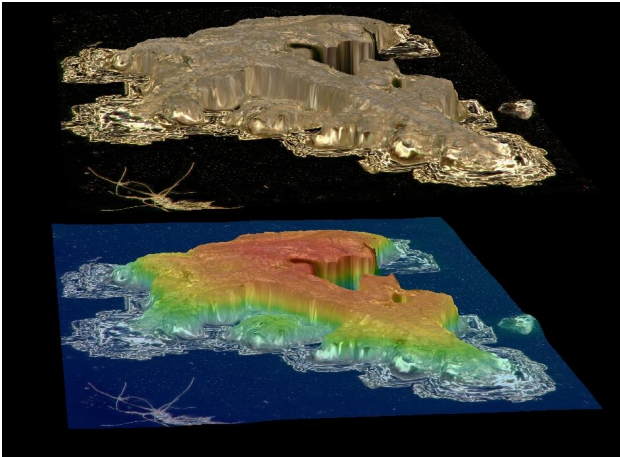


Figure 8: *Having control of all coordinates, the object is well-determined and can be displayed and measured arbitrarily.*

## 9.2   Focus stacking with a normal camera

In contrast to focus-stacked pictures taken by a microscope, focus stacking is a bit more complicated in ordinary photography: In commercially available cameras, the position of the sensor plane is fixed and the position of the lens center $C$ moves forward and backward on the optical

axis. If we focus on points that are very far away, $C$ lies in front of the sensor plane at a distance $f$ (if $d^* = f$ then $d = \infty$). If we photograph a two-dimensional shape – such as, for instance, a drawing – that lies in a plane parallel to the sensor plane at a distance of $s = d + d^*$ and focus it, the center $C$ will have the position at a distance $d^*$ from the sensor plane that we want to calculate.

With the formula (6), the following applies:

$$s = d^{*2}/(d^* - f) \quad \text{or} \quad d^{*2} - sd^* + sf = 0 \tag{7}$$

The ambiguous solution of this quadratic equation is

$$d^* = \frac{s}{2} \pm \sqrt{\frac{s^2}{4} - sf}.$$

In order for the expression below the root not to be negative, $s \geq 4f$ must apply. This is, indeed, always the case because of the requirement $d > f$ (if $d = d^* = 2f$, the solutions coincide). Furthermore, both solutions are always valid, even though one would – for practical reasons – tend to stick to *one* algebraic sign when computing a series of camera positions.
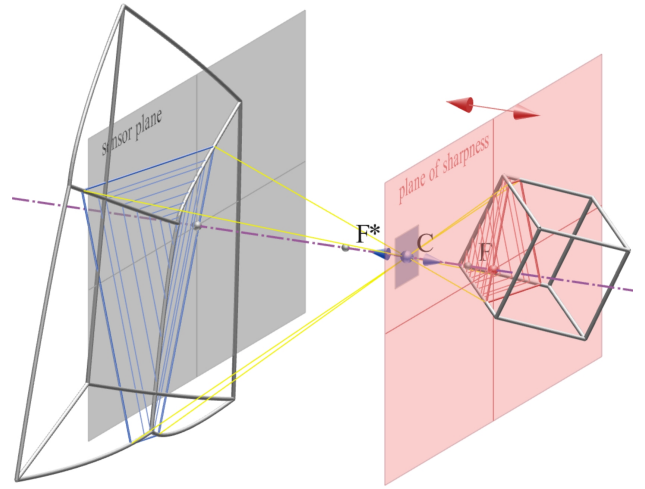


Figure 9: *When the center C of the lens system (and therefore also the focal point F ) is moving along the optical axis (with fixed sensor plane π), the plane of sharpness which corresponds to the sensor plane is moving in parallel. Its intersection lines with the spatial object are depicted in sharp focus, but in an absolute size that depends on the distance $\overline{C\pi}$.*

If the lens system lies within the computed distance $d^*$ in front of the fixed sensor plane $\pi$, our two-dimensional shape will firstly be rendered sharp overall on the sensor, and secondly, it will appear *similar*, and thus perspectively undistorted, even though it will not keep its original size.
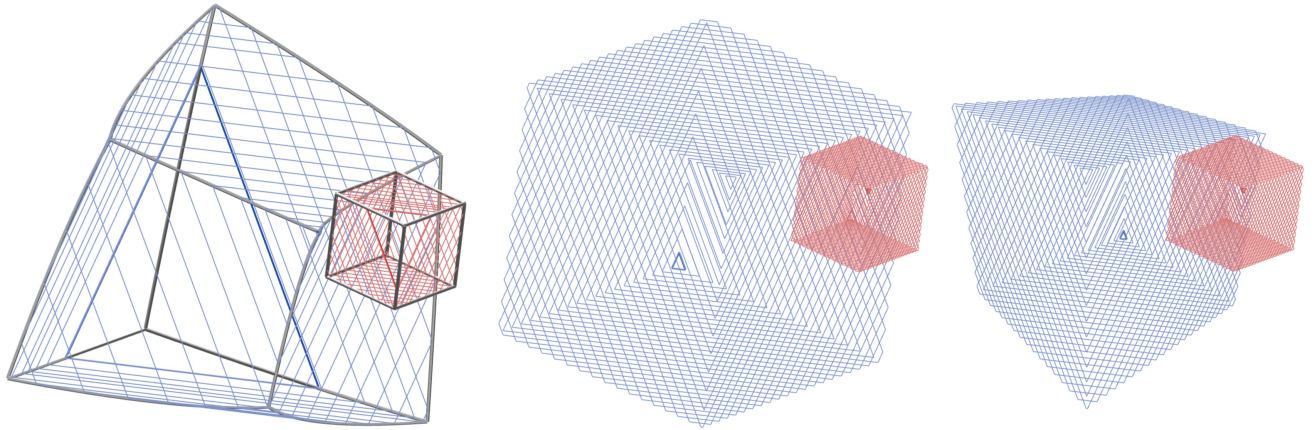
Figure 10: *A spatial object (in this case a red cube) is "scanned" by a "sweeping focal plane." Only the intersections with the plane are depicted in the sensor plane. If the corresponding images of the section are not scaled, the result is neither a central nor a normal projection (image on the left). Scaled with the factor in Equation 8, the image is a normal projection (middle image); scaled with the factor in Equation 9 as in the image to the right, the result is a perfect central projection (= "perspective".) In the latter case, the center of the perspective can vary almost arbitrarily.*

Let us now turn back to three-dimensional objects. If we take a series of photographs while purposefully varying the distance of the lens center, we will get photographs in which one section line of the object is rendered sharp *and largely undistorted* (it is merely scaled.)

Figure 9 illustrates this matter: in a simulation of this process, a cube was mapped by way of layers, which can be triangles, quadrangles, pentagons or hexagons. However, if we now simply put these pictures on top of one another, we will end up with strangely distorted perspectives (see also Figure 10 on the left).

Straight lines – such as the edges of the cube – are depicted as curved (it is possible to show that they form parabolas.) The reason for this is of course that, owing to the different distance of the lens center from the sensor plane, the section lines are scaled proportionately to this distance.

## 10 Converting the scanning process into normal and central projections

Strictly speaking, we scanned our object three-dimensionally in this way – even though we must bear in mind that only those section lines were recorded that were visible from the respective center. Let us now conduct some skilful scaling, in order to compute the relations in the visible three-dimensional real space during the scanning process.

Let $t$ be a line segment in the plane of sharpness, and thus in space, and $t^*$ the line segment parallel to it in the sensor plane $\pi$. According to the intercept theorems, the following applies: $t : d = t^* : d^*$. With the scaling factor

$$\lambda = d/d^*, \tag{8}$$

we can thus calculate the genuine length $t$ from the image length. If we scale all pictures of the series, with the factor changing from one picture to another, we get a *normal projection* of the object (see Figure 10, middle). This is remarkable insofar as it is *impossible* to achieve a normal projection with a single photograph, except if we used an astronomical telescope with an almost infinite focal length.[5]

In order to achieve an exact central projection (perspective), which exclusively relies on unambiguously recorded points, we will choose a position as the center where the lens center used to be when the last still visible points of the object to be depicted appeared sharp ($d = d_m$ maximal $\Rightarrow d^* = d_m^*$ minimal). The $i$th picture will then not only be scaled according to the formula (8), with the factor $\lambda_i = d_i/d_i^*$, but additionally with the factor $d_m^*/d_m$: If we now feed the image series into a software designed to recognize sharp pixels, we will get a picture of graphical precision that is sharp and perspectively correct, as can be seen in Figure 10 on the right.

$$\mu = \frac{d_i}{d_i^*} \cdot \frac{d_m^*}{d_m} \tag{9}$$

---

[5]There is, however, one limitation: even from a number of positions on the optical axis, we cannot always see as much of a surface as we would in a genuine normal projection. Just think, for example, of a spaceship directly approaching the moon. From its position, we will never be able to see 50% of the moon's surface, the way we do from Earth.

Figure 11: *A square stamp of typical macro size is being focus-stacked. With the application of the corresponding scalings of the images, the result is a geometrically perfect perspective.*

The square stamp in Figure 11 passes the relatively strict geometrical tests that can be used in order to test the correctness of a perspective, and the same is true of the "geometric still life" in Figure 12. This is important because we do not usually photograph miniature geometrical figures in practice, but living beings and natural objects. Creating a *full-size* sharp photograph of the stamp would be a classic task of macro photography, while the still life is already a medium-sized scene and thus easier to photograph with a sharp focus overall.



Figure 12: *A typical geometric scene (cube, square, cylinder of revolution). From the geometric point of view, the stacked image fulfills all requirements of a single central projection.*

## 11 Outlook

Speaking from a mathematical/geometrical point of view, it is important to note that much more can be done with a series of pictures of an object, owing to the fact that these pictures provide information of the object's location in space – one example would be 3D models. In any case, focus stacking on the macro level should make it possible to achieve results that would rival those of laser scanners, if they were done under laboratory conditions – even though the technology behind it is simpler, quicker, and cheaper. Using the above described geometrical insights, methods like the ones proposed by [6] could be enhanced.



Figure 13: *Here, only three photos were stacked, allowing major parts of the praying mantis to appear sharp. The blurred rest of the stacked photo is deliberate.*

If the objects that we want to photograph happen to be small animals, we are faced with the additional problem that these seldom tend to freeze in place, and usually at least move their feelers or individual limbs (Figure 13). In such cases, the image series should be processed in the tenth of a second at the most, which will probably be possible in a few years' time, bearing in mind the rapid technological advancement in recent years. Currently, commercially available cameras still need a full half second for a complete series of 8 to 10 pictures – the bottleneck does not occur when saving the pictures but is a result of the continuous re-adjustment of the focus. In order to depict as many parts of the object's surface as possible, and also for additional accuracy, one could use several rigidly

connected cameras simultaneously. The registration of the surface parts should easily be possible since all camera positions are well known.

From an aesthetic point of view, we often only need two or tree pictures of an insect for impressive photographs. In Figure 13, it was important to focus on the tongs and eyes of the praying mantis – it is secondary that the rest of its body appears blurred.

# References

[1] G. GLAESER, 3D-Images in Photography?, *J. Geom. Graph.* **13** (1) (2009), 113–120.

[2] P. W. HAWKES, E. KASPER, *Principles of Electron Optics*, Volume 1: Basic Geometrical Optics (2nd edition), Academic Press (2018), 256–257.

[3] N. NEVEROVA, N. H. KONIK, Edge-based method for sharp region extraction from low depth of field images, *Visual Communications and Image Processing* (2012), 1–6.

[4] L. RENTING ET AL., Image partial blur detection and classification, *IEEE Conference on Computer Vision and Pattern Recognition*, (2008).

[5] C. ZHANG ET AL., Extended depth-of-field via focus stacking and graph cuts, *IEEE International Conference on Image Processing* (2013).

[6] G. KONTOGIANNI ET AL., Enhancing Close-up Image Based 3D Digitisation with Focus Stacking. *International Archives of the Photogrammetry, Remote Sensing & Spatial Information Sciences* **42** (2017).

**Georg Glaeser**
e-mail: georg.glaeser@uni-ak.ac.at

Department of Geometry
University of Applied Arts Vienna
Oskar Kokoschka-Platz 2, A-1010 Vienna, Austria

VLADIMIR VOLENEC
EMA JURKIN
MARIJA ŠIMIĆ HORVATH

# Covertex Inscribed Triangles of Parabola in Isotropic Plane

**Covertex Inscribed Triangles of Parabola in Isotropic Plane**

**ABSTRACT**

In the paper the concept of a covertex inscribed triangle of a parabola in an isotropic plane is introduced. It is a triangle inscribed to the parabola that has the centroid on the axis of parabola, i.e. whose circumcircle passes through the vertex of the parabola. We determine the coordinates of the triangle centers, and the equations of the lines, circles and conics related to the triangle.

**Key words:** isotropic plane, triangle, parabola

**MSC2010:** 51N25

**Covertex trokuti upisani paraboli u izotropnoj ravnini**

**SAŽETAK**

U radu se uvodi pojam covertex trokuta upisanog paraboli u izotropnoj ravnini. To je trokut upisan paraboli čije težište leži na osi parabole, tj. čija opisana kružnica prolazi tjemenom parabole. Određuju se koordinate točaka te jednadžbe pravaca, kružnica i konika povezanih s tim trokutom.

**Ključne riječi:** izotropna ravnina, trokut, parabola

## 1 Motivation

The following theorem, which can be found in [10], is a well-known fact from the geometry of Euclidean plane:
*Let $A, B, C$ be three points on a parabola $\mathcal{P}$ different from its vertex and different mutually. These are the equivalent statements:*

$1^0$ *The normal lines to $\mathcal{P}$ at $A, B, C$ are concurrent.*

$2^0$ *The centroid of the triangle $ABC$ lies on the axis of parabola $\mathcal{P}$.*

$3^0$ *The circumcircle of the triangle $ABC$ passes through the vertex of parabola $\mathcal{P}$.*

The perpendicularity is not defined in the isotropic plane, and often an isotropic line plays a role of a line perpendicular to a given one. Therefore, every normal to $\mathcal{P}$ passes through the absolute point. From that point of view, the property $1^0$ is fulfilled for any three points on the parabola, and it is interesting to study the triangles having properties $2^0$ and $3^0$.

The result above together with other results stated in [10] inspired the authors to write this paper.

## 2 Introduction

Let us start by recalling some basic facts about the isotropic plane. The isotropic plane is a real projective metric plane whose absolute figure is a pair consisting of an *absolute point* $\Omega$ and an *absolute line* $\omega$ incident to it, [11], [12]. The *isotropic points* are the points incident with the absolute line $\omega$ and the *isotropic lines* are the lines passing through the absolute point $\Omega$.

In the affine model of the isotropic plane where the coordinates of the points are defined by $x = \frac{x_0}{x_2}$, $y = \frac{x_1}{x_2}$, the absolute line has the equation $x_2 = 0$ and the absolute point has the coordinates $(0 : 1 : 0)$.

Two lines are *parallel* if they pass through the same isotropic point, and two points are *parallel* if they are incident with the same isotropic line. For two non-parallel points $A = (x_A, y_A)$ and $B = (x_B, y_B)$, a *distance* is defined

by $d(A,B) = x_B - x_A$, and for two parallel points, $x_A = x_B$, a *span* is defined by $s(A,B) = y_B - y_A$. For two non-parallel lines $p$ and $q$, given by the equations $y = k_p x + l_p$ and $y = k_q x + l_q$, an *angle* is defined by $\angle(p,q) = k_q - k_p$. All these quantities are oriented.

A triangle in the isotropic plane is called *allowable* if non of its sides is an isotropic line. In our study only such triangles are considered.

The midpoint of the points $A$ and $B$ is defined as $M = \left(\frac{x_A + x_B}{2}, \frac{y_A + y_B}{2}\right)$, while the bisector of the lines $p$ and $q$ is given by the equation $y = \frac{k_p + k_q}{2} x + \frac{l_p + l_q}{2}$.

A *normal line* to a line $l$ at a point $P$ is the isotropic line $n$ passing through $P$. A distance from $P$ to $l$ is defined as the span $s(N,P)$, where $N$ is the intersection point of $l$ and $n$, i.e. the point on $l$ parallel to $P$.

The classification of conics in the isotropic plane can be found in [2] and [11]. A *circle* is a conic touching the absolute line $\omega$ at the absolute point $\Omega$. The equation of such a circle is given by

$$y = ux^2 + vx + w, \quad u \neq 0, \quad u,v,w \in \mathbb{R}.$$

A *parabola* is a conic touching the absolute line at a point different from the absolute point. By choosing a suitable coordinate system every parabola can be represented by the equation

$$y^2 = x. \tag{1}$$

It has vertex (focus) at $O = (0,0)$, the $x$-axis as its axis, and $y$-axis as its directrix. A numerous properties of parabola were discussed in [13], [15] and [19].

## 3 Covertex Inscribed Triangles of Parabola

Let $A = (a^2, a), B = (b^2, b), C = (c^2, c)$ be three points on the parabola $\mathcal{P}$ given by (1) different from its vertex and different mutually. Thus, $a$, $b$, $c$ are mutually different nonzero real numbers. It can be easily checked that $A, B, C$ lie on the circle $\mathcal{C}$ with equation

$$(a+b)(b+c)(c+a)y = \tag{2}$$
$$-x^2 + (a^2 + b^2 + c^2 + ab + bc + ca)x + abc(a+b+c).$$

The circle $\mathcal{C}$ passes through the vertex $O = (0,0)$ precisely when

$$a + b + c = 0. \tag{3}$$

In that case the centroid $G = \left(\frac{a^2+b^2+c^2}{3}, \frac{a+b+c}{3}\right)$ of the triangle $ABC$ lies on the axis of the parabola $\mathcal{P}$, and we proved:

**Theorem 1** *A triangle inscribed to a parabola has the centroid on the axis of parabola if and only if its circumcircle passes through the vertex of parabola.*
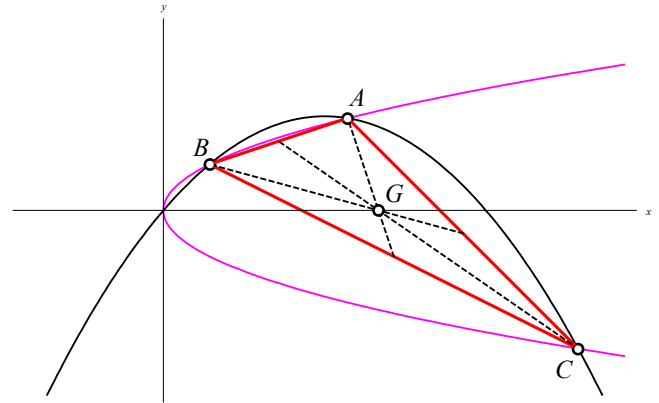


Figure 1: *Covertex inscribed triangle of a parabola*

The triangles having the property from Theorem 1 are called the *covertex inscribed triangles* of the parabola. If such a triangle $ABC$ has vertices $A = (a^2, a)$, $B = (b^2, b)$, $C = (c^2, c)$, the equations of its sides are:

$$\begin{aligned}
AB & \quad \dots \quad x + cy + ab = 0, \\
BC & \quad \dots \quad x + ay + bc = 0, \\
CA & \quad \dots \quad x + by + ca = 0.
\end{aligned} \tag{4}$$

Considering (3) we will use the standard notation:

$$p = abc, \quad q = ab + bc + ca. \tag{5}$$

The following relations are interesting, useful and their validity can easily be proved:

$$\begin{aligned}
a^2 &= bc - q, \\
a^3 &= p - aq, \\
a^2 + b^2 + c^2 &= -2q, \\
a^2b^2 + b^2c^2 + c^2a^2 &= q^2, \\
a^4 + b^4 + c^4 &= 2q^2.
\end{aligned}$$

The equation (2) of the circumcircle $\mathcal{C}$ of $ABC$ now takes the form

$$py = x^2 + qx, \tag{6}$$

the centroid is $G = \left(-\frac{2}{3}q, 0\right)$, and the Euler line has the equation $x = -\frac{2}{3}q$, [6].

The properties of an allowable triangle in the isotropic plane have been studied in numerous papers, [3], [4], [5], [6], [7], [8], [14], [16], [18]. The observed triangle was settled in the standard position having the circumcircle with the equation $y = x^2$ and the vertices of the form $A = (a, a^2)$, $B = (b, b^2), C = (c, c^2)$, where $a + b + c = 0$. The same notations $p = abc$, $q = ab + bc + ca$ were used as well. Therefore, it is not of our interest to prove the theorems on the

special case of covertex inscribed triangles of parabola. Instead we determine the coordinates of the triangle centers, and the equations of the lines, circles and conics related to the triangles.

The midpoint $A_m$ of the points $B$ and $C$ has the coordinates $A_m = \left(-q - \frac{1}{2}a^2, -\frac{1}{2}a\right)$ and lies on the circle with the equation

$$py = -2x^2 - 3qx - q^2. \tag{7}$$

Indeed,

$$-2\left(q + \frac{1}{2}a^2\right)^2 + 3q\left(q + \frac{1}{2}a^2\right) - q^2$$
$$= -\frac{1}{2}a^4 - \frac{1}{2}a^2q = -\frac{1}{2}a\left(a^3 + qa\right) = -\frac{1}{2}ap.$$

It can be proved similarly that the midpoints $B_m$, $C_m$ of the sides $AC$, $AB$, respectively, also lie on the circle given by (7). Thus, that circle is the *Euler circle* of the triangle $ABC$. Let us now prove that the circle having the equation

$$4py = x^2 \tag{8}$$

is the *inscribed circle* of the triangle $ABC$. The line $BC$ has the equation $x + ay + bc = 0$ given in (4). The intersection point of $BC$ and the circle (8) is the point $D = \left(-2bc, \frac{bc}{a}\right)$ having the intersection multiplicity 2. Therefore, $D$ is the contact point of $BC$ and (8). In the similar way, it can be shown that the lines $CA$ and $AB$ also touch the circle given by (8).

The inscribed circle and Euler circle of a triangle touch each other externally in a point called *Feuerbach point*, and their common tangent is called the *Feuerbach line* of the considered triangle, [1]. So, we prove:

**Theorem 2** *The Feuerbach point of the covertex inscribed triangle ABC of the parabola $\mathcal{P}$ is*

$$\Phi = \left(-\frac{2}{3}q, \frac{1}{9p}q^2\right) \tag{9}$$

*and its Feuerbach line is given by the equation*

$$3qx + 9py + q^2 = 0. \tag{10}$$

**Proof.** By eliminating $y$ in (7) and (8), the equation $9x^2 + 12qx + 4q^2 = 0$ with double root $x = -\frac{2}{3}q$ is obtained. From (8) we get $y = \frac{1}{9p}q^2$. The radical axis of the inscribed circle and Euler circle is obtained by eliminating the terms next to $x^2$ in (7) and (8). Thus, the line having the equation $3qx + 9py + q^2 = 0$ is their common tangent. □

In the isotropic plane the principle of projective duality is preserved. The dual of the triangle inscribed circle is its circumcircle, while the dual of the Euler circle is the circle inscribed to the triangle formed by angle bisectors of

the considered triangle, [7]. The circumscribed circle and the dual Euler circle of the triangle touch each other at one point, so-called *dual Feuerbach point*, and their common tangent is called *dual Feuerbach line*.

**Theorem 3** *The dual Feuerbach point of the covertex inscribed triangle ABC of the parabola $\mathcal{P}$ is*

$$\Phi' = \left(-\frac{2}{3}q, -\frac{2}{9p}q^2\right) \tag{11}$$

*and its dual Feuerbach line is given by the equation*

$$3qx + 9py + 4q^2 = 0. \tag{12}$$

**Proof.** The equations of the sides $CA$, $AB$ from (4) can be written in the form $cx + bcy + ac^2 = 0$, $bx + bcy + ab^2 = 0$, and their angle bisector has equation $-ax + 2bcy + a(b^2 + c^2) = 0$, which because of $-b^2 - c^2 = q + bc$, and after multiplying by $a$, turns to $2py = a^2x + a^2q + ap$. By eliminating the terms next to $x^2$ in this equation and in the equation of the circle

$$8py = -x^2 - 4qx - 4q^2 \tag{13}$$

we obtain the equation $x^2 + 4(a^2 + q)x + 4(a^2q + q^2 + ap) = 0$. Because of

$$a^2q + q^2 + ap = bcq + a^2bc = b^2c^2,$$

it turns to the equation $x^2 + 4bcx + 4b^2c^2 = 0$ having a double root. Therefore, the observed angle bisector touches the circle (13). The same fact holds for the other two angle bisectors of the triangle $ABC$ as well. Thus, (13) is the equation of the dual Euler circle of $ABC$. Now by eliminating $y$ in (6) and (13) we get equation $9x^2 + 12qx + 4q^2 = 0$ with a double root $x = -\frac{2}{3}q$. Hence, the point $\left(-\frac{2}{3}q, -\frac{1}{9p}q^2\right)$ is their contact point. By eliminating the terms next to $x^2$ in (6) and (13), the equation (12) of their radical axis is obtained. □

The *orthic axis* of the triangle is the radical axis of a pencil of circles consisting of some important circles of that triangle as the circumcircle, Euler circle and polar circle, see [1] and [14].

**Theorem 4** *The orthic axis of the covertex inscribed triangle ABC of the parabola $\mathcal{P}$ is given by the equation*

$$qx + 3py + q^2 = 0. \tag{14}$$

**Proof.** By eliminating the terms next to $x^2$ in the equations (6) and (7) of the circumcircle and Euler circle of the triangle $ABC$, the equation (14) of their radical axis is obtained. □

**Theorem 5** *The polar circle of the covertex inscribed triangle ABC of the parabola $\mathcal{P}$ has the equation*

$$2py = -x^2 - 2qx - q^2. \tag{15}$$

**Proof.** The polar of the point $(u,v)$ with respect to the circle (15) has the equation $p(y+v) = -xu - q(x+u) - q^2$. Therefore, the polar of $A = (a^2,a)$ has the equation $py + (q+a^2)x + (q+a^2)q + ap = 0$, i.e. $py + bcx + bc(q+a^2) = 0$, and finally $x + ay + bc = 0$ being the equation of the side $BC$. Similarly we get that the polars of $B$ and $C$ are the sides $CA$ and $AB$, respectively. □

The circles of the pencil mentioned above intersect each other in the points having coordinates

$$(-q, 0), \quad \left(-\frac{q}{3}, -\frac{2}{3p}q^2\right).$$

This can be easily proved by using e.g. (6) and (7).

The *Gergonne point* of the triangle $ABC$ is the intersection point of three cevians $AD$, $BE$, $CF$ defined by the contact points $D$, $E$, $F$ of the inscribed circle, [3], and we have:

**Theorem 6** *The Gergonne point of the covertex inscribed triangle ABC of the parabola $\mathcal{P}$ has the coordinates*

$$\Gamma = \left(\frac{9p^2}{q^2}, -\frac{3p}{q}\right). \tag{16}$$

**Proof.** The line with the equation $qx + (3p - aq)y = 3ap$ obviously passes through the vertex $A = (a^2,a)$. It also passes through the contact point $D = \left(-2bc, \frac{bc}{a}\right)$ of the side $BC$ and the inscribed circle of the triangle $ABC$ since

$$-2bcq + 3b^2c^2 - bcq = 3bc(bc - q) = 3ap.$$

Thus, the observed line is the cevian $AD$. On the other hand, it also passes through the point $\Gamma$ given in (16). Since the analogue statements hold for the lines $BE$ and $CF$, $\Gamma$ is the Gergonne point of the triangle $ABC$. □

**Corollary 1** *The Gergonne point of the covertex inscribed triangle ABC of the parabola $\mathcal{P}$ lies on the parabola $\mathcal{P}$*

Corollary 1 together with Theorem 1 present new geometric results in the isotropic plane.
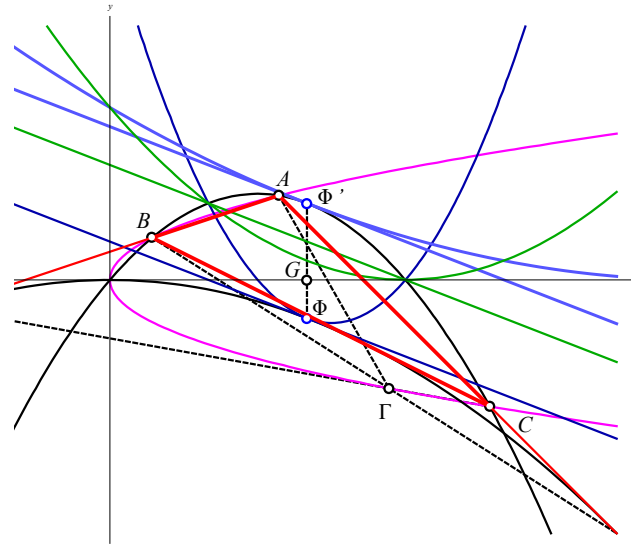


Figure 2: *The centroid G, Feuerbach point $\Phi$, dual Feuerbach point $\Phi'$ and Gergonne point $\Gamma$ of the covertex inscribed triangle ABC of a parabola*

**Theorem 7** *Every conic circumscribed to the covertex inscribed triangle ABC of the parabola $\mathcal{P}$ has the equation of the form*

$$Ax^2 + 2Bxy + Cy^2 + (qA - C)x + (2qB - pA)y - 2pB = 0, \tag{17}$$

*the axis with equation*

$$Bx + Cy + qB - \frac{1}{2}pA = 0 \tag{18}$$

*and the center with the coordinates*

$$M = \left(\frac{2qB^2 - pAB - qAC + C^2}{2(AC - B^2)}, \frac{pA^2 - qAB - BC}{2(AC - B^2)}\right). \tag{19}$$

**Proof.** Every conic is given by the equation of the form

$$Ax^2 + 2Bxy + Cy^2 + 2Dx + 2Ey + F = 0. \tag{20}$$

The points $A = (a^2,a)$ and $B = (b^2,b)$ lie on the conic precisely when the following equalities hold:

$$a^4A + 2a^3B + a^2C + 2a^2D + 2aE + F = 0,$$
$$b^4A + 2b^3B + b^2C + 2b^2D + 2bE + F = 0. \tag{21}$$

By subtracting the two upper equations and dividing by $a - b$ we get

$$(a^2 + b^2)(a+b)A + 2(a^2 + ab + b^2)B + (a+b)C$$
$$+ 2(a+b)D + 2E = 0,$$

i.e.

$$(cq+p)A - 2qB - cC - 2cD + 2E = 0 \qquad (22)$$

since

$$(a^2+b^2)(a+b) = (-q-ab)(-c) = cq+p.$$

Similarly, we get

$$(bq+p)A - 2qB - bC - 2bD + 2E = 0,$$
$$(aq+p)A - 2qB - aC - 2aD + 2E = 0.$$

It immediately follows $pA - 2qB + 2E = 0$, and from (22) also $qA - C - 2D = 0$. Thus, $2D = qA - C$ and $2E = 2qB - pA$ are valid. From (20) we get $(a^4 + a^2q - ap)A + 2(a^3+aq)B + F = 0$, and finally $F = -2pB$ since $a^3+aq = p$. We proved that the conic circumscribed to the triangle $ABC$ has to have the equation of the form (17).

The equation (20) can be written in homogeneous coordinates as follows

$$Ax_0^2 + 2Bx_0x_1 + Cx_1^2 + 2Dx_0x_2 + 2Ex_1x_2 + Fx_2^2 = 0,$$

and the point $(u_0 : u_1 : u_2)$ has the polar with the equation

$$Au_0x_0 + B(u_1x_0 + u_0x_1) + Cu_1x_1 + D(u_0x_2 + u_2x_0)$$
$$+ E(u_1x_2 + u_2x_1) + Fu_2x_2 = 0. \qquad (23)$$

Particularly, the polar of the absolute point $\Omega = (0 : 1 : 0)$ is given by the equation $Bx_0 + Cx_1 + Ex_2 = 0$, i.e. in affine coordinates $Bx + Cy + E = 0$. Thus, when the conic is given by the equation (17), its axis is given by the equation (18). The equation (23) written in the form

$$(Au_0 + Bu_1 + Du_2)x_0 + (Bu_0 + Cu_1 + Eu_2)x_1$$
$$+ (Du_0 + Eu_1 + Fu_2)x_2 = 0$$

is the equation of the absolute line $x_2 = 0$ precisely when $Au_0 + Bu_1 + Du_2 = 0$ and $Bu_0 + Cu_1 + Eu_2 = 0$. Therefore, the coordinates of the point $M = \left(\frac{u_0}{u_2}, \frac{u_1}{u_2}\right) = (u,v)$ have to satisfy the equations $Au + Bv + D = 0$ and $Bu + Cv + E = 0$, which leads to

$$M = \left(\frac{BE-CD}{AC-B^2}, \frac{BD-AE}{AC-B^2}\right).$$

So, when the conic is given by (17), its center is given by (19). $\qquad \square$

The properties of the *Steiner ellipse*, *Steiner axis* and *Steiner point* of a triangle in the isotropic plane were studied in details in [8] and [18]. Here we prove the following two theorems:

**Theorem 8** *The Steiner ellipse of the covertex inscribed triangle ABC of the parabola $\mathcal{P}$ has the equation*

$$3qx^2 + 9pxy - q^2y^2 + 4q^2x + 6pqy - 9p^2 = 0, \qquad (24)$$

*while the Steiner axis is given by*

$$9px - 2q^2y + 6pq = 0. \qquad (25)$$

**Proof.** By inserting $A = 3q$, $B = \frac{9}{2}p$, $C = -q^2$ into (17), (18), (19), the circumscribed conic (24) with the axis (25) and the center $M = \left(-\frac{2}{3}, 0\right)$ is obtained. The point $M$ is the centroid $G$ of the triangle $ABC$, and therefore (24) is the equation of the Steiner ellipse. $\qquad \square$

**Theorem 9** *The Steiner point of the covertex inscribed triangle ABC of the parabola $\mathcal{P}$ has the coordinates*

$$S = \left(\frac{9p^2}{q^2}, \frac{81p^3}{q^4} + \frac{9p}{q}\right). \qquad (26)$$

**Proof.** The coordinates of the point $S$ satisfy the equations (6) and (24). So, it is the intersection of the circumcircle and the Steiner ellipse of the triangle $ABC$. $\qquad \square$

The isogonal conjugate $P'$ of a point $P$ with respect to triangle $ABC$ is constructed by reflecting the lines $AP$, $BP$, $CP$ about the angle bisectors at the points $A$, $B$, $C$, respectively. The three reflected lines then concur at the isogonal conjugate $P'$. The isogonality in the isotropic plane was studied in [9].

**Theorem 10** *The isogonal point $P' = (x', y')$ of the point $P = (x,y)$ with respect to the covertex inscribed triangle ABC of the parabola $\mathcal{P}$ has the coordinates*

$$x' = -\frac{qx^2 + pxy + q^2x - p^2}{x^2 + qx - py},$$
$$y' = \frac{qxy + py^2 - px + q^2y - pq}{x^2 + qx - py}. \qquad (27)$$

**Proof.** If a point $P = (u,v)$ is given, then the slope of the line $AP$ equals to $k = \frac{v-a}{u-a^2}$. The line isogonal to the line $AP$ with respect to the lines $AB$ and $AC$ with slopes $-\frac{1}{c}$ and $-\frac{1}{b}$, respectively, has the slope

$$-\frac{1}{c} - \frac{1}{b} - k = \frac{a}{bc} - \frac{v-a}{u-a^2} = \frac{au - bcv + aq}{bcu - ap}.$$

and the equation

$$(bcv - au - aq)x + (bcu - ap)y = aqu + apv - a^2p - a^3q. \qquad (28)$$

Similarly, the line isogonal to the line $BP$ with respect to the lines $BC$ and $BA$ has the equation

$$(cav - bu - bq)x + (cau - bp)y = bqu + bpv - b^2p - b^3q. \qquad (29)$$

By subtracting (28) and (29) and then dividing by $a - b$ we get

$$(cv + u + q)x + (cu + p)y = -qu - pv - cp - q^2.$$

So, we conclude that the following two equalities have to hold

$$(u + q)x + py = -qu - pv - q^2, \quad vx + uy = -p.$$

Solving the system of equations, we get

$$x = -\frac{qu^2 + puv + q^2u - p^2}{u^2 + qu - pv}, y = \frac{quv + pv^2 - pu + q^2v - pq}{u^2 + qu - pv},$$

which finishes the proof. □

The symmedian center $K$ is the isogonal conjugate of the triangle centroid $G$. Therefore we have:

**Theorem 11** *The symmedian center $K$ of the covertex inscribed triangle $ABC$ of the parabola $\mathcal{P}$ has the coordinates*

$$K = \left( -\frac{2q^3 + 9p^2}{2q^2}, \frac{3p}{2q} \right) \tag{30}$$

*and the Brocard diameter is given by*

$$x = -\frac{2q^3 + 9p^2}{2q^2}.$$

**Proof.** The claim follows from (27) after inserting $x = -\frac{2}{3}q$, $y = 0$. □

**Theorem 12** *The isogonal image of the isotropic line $x' = m$ with respect to the covertex inscribed triangle $ABC$ of the parabola $\mathcal{P}$ is a special hyperbola circumscribed to $ABC$ having equation*

$$(q + m)x^2 + pxy + q(q + m)x - mpy - p^2 = 0. \tag{31}$$

**Proof.** It follows directly from the first equation in (27). □

The isogonal image of the Euler line, so-called *Jeřabek hyperbola*, and the isogonal image of the Brocard diameter, so-called *Kiepert hyperbola*, in the case of standard triangle were studied in detailed in [5] and [16]. Here we prove

**Theorem 13** *The Jeřabek hyperbola of the covertex inscribed triangle $ABC$ of the parabola $\mathcal{P}$ is given by*

$$qx^2 + 3pxy + q^2x + 2pqy - 3p^2 = 0, \tag{32}$$

*while its Kiepert hyperbola is given by*

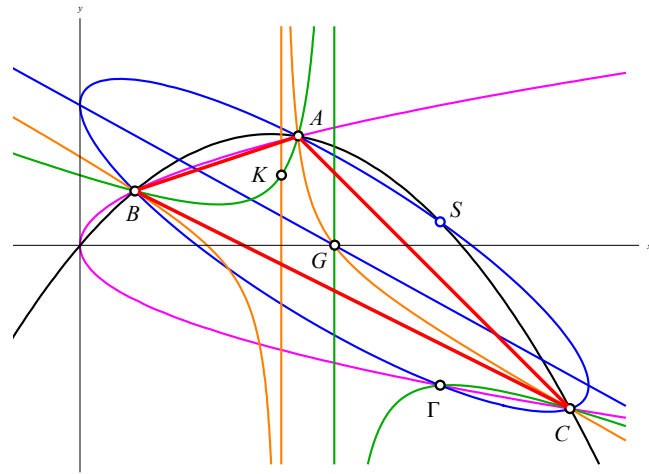$$9px^2 - 2q^2xy + 9pqx - (2q^3 + 9p^2)y + 2pq^2 = 0. \tag{33}$$



Figure 3: *The centroid G, symmedian center K and Steiner point S of the covertex inscribed triangle ABC of a parabola. The Steiner axis and Steiner ellipse are marked in blue, the Euler line and Jeřabek hyperbola are marked in green, while the Brocard diameter and Kiepert hyperbola are marked in orange.*

**Proof.** The equations (32) and (33) follow directly from Theorem 12 by inserting $m = -\frac{2}{3}q$ and $m = -\frac{2q^3 + 9p^2}{2q^2}$ into (31) for the Euler line and Brocard diameter, respectively. □

The concept of reciprocity with respect to the standard triangle in the isotropic plane was introduced and studied in [17]. Here we prove the following theorem:

**Theorem 14** *The lines given by the equations*

$$Ux + Vy + W = 0 \tag{34}$$

*and*

$$U'x + V'y + W' = 0, \tag{35}$$

*where*

$$U' = qU^2 + V^2 - UW, \qquad V' = pU^2 - VW,$$
$$W' = q^2U^2 + qV^2 + W^2 - pUV - 2qUW, \tag{36}$$

*are reciprocal lines with respect to the covertex inscribed triangle $ABC$ of the parabola $\mathcal{P}$.*

**Proof.** Let the line having the equation (34) be given. The points

$$D = \left( \frac{bcV - aW}{aU - V}, \frac{W - bcU}{aU - V} \right),$$
$$D' = \left( \frac{qV + aW - aqU - pU}{aU - V}, \frac{qU + aV - W}{aU - V} \right) \tag{37}$$

lie on the line $BC$ given by $x + ay + bc = 0$, and they are isotomic conjugate since they have the same midpoint as the points $B$ and $C$. Indeed,

$$\frac{bcV - aW}{aU - V} + \frac{qV + aW - aqU - pU}{aU - V} = -q - bc = b^2 + c^2,$$

$$\frac{W - bcU}{aU - V} + \frac{qU + aV - W}{aU - V} = -a = b + c.$$

The point $D$ obviously lies on the line (34), and point $D'$ on the line (35). Thus, the lines (34) and (35) intersect the line $BC$ in the isotomic conjugate points of the side $BC$. The similar claims can be proved for the sides $AB$ and $CA$ as well. Therefore, the lines (34) and (35) are reciprocal with respect to the triangle $ABC$. □

Using Theorem 14 it can be easily shown that the orthic axis of the triangle $ABC$ is reciprocal to its Steiner axis, while the Euler line of the triangle is reciprocal to its Feuerbach line.

The concepts of equicevian points and equiangular lines of the triangle in the isotropic plane were studied in [4] where a number of their significant properties was considered. A point $P$ such that the points $D = AP \cap BC$, $E = BP \cap CA$, $F = CP \cap AB$ satisfy the equalities

$$d(A, D) = d(B, E) = d(C, F) = t^2, \quad t \neq 0, \qquad (38)$$

is called the *equicevian point* of the triangle $ABC$. It is known that each allowable triangle in the isotropic plane has two equicevian points.

**Theorem 15** *The equicevian points of the covertex inscribed triangle ABC of the parabola $\mathcal{P}$ are of the form*

$$P = \left( \frac{2}{3}(t^2 - q), \frac{3p}{t^2} \right), \qquad (39)$$

*where $t^2 = \pm q$.*

**Proof.** Let us look for a point $P$ such that (38) is fulfilled. The abscissa of the point $D$ equals $a^2 + t^2$, and the equality

$$\frac{d(B, D)}{d(C, D)} = \frac{t^2 + a^2 - b^2}{t^2 + a^2 - c^2}$$

follows. Similarly we get

$$\frac{d(C, E)}{d(A, E)} = \frac{t^2 + b^2 - c^2}{t^2 + b^2 - a^2}, \quad \frac{d(A, F)}{d(B, F)} = \frac{t^2 + c^2 - a^2}{t^2 + c^2 - b^2}.$$

According to Ceva's theorem, which also holds in the isotropic plane, the lines $AD$, $BE$ and $CF$ pass through the point $P$ if and only if $d(B, D)d(C, E)d(A, F) + d(C, D)d(A, E)d(B, F) = 0$, i.e.

$$(t^2 + a^2 - b^2)(t^2 + b^2 - c^2)(t^2 + c^2 - a^2)$$
$$+ (t^2 + a^2 - c^2)(t^2 + b^2 - a^2)(t^2 + c^2 - b^2) = 0,$$

which holds precisely when

$$2t^6 + 2t^2 \left( b^2 c^2 + c^2 a^2 + a^2 b^2 - a^4 - b^4 - c^4 \right) = 0,$$

i.e.

$$2t^6 - 2q^2 t^2 = 0.$$

As $t \neq 0$, it has to be $t^4 - q^2 = 0$, which leads to $t^2 = \pm q$. The line $BC$ has the equation $y = -\frac{1}{a}x - \frac{bc}{a}$, so the ordinate of the point $D$ equals $\frac{1}{a}\left(-a^2 - t^2 - bc\right) = \frac{1}{a}\left(q - 2bc - t^2\right)$. Therefore,

$$D = \left( a^2 + t^2, \frac{1}{a}\left(q - 2bc - t^2\right) \right).$$

It can be easily checked that the coordinates of the points $A$ and $D$ satisfy the equation

$$(t^2 - 2q + 3bc)x + at^2 y = 2a^2 t^2 - 2a^2 q + 3ap.$$

Thus, that is the equation of the line $AD$. Some short calculation shows that the same line passes through the point $P = \left( \frac{2}{3}\left(t^2 - q\right), \frac{3p}{t^2} \right)$. The equivalent statements holds for the lines $BE$ and $CF$. Thus the point $P$ is equicevian point of the triangle $ABC$. □

The equicevian points of the standard triangle considered in [4] are so to say equal. It is not like that in the case of the covertex inscribed triangle of the parabola. Here the equicevian points are given by the coordinates

$$P_1 = \left( 0, \frac{3p}{q} \right), \quad P_2 = \left( -\frac{4q}{3}, -\frac{3p}{q} \right). \qquad (40)$$

They are symmetrical with respect to the centroid $G$ of the triangle and they lie on its Steiner axis. It is also known that they are the foci of its circumscribed Steiner ellipse of the triangle $ABC$, [4]. But in the case of the covertex inscribed triangle, it can be noticed that one of them, the point $P_1$, lies on the vertex tangent (directrix) of parabola $\mathcal{P}$. So, an interesting geometric fact can be stated:

**Theorem 16** *The circumscribed Steiner ellipse of the covertex inscribed triangle ABC of the parabola $\mathcal{P}$ touches the directrix of parabola $\mathcal{P}$ at one of the foci.*

A line $l$ such that the points $D' = l \cap BC$, $E' = l \cap CA$, $F' = l \cap AB$ satisfy the equalities

$$\angle(BC, AD') = \angle(CA, BE') = \angle(AB, CF') = \varphi, \quad \varphi \neq 0, \qquad (41)$$

is called the *equiangular line* of the triangle $ABC$. It was proved in [4] that each allowable triangle has two equiangular lines.

**Theorem 17** *The equiangular lines of the covertex inscribed triangle ABC of the parabola $\mathcal{P}$ have the equations*

$$qx - 3py + q^2 + \frac{9}{q}p^2 = 0, \quad qx + py + q^2 + \frac{3}{q}p^2 = 0. \quad (42)$$

**Proof.** Because of (41) the line $AD'$ has the slope $\varphi - \frac{1}{a}$, and its equation is

$$y = \left(\varphi - \frac{1}{a}\right)x + 2a - a^2\varphi. \quad (43)$$

From (43) and the equation $y = -\frac{1}{a}x - \frac{bc}{a}$ of the line $BC$ we get the coordinates of the point $D'$

$$x_{D'} = \frac{1}{a\varphi}\left(a^3\varphi - 2a^2 - bc\right),$$

$$y_{D'} = \frac{1}{a^2\varphi}\left(2a^2 + bc - a^3\varphi - p\varphi\right).$$

Analogously, we obtain the coordinates of the point $E'$

$$x_{E'} = \frac{1}{b\varphi}\left(b^3\varphi - 2b^2 - ca\right),$$

$$y_{E'} = \frac{1}{b^2\varphi}\left(2b^2 + ca - b^3\varphi - p\varphi\right).$$

Using the equalities $a + b = -c$ and $a^2 + ab + b^2 = -q$, the slope of the line $D'E'$ is calculated

$$\frac{1}{ab} \cdot \frac{a^2b^2\varphi + cp\varphi - cq}{2ab + c^2 + p\varphi} = \frac{1}{p} \cdot \frac{abp\varphi + c^2p\varphi - c^2q}{2ab + c^2 + p\varphi}.$$

Similarly, we determine the slope of the line $D'F'$

$$\frac{1}{p} \cdot \frac{acp\varphi + b^2p\varphi - b^2q}{2ac + b^2 + p\varphi}.$$

The points $D'$, $E'$ and $F'$ are collinear precisely when

$$\frac{abp\varphi + c^2p\varphi - c^2q}{2ab + c^2 + p\varphi} - \frac{acp\varphi + b^2p\varphi - b^2q}{2ac + b^2 + p\varphi} = 0,$$

which is equivalent to $p^2\varphi^2 - q^2 = 0$. Thus,

$$\varphi = \pm\frac{q}{p}.$$

Therefore, the slope of the line $D'E'$ equals

$$\frac{1}{p} \cdot \frac{\pm abq \pm c^2q - c^2q}{2ab + c^2 \pm q} = \frac{1}{p} \cdot \frac{\pm 2abq \mp q^2 - abq + q^2}{3ab - q \pm q}.$$

So, we get two lines with slopes $\frac{q}{3p}$ and $-\frac{q}{p}$. Since equiangular lines of a triangle pass through its symmedian center, [4], which is now given by (30), their equations are of the form (42). □

## References

[1] J. BEBAN-BRKIĆ, R. KOLAR-ŠUPER, V. VOLENEC, Z. KOLAR-BEGOVIĆ, On Feuerbach's Theorem and a Pencil of Circles in the Isotropic Plane, *J. Geom. Graph.* **10** (2006), 125–132.

[2] J. BEBAN-BRKIĆ, M. ŠIMIĆ, V. VOLENEC, On Foci and Asymptotes of Conics in Isotropic Plane, *Sarajevo J. Math.* **3** (**16**) (2007), 257–266.

[3] J. BEBAN-BRKIĆ, V. VOLENEC, Z. KOLAR-BEGOVIĆ, R. KOLAR-ŠUPER, On Gergonne point of the triangle in isotropic plane, *Rad Hrvat. Akad. Znan. Umjet. Mat. Znan.* **515** (2013), 95–106.

[4] Z. KOLAR-BEGOVIĆ, R. KOLAR-ŠUPER, V. VOLENEC, Equicevian points and equiangular lines of a triangle in an isotropic plane, *Sarajevo J. Math.* **11** (2015), 101–107.

[5] Z. KOLAR-BEGOVIĆ, R. KOLAR-ŠUPER, V. VOLENEC, Jeřabek Hyperbola of a Triangle in an Isotropic Plane, *KoG* **22** (2018), 12–19.

[6] R. KOLAR-ŠUPER, Z. KOLAR-BEGOVIĆ, V. VOLENEC, J. BEBAN-BRKIĆ, Metrical relationships in standard triangle in an isotropic plane, *Math. Commun.* **10** (2005), 149–157.

[7] R. KOLAR-ŠUPER, Z. KOLAR-BEGOVIĆ, V. VOLENEC, Dual Feuerbach theorem in an isotropic plane, *Sarajevo J. Math.* **6** (2010), 109–115.

[8] R. KOLAR-ŠUPER, Z. KOLAR-BEGOVIĆ, V. VOLENEC, Steiner point of a triangle in an isotropic plane, *Rad Hrvat. Akad. Znan. Umjet. Mat. Znan.* **20** (**528**) (2016), 83–95.

[9] R. KOLAR-ŠUPER, Z. KOLAR-BEGOVIĆ, V. VOLENEC, J. BEBAN-BRKIĆ, Isogonality and inversion in an isotropic plane, *Int. J. Pure Appl. Math.* **44** (**3**) (2008), 339–346.

[10] J. PLANE, Recherches géométriques sur les normales a une parabole issues d'un même point, *Nouv. Ann. Math.* **11** (1911), 241–261.

[11] H. SACHS, *Ebene isotrope Geometrie*, Vieweg-Verlag, Braunschweig-Wiesbaden, 1987.

[12] K. STRUBECKER, Geometrie in einer isotropen Ebene, *Math. Naturwiss. Unterr.* **15** (1962-63), 297-306, 343-351, 385-394.

[13] M. Šimić Horvath, V. Volenec, J. Beban-Brkić, On parabolas related to cyclic quadrangle in isotropic plane, *Rad Hrvat. Akad. Znan. Umjet. Mat. Znan.* **20** (**528**) (2016), 97–107.

[14] V. Volenec, J. Beban-Brkić, R. Kolar-Šuper, Z. Kolar-Begović, Orthic axis, Lemoine line and Longchamp's line of the triangle in $I_2$, *Rad Hrvat. Akad. Znan. Umjet. Mat. Znan.* **503** (2009), 13–19.

[15] V. Volenec, E. Jurkin, M. Šimić Horvath, Parabola in Isotropic Plane, *manuscript*

[16] V. Volenec, Z. Kolar-Begović, R. Kolar-Šuper, Kiepert hyperbola in an isotropic plane, *Rad Hrvat. Akad. Znan. Umjet. Mat. Znan.* **22** (**534**) (2018), 129–143.

[17] V. Volenec, Z. Kolar-Begović, R. Kolar-Šuper, Reciprocity in an isotropic plane, *Rad Hrvat. Akad. Znan. Umjet. Mat. Znan.* **519** (2014), 171–181.

[18] V. Volenec, Z. Kolar-Begović, R. Kolar-Šuper, Steiner's ellipses of the triangle in an isotropic plane, *Math. Pannon.* **21** (2) (2010), 229–238.

[19] V. Volenec, M. Šimić Horvath, E. Jurkin, Circles of curvature at points of parabola in isotropic plane, *manuscript*

**Vladimir Volenec**
e-mail: volenec@math.hr

Faculty of Science, University of Zagreb
Bijenička cesta 30, HR-10000 Zagreb, Croatia

**Ema Jurkin**
orcid.org/0000-0002-8658-5446
e-mail: ema.jurkin@rgn.hr

Faculty of Mining, Geology and Petroleum Engineering, University of Zagreb

Pierottijeva 6, HR-10000 Zagreb, Croatia

**Marija Šimić Horvath**
orcid.org/0000-0001-9190-5371
e-mail: msimic@arhitekt.hr

Faculty of Architecture, University of Zagreb

Kačićeva 26, HR-10000 Zagreb, Croatia

RUŽICA KOLAR-ŠUPER

# Bouvaist Cubic of a Triangle in an Isotropic Plane

**Bouvaist Cubic of a Triangle in an Isotropic Plane**

**ABSTRACT**

The cubic in an isotropic plane which passes through the intersections of the sides of an orthic triangle with the sides of a complementary triangle of a given triangle, and through the point which is complementary to the Steiner point of triangle is studied in this paper. It is proved that its non-isotropic asymptote is parallel to Lemoine line of a given triangle.

**Key words:** isotropic plane, Bouvaist cubic, point complementary to the Steiner point

**MSC2010:** 51N25

**Bouvaistova kubika trokuta u izotropnoj ravnini**

**SAŽETAK**

U članku se proučava kubika koja prolazi kroz sjecišta stranica ortotrokuta i komplementarnog trokuta danog trokuta i kroz točku komplementarnu Steinerovoj točki tog trokuta. Dokazuje se da je neizotropna asimptota kubike paralelna s Lemoineovim pravcem danog trokuta.

**Ključne riječi:** izotropna ravnina, Bouvaistova kubika, komplementarna točka Steinerovoj točki

In [1], Bouvaist showed the existence of a cubic in Euclidean geometry, which passes through all nine intersections of the sides of an orthic triangle and a complementary triangle of a given triangle and through a point complementary to the Steiner point of that triangle. He proved that this cubic is circular and its real asymptote is parallel to the Lemoine line of a given triangle.

It will be shown in this paper that some analogous statement holds in the isotropic plane as well.

The isotropic (or Galilean) plane is a projective–metric plane, where the absolute consists of one line, i.e., the absolute line $\omega$, and one point on that line, i.e., the absolute point $\Omega$. The lines through the point $\Omega$ are isotropic lines, and the points on the line $\omega$ are isotropic points (the points at infinity). Two points $P_1 = (x_1, y_1)$, $P_2 = (x_2, y_2)$ with $x_1 = x_2$ are said to be *parallel*, and we shall say they are on the same *isotropic* line. Any isotropic line is perpendicular to any non-isotropic line.

A triangle is said to be *allowable* if none of its sides is isotropic. Each allowable triangle ABC can be set by a suitable choice of the coordinate system in the *standard position*, in which its circumscribed circle has the equation $y = x^2$, and its vertices are the points $A = (a, a^2)$,   $B = (b, b^2)$,   $C = (c, c^2)$, where $a + b + c = 0$. We shall say then that *ABC* is a *standard triangle*. To prove geometric facts for each allowable triangle it is sufficient to give a proof for the standard triangle (see [3]).

With the labels

$$p = abc \quad \text{and} \quad q = bc + ca + ab$$

a number of useful equalities are proved in [3], as e.g.

$$a^2 = bc - q,$$
$$(b - c)^2 = -(q + 3bc),$$
$$(c - a)(a - b) = 2q - 3bc.$$

In [3], it is proved that the sides $B_h C_h$ and $B_m C_m$ of the orthic triangle $A_h B_h C_h$ and the complementary triangle

$A_m B_m C_m$ of the standard triangle have the equations:

$$y - 2ax + q - 2bc = 0,$$

$$y + ax + q - \frac{bc}{2} = 0,$$

and the equations of their other sides are obtained by a cyclic permutation $a \to b \to c \to a$. That is why every cubic through all nine intersections of the sides of these two triangles has the equation of the form:

$$\prod (y - 2ax + q - 2bc) - \lambda \prod \left( y + ax + q - \frac{bc}{2} \right) = 0, \quad (1)$$

where $\prod$ denotes the product of three factors, the first of which is written, and the other two arise from the first one by cyclic permutations $a \to b \to c \to a$.

In [4], it is shown that the point

$$S = \left( \frac{3p}{2q}, -\frac{9p^2}{2q^2} - q \right)$$

is complementary to the Steiner point of the standard triangle $ABC$. For that point we obtain

$$y - 2ax + q - 2bc = -\frac{9p^2}{2q^2} - \frac{3ap}{q} - 2bc$$

$$= -\frac{bc}{2q^2} (9a^2 bc + 6a^2 q + 4q^2)$$

$$= -\frac{bc}{2q^2} [9bc(bc - q) + 6q(bc - q) + 4q^2]$$

$$= \frac{bc}{2q^2} (2q^2 + 3bcq - 9b^2 c^2)$$

$$= \frac{bc}{2q^2} (q + 3bc)(2q - 3bc)$$

$$= -\frac{bc}{2q^2} (b - c)^2 (c - a)(a - b),$$

$$y + ax + q - \frac{bc}{2} = -\frac{9p^2}{2q^2} + \frac{3ap}{2q} - \frac{bc}{2}$$

$$= -\frac{bc}{2q^2} (9a^2 bc - 3a^2 q + q^2)$$

$$= -\frac{bc}{2q^2} [9bc(bc - q) - 3q(bc - q) + q^2]$$

$$= -\frac{bc}{2q^2} (4q^2 - 12bcq + 9b^2 c^2),$$

$$= -\frac{bc}{2q^2} (2q - 3bc)^2$$

$$= -\frac{bc}{2q^2} (c - a)^2 (a - b)^2$$

and then

$$\prod (y - 2ax + q - 2bc) = -\frac{a^2 b^2 c^2}{8q^6} (b - c)^4 (c - a)^4 (a - b)^4,$$

$$\prod \left( y + ax + q - \frac{bc}{2} \right) = -\frac{a^2 b^2 c^2}{8q^6} (b - c)^4 (c - a)^4 (a - b)^4.$$

Thus, the cubic of the pencil of the cubics with equation (1) passes through the point $S$ if one takes $\lambda = 1$ (Figure 1).

If that cubic of the allowable triangle $ABC$, which passes through the intersections of the sides of its orthic triangle with the sides of its complementary triangle, and through the point $S$ complementary to the Steiner point of the triangle $ABC$ (Figure 1), is called the *Bouvaist cubic* of that triangle, then we have:

**Theorem 1** *The Bouvaist cubic $\mathcal{B}$ of the standard triangle $ABC$ has the equation:*

$$(y - 2ax + q - 2bc)(y - 2bx + q - 2ca)$$

$$(y - 2cx + q - 2ab) - \left( y + ax + q - \frac{bc}{2} \right) \quad (2)$$

$$\left( y + bx + q - \frac{ca}{2} \right) \left( y + cx + q - \frac{ab}{2} \right) = 0.$$

Let us now find the intersection points of the cubic (2) and the absolute line. We have to solve the equation

$$(y - 2ax)(y - 2bx)(y - 2cx) - (y + ax)(y + bx)(y + cx) = 0,$$

which can also be written in the following form:

$$-3(a + b + c)xy^2 + 3(bc + ca + ab)x^2 y - 9abcx^3 = 0,$$

and finally as $3qx^2 y - 9px^3 = 0$. We have the double solution $x = 0$ and the solution $y = \frac{3p}{q} x$, which means that the cubic has an asymptote with a slope $\frac{3p}{q}$, which is by [2] a slope of the Lemoine line $\mathcal{L}$ of the triangle $ABC$. We obtained:

**Theorem 2** *The non-isotropic asymptote of Bouvist cubic of an allowable triangle is parallel to the Lemoine line of a given triangle. Absolute point is an intersection point of the Bouvaist cubic and absolute line with intersection multiplicity 2.*
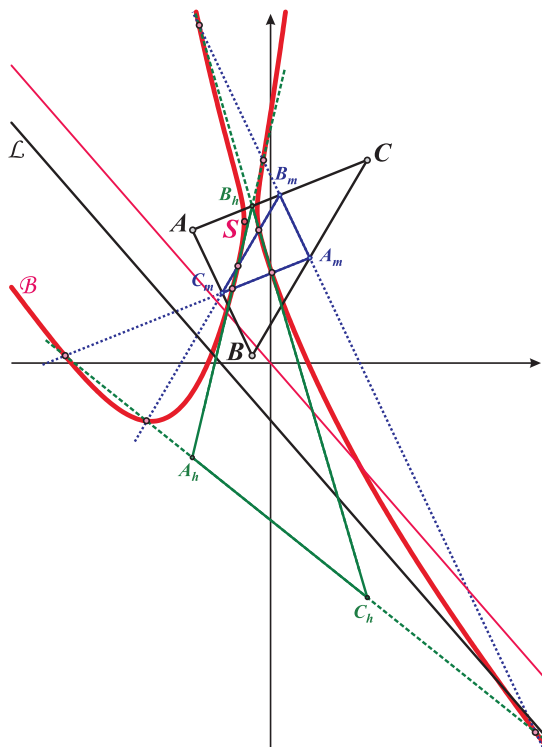
Figure 1: *Bouvaist cubic of a triangle ABC in isotropic plane*

## References

[1] R. BOUVAIST, *Généralization de la question 2811*, Mathesis **48** (1934), 451–452.

[2] Z. KOLAR–BEGOVIĆ, R. KOLAR–ŠUPER, J. BEBAN–BRKIĆ, V. VOLENEC, Symmedians and the symmedian centre of the triangle in an isotropic plane, *Math. Pannon.* **17** (2006), 287–301.

[3] R. KOLAR-ŠUPER, Z. KOLAR-BEGOVIĆ, V. VOLENEC, J. BEBAN-BRKIĆ, Metrical relationships in a standard triangle in an isotropic plane, *Math. Commun.* **10** (2005), 149–157.

[4] R. KOLAR-ŠUPER, Z. KOLAR-BEGOVIĆ, V. VOLENEC, Steiner point of a triangle in an isotropic plane, *Rad Hrvat. Akad. Znan. Umjet. Mat. Znan.* **20** 528 (2016), 83–95.

**Ružica Kolar–Šuper**
orcid.org/0000-0002-8945-2745
e-mail: rkolar@foozos.hr

Faculty of Education, University of Osijek
Cara Hadrijana 10, 31 000 Osijek, Croatia

**SIMONE PORRO**
**LUIGI COCCHIARELLA**

# Use of a Game Engine Artificial Intelligence to Represent People Flows in Architectural Spaces via Geometry and Graphics

**Use of a Game Engine Artificial Intelligence to Represent People Flows in Architectural Spaces via Geometry and Graphics**

**ABSTRACT**

The digital and the related technological evolution in recent years have shifted to words such as *Virtual Reality and Artificial Intelligence*. The wider use of these and other technologies in architecture has been far limited by a lack of IT tools with which architects could interface since they have been made available in the last few years only. The evolution of the tools used by the architect can be condensed and simplified into a sequence of three stages: *Drawing Board, CAD systems, Game Engines*. The frames of this sequence, in addition to indicating instruments, are representative of the historical context in which they have been or are still being used. This study, based on a Master thesis recently discussed at the Politecnico di Milano [14], examines the role that *Game Engines* can play in the graphic representation and design processes. More specifically, it takes a closer look at the Unreal Engine as a tool for creating a real-time design environment and using Artificial Intelligence (AI) technologies to represent user flows in the space as valuable support and a relevant part of the design strategies aiming at implementing and evaluating design options. For this purpose, various simulations have been carried out both considering users' flows based on assigned spaces, and generating spaces based on the users' flows.

**Key words:** artificial intelligence, flows, parametric modeling, dynamic environment, game engines, simulations, unreal engine

**MSC2010:** 00A66, 51N05, 01A05, 97U99

**Upotreba game enginea umjetne inteligencije u svrhu predstavljanja protoka ljudi u arhitektonskim prostorima pomoću geometrije i grafike**

**SAŽETAK**

Digitalna i njoj pripadajuća tehnološka evolucija posljednjih godina pretvorila se u riječi kao *Virtualna stvarnost i umjetna inteligencija*. Šira upotreba ovih, ali i drugih tehnologija u arhitekturi dosta je ograničena zbog nedostatka IT alata s kojima su se arhitekti susretali s obzirom na to da su bili dostupni jedino u posljednjih nekoliko godina. Evolucija alata koju koriste arhitekti može biti komprimirana i pojednostavljena promatrajući je u tri faze: *crtaća ploča, CAD sustavi, game enginei*. Okviri ovih faza predstavnici su povijesnog konteksta u kojem su se koristili ili se još uvijek koriste. Ovo proučavanje koje se temelji na diplomskom radu nedavno obrađenom na Politecnico di Milano [14], ispituje ulogu koju *game enginei* mogu igrati u grafičkoj prezentaciji i procesu projektiranja. Konkretnije, bliže sagledava Unreal Engine kao alat za stvaranje okoline projektiranja u stvarnom vremenu i koristeći tehnologije Umjetne inteligencije predstavlja korisničko razmišljanje u prostoru kao korisnu podršku i važan dio strategija projektiranja s ciljem implementacije i evaluacije projektantskih opcija. Za ovu svrhu, brojne simulacije su izvedene uzimajući u obzir i protoke korisnika temeljene na konkretnom prostoru, ali i generiranje prostora temeljeno na protocima korisnika.

**Ključne riječi:** umjetna inteligencija, protoci, parametarsko modeliranje, dinamično okruženje, game enginei, simulacije, unreal engine

## 1 Play and serious game definition

To understand how real-time engines integrate in the Geometrical and Architectural context, we need to start from upstream, as they fit into the digitization process, looking at similarities and contact points with Geometry and Architecture, as well as at what architecture can get from these digital engines. To this end it is necessary to remind meaning and definition of Game and Play in relation to the topic. The discipline behind this world is called *Game Studies* or

*Ludology*. This sector studies games in general, the act of playing, the player and the culture behind her/him, contextualizing the historical playground. As we could expect, the research fields falling within this sector are various and vast, involving anthropology and sociology, as well as psychology, over and above scientific and technical areas. All these aspects contribute to define the design of a game concerning both the player and the game itself and of course in relation to the user. Not to be confused *Game Studies* or *Ludology*, is about the study of video games, which is simply a branch of a much broader context dealing with *Digital Games*. In the playful context before the introduction of the digital, a publication having a discreet influence and still taken as a reference nowadays was *Homo Ludens* by John Huizinga in 1944, as well as the subsequent discussions, in which he highlighted the importance of the "Play" element inside of a culture. Huizinga argued that play is a factor of primary and fundamental importance for a society. According to this point of view, he brings the highest human achievements back as a product of the creativity of the game.

The common perspective that play is only one form of culture among many is a modern deformation, and a concept wrong in itself. On the point Huizinga expresses a simple contradiction: if the game were the product of human culture there would be no play outside of it, but this is not so since the game is much older and is already shown in nature, as shown for example in the animals plays. Therefore, since the Game exists before culture and before mankind himself, one can think, opposite, that culture is born through the Game. In the biological field, indeed, an attempt has been made to give explanations and formulate theories that try to define the game as a function of life, explaining the game as something that serves biological purposes. Even Huizinga asks: why do we play? Whatever the answer, be it biological or not, in the end there is always a relation with satisfaction, or with the pleasure of playing that escapes any logical analysis, that is, precisely, what Huizinga says is the essence of the game. In the Game there is an immaterial, conscious element of the individual, which manifests itself in the physical existence through the game itself. The Game is the door that connects material and immaterial, real and virtual. From these premises it is clear that the Game has a much higher value than one would normally attribute to it, which transcends both the biological and cultural activity of the individual who performs it. It is an act having within itself an immaterial, archetypal and creative sense.

Moreover, at the time the author had already tried to free the issue from another common but false opinion, which saw the concept of Game as the opposite of seriousness. Huizinga pointed out that this opposition of facts does not hold up since the Game can be both serious and not serious, and although there may be an oscillation between these two opposites the Game still remains Game, showing its own identity. On this subject in 1970 Clark C. Abt introduced the phrase "serious games", which he defined as follows: "... these games have an explicit and carefully thought-out educational purpose and are not intended to be played primarily for amusement" [2, p. 9]. Today the same idea is generally expressed as "games that aim at training, educating, persuading or communicating values and ideas" [5, p. 26]. In this context, according to the definition above, "serious games" are no longer Game, or at least they are not in their purest form, as they are exploited for a certain purpose. In a Broader sense, quoting Juul, "a rule-based formal system with a variable and quantifiable outcom" [9, p. 35]. Concerning the seriousness of a Game, in support of the thesis that the words *serious* and *game* are not necessarily two opposites of the same aspect, a historical example can be taken as a reference from Von Neumann and the Game Theory. Beyond the name, which can make you mislead, contrary to what you might think, he does not talk about Game in the common sense of the term, although it is precisely from the observation of that common context that Game is born. With the title: *Theory of Games and Economic Behavior*, he essentially put mathematical aspects at the base of studying and analysing the decisions of a subject in certain situations of conflict with other rivals. In other words, he intended to predict the behavior of individuals in situations that can lead to the division or the winning of something in monetary terms or more generally in utilitarian terms. The theory therefore applies to an infinite number of scenarios, of various nature and complexity, which can range from chess games to the financial or economic market contexts. The most interesting aspect of this story is that it shows a different definition of Game. This point of view began to be used to evaluate behaviors and choices of the "players", no longer understood as acts aimed at a mere fun or without a completely defined purpose, but on the contrary, as actions having a plan or a strategy behind, and aiming at specific purposes.

More recently Alessandro Baricco, in the book titled *The Game* [3] describing the world in which we live in and the digital revolution that underlies it, shows how this process of *gamification* is definitely connected to our society, more profoundly than we think. Baricco starts from a simple similarity: *Table football*, *Pinball*, *Video game*. A similarity that traces some historical stages of the technological evolution of the digital. Well, starting from this path he realizes that it reveals a substantial mutation behind the use of more and more technologically evoluted Games. In a *Table football* the feeling is natural, the noises are real, you have to physically do a certain movement, a certain effort and even the ball is real. It is no more than a physical game. If you switch to the *Pinball* (flipper) the situation begins to change. Many of the noises become electrical, and a screen appears that begins to take some importance.

The ball is closed under a glass and the physical sensation is reduced. There are only two keys, whose consistency becomes much softer and different from the resistance of table football. This passage is a sort of preparation for the last passage, says Baricco, a kind of "limbo" to the final step, which is the video game, of which *Space Invaders* is the key reference and prototype. Here everything has been transferred to the screen, physical remains are only the keys that act as a link between the digital world and the real world. The sounds have become completely artificial. The rhythms change, much faster, with a different concept of time, in a way more liquid. Everything has turned into sequences of bits, numbers that are translated into images, sounds, actions, etc. These games have an explicit and carefully thought-out educational purpose and are not intended to be played primarily for amusement. It slips into a dematerialized world, with a different density, in other words, as he says, in "the pure essence of the game". In this similarity the passage is not only in terms of digitization. If on the one hand you have loss in movement or reality, on the other hand you have much in exchange. If the table football, that is, just one physical device, offered only one possibility of Game, the digital engine beyond the screen potentially offered an infinite number of simulated "realities". What Baricco also points out is that the same mentality that led to the evolution of the Game has revolutionized and is still revolutionizing the companies. According to the author this phenomenon exploded with worldwide resonance in 2007 when Steve Jobs presented the *iPhone*. In that context, a further transition to digitization was established. The keyboard characterizing the fromer smartphones disappeared, and in its place a touch screen with icons to press appeared. Well, in hindsight, the iPhone itself is built like a Game device, and only the purpose for which it is used changes, including games. In addition to make phone calls (the original function still in the name), from that moment on with one single device you could send emails or write texts, take pictures or make movies, and (of course) also play in the classic sense of the term. Then on the one hand we have the Game with the aim of having fun or, as Huizinga would say, without any other necessary purpose if not that of the mere fun (let us say *funny game*). On the other hand we have the Game aimed at carrying out activities related to the everyday life (let us say *serious game*). So far, the definition of *Game* as it is intended in this discussion is not necessarily seen as a playful aspect, but much more as a tool that through the Play, intended as a productive factor, can lead into creative, and generative results, in the context in which it is applied. A metaphor of that can be seen in terms of an engine element that if inserted in a car results in allowing motion, where the Play is movement for transporting purposes, while, if applied to a children's carousel generates fun, and the Play is for entertainment and pastime.

## 2 Architecture and geometrical serious games

Once you understand what is meant by Game, it is interesting to note how this could be integrated into the geometrical and architectural context and what are the common points between the two worlds. As you may have already guessed for simplicity, we will no longer use the words "serious game", but simply: *Game*. Letting people understand that it is neither our intent to trivialize the matter in discussion, nor to diminish other related matters. It is for the pure sake of simplicity. Well, if we analyze the structure of a Game, it is generally formed by a visual, two-dimensional or three-dimensional part, managed by the *Game Designer*, and by a structural, scripting, computer-guided part precisely arranged by the *Programmer*. The same can be said for Architecture that comes from the right dialogue between an aesthetic compositional part, and a structural engineering part. And even Geometry can be seen as the result of a process and its 'aesthetic' representation. Therefore, Game, Architecture and Geometry, share the same conformation processes. They, indeed, share similar structural aspects concerning their 'composition'. The similarity established by Baricco among table football, pinball, and videogame in relation to how the digital has historically changed, shows in time-lapse some key moments of the digital evolution of the Game, which in parallel could correspond to innovations in Architectural design and in Geometry. To summarize, in all these three fields we have gone on to an ever smaller physicality as well as to a translation of graphic operations for visual purposes into the form of codes, numbers, bits. Since even architectural and geometrical are involved in the digital revolution, the same time-lapse logic proposed by Baricco for Games can be applied to these contexts, with special reference to the tools used, where an interesting comparison would emerge. The similarity here proposed in relation to digital graphics for architecture is the following: *Drawing Board*, *Cad Systems*, *Game Engine*.
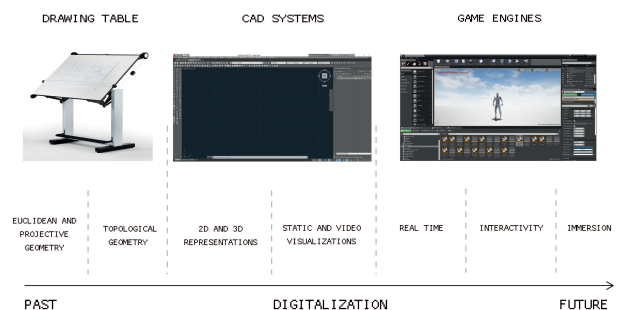


Figure 1: *Timeline of frames and functionalities of tools used by architects*

Each step of the sequence symbolically represents a frame of a wider context, in which there is a change of both the tools or the software and above all the potential that the technological evolution offers. From the analogue of the Drawing Board we have moved on to the CAD Systems in which the space is digitized in its two and three-dimensional forms, up to the last step in which beyond the digital space also the temporal component is simulated. It is interesting to note some fundamental mutations if you switch between the chain frames. When designing with pencils, ink pen, paper and tracing paper on drawing tables, everything was physical. You paid for the mistakes with ink at the time, and all the instruments had a certain consistency, certain smells and noises, and thicknesses. At the time you got your hands dirty and there was a certain slowness in all the processes, from pulling a line of which you made sure its sweetness, to its cancellation. With Cad software the situation has changed: pencils and ink no longer exist, lines are produced by a command as well as their cancellation, the tracing papers are called layers, you don't have to pour or remove them on the drawing, now they are activated and deactivated with a click. The physical drawing board no longer exists, or rather exists the digital counterpart, which has become usually black. Not only the graphic model developed is no longer limited to the two dimensions of the drawing board but it also acquires the third dimension, the extrusion along the Z axis. The only connection left with the drawing board is the paper, still used to print on what is digitally produced, while nowadays also 3D printers started to take off. Much has been lost with Cad Software, but in return it has also achieved quite a bit: production speed, graphic cleaning, management of every aspect of the design, etc. The last step in this chain is about *Game Engines*. Not so much for their current level of use but more for the potential they offer compared to the Cad frame. Game Engines allow to work with an element not well managed by Cad software: *time*. That brings two main important features: the visualization and representation of the scene in real time, with the possibility of integrating the model in Virtual Reality, and the possibility of creating, through computer codes or scripts, possible interactions between the user the element of a scene or the scene itself. In other words, all the information as well as the process that governs them will be condensed into a single three-dimensional model accessible with any screen or with a viewer, and controlled by visual interfaces. Goodbye to paper. Because the information moves towards digitalization a further aspect needs to take into account called *Gameplay*, in other words: the experience that comes from the act of playing. Since there is a more and more explicit dialogue between the spatial and the geometrical components, the rules and processes behind it (Game) and the temporal components (Play) it would be crucial consider

also this interaction between the game's response and the user, which "can generate outcomes that never could have been imagined beforehand". [12]

**Game Engine choices and mapping**

The choice of the *Game Engine* as a design and representation tool was based on different factors. First of all, together with Unity it is the most used software program among game engines for architectural purposes. A research conducted by CGarchitects shows that it is the most used among Real Time Engines. Responses were gathered between November 30 2017 and February 3 2018 via CGarchitect's community (social media & email newsletter) and through Facebook groups associated with real-time engines and architectural visualization. 997 Responses came from Social media and 1,066 responses came from email newsletter subscribers. Second reason for the choice is due to a series of characteristics that other competitor software programs considered do not offer yet, or they do not offer with the same quality. As you can see in the Fig. 2 [Top Left] shows that Unreal is between the most used in the architectural field as a visualization tool and also the most used for experimental purposes among general renderer software [Top Right]. What's also interesting is the use of Unreal Engine in the real time research field [Down].

Although the programming is not the architect's own discipline, the software comes in handy giving the possibility to program through a *visual scripting editor* called Blueprint. This type of interaction with the software partly recalls Grasshopper, however it should be noted that the two software programs work on different contexts, from which a different type of programming in the two cases follows. In particular, Grasshopper is largely based on geometric properties of which the architect has knowledge and s/he is more familiar with, indeed Grasshopper is a plug-in of a well-known NURBS modeler, Rhinoceros. It is not so for Unreal Engine, a much more eclectic software that must interface with software programs developed in a wide spectrum of disciplinary fields, and therefore is a much purer kind of programming software in its essence. This aspect, while on the one hand broadens the range of its programming possibilities, on the other hand clearly complicates the process, especially from those who are not accustomed to these approaches, or at least to this specific software. Another fundamental difference lies in being a software that mainly pertains to the temporal aspects, although it effectively integrates the spatial part with which it must interface. This aspect shifts the context of its use more to the simulative and experiential side of the represented space, on which the work that follows is based.
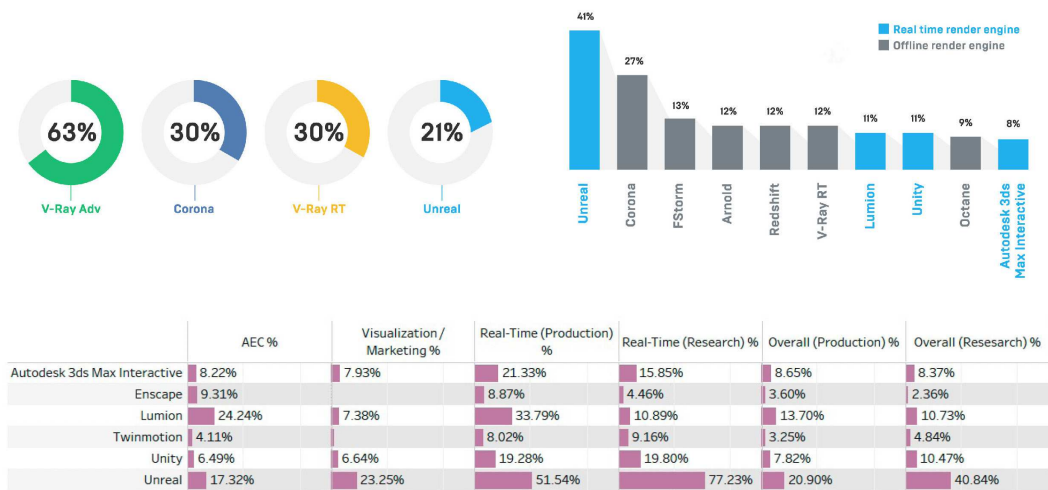
| | AEC % | Visualization / Marketing % | Real-Time (Production) % | Real-Time (Research) % | Overall (Production) % | Overall (Resesarch) % |
|---|---|---|---|---|---|---|
| Autodesk 3ds Max Interactive | 8.22% | 7.93% | 21.33% | 15.85% | 8.65% | 8.37% |
| Enscape | 9.31% | | 8.87% | 4.46% | 3.60% | 2.36% |
| Lumion | 24.24% | 7.38% | 33.79% | 10.89% | 13.70% | 10.73% |
| Twinmotion | 4.11% | | 8.02% | 9.16% | 3.25% | 4.84% |
| Unity | 6.49% | 6.64% | 19.28% | 19.80% | 7.82% | 10.47% |
| Unreal | 17.32% | 23.25% | 51.54% | 77.23% | 20.90% | 40.84% |

Figure 2: *[Top Left] Percentage of use of rendering engines for visualization purposes. [Top Right] Percentage of experimental use of rendering engines. [Down] Percentage of use of Real Time Engines between different contexts. (Images above taken from https://www.unrealengine.com/en-US/blog/cgarchitect-survey-shows-shift-to-real-time-rendering) (Image below taken from http://www.cgarchitect.com/2018/02/2018-architectural-visualization-rendering-engine-survey)*

Fig.3 shows a general mapping of the main functionalities within UE4 (Unreal Engine release 4). This map was based primarily on those features useful to architectural and geometrical practice. Several other features are available, there are more than two hundred plugins available and it is not excluded that combined together they could generate other useful tools. However, it should be noted that the true strength and effectiveness of what can be pro-duced with this software, outside of mere visualizations or architectural walkthroughs, lies in the combination of these tools among them, thanks in particular to the functionalities of scripting. A general classification can be done within two categories: *visualization* and *parameterization* but in a way it's a simplification since there are other functions in-between them.
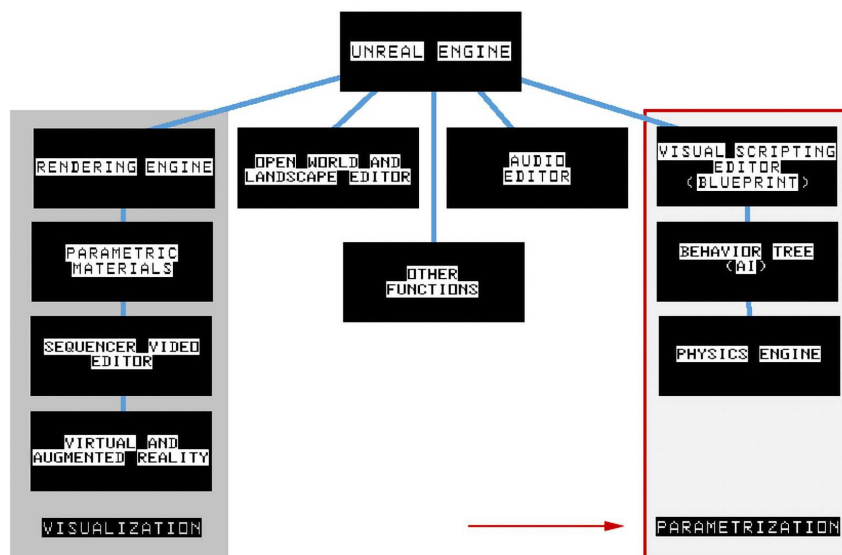


Figure 3: *General mapping of Unreal Engine: right block shows the set of functions we used*

## Playing Architecture

For the Master dissertation, as well as for this paper, a closer look at the *Unreal Engine* release 4 (UE4) has been taken, as a tool for creating a real-time design environment and for using Artificial Intelligence (AI) technologies to represent users' flows in the space, which can be adopted to carry out design strategies and to evaluate design options. For this purpose, several simulations have been developed, either considering the pedestrian planar flows interlinked with the form of space, either parametrically generating spaces on the bases of the number of users. The first series of tests is based on pre-assigned spatial contexts. In order to test the AI programmed sets, different situations were figured out and modeled in advance. Given the assigned space, a series of points has been subsequently assigned, working as 'attractors' according to possible users' interest locations, and a virtual robot (silhouette) has been placed to explore the various possible paths, based on a random sequences of movements towards the assigned attractor-points. In order to graphically represent the visual simulations, the silhouette has been equipped with a tracing video-camera system shoving at the same time its movements and the scene from the camera point of view, and allowing to reproduce in real-time the flows as graphic diagrams in the space. The AI system was also tested in a 3D spatial context characterized by differences in heights, such as inclined corridors, vertical lifts, and so on, connecting the floors. A second series of tests has been carried out considering the inverse process, that is, implementing a generative system able to create new spaces, such as rooms and paths, according to the needs emerged from the real-time analysis of the parametrically assigned users' flows. Therefore, a generative algorithm was set, able to update the geometry of space according to the number of people supposed to 'need space': in other words, space expanded according to the number of users. This generative process is based on a preliminary evaluation of the entire scenario, which essentially controls the generation itself in order to match 'rooms and paths' with the number of users. What we developed here with *Unreal Engine* would only show the power and the potentiality of this typology of software, which is still to be fully discovered, since it has been available only few years ago, and the software houses are only recently getting increasingly interested in the architectural field. However, considering the present state of art, we tried to propose some tests on if and how it is possible to use the system outside of its native target environment, adapting it to an architectural design spatial context. In our case the Master thesis, which was at the origin of this work, was confined to focusing on the use of

UE4 to realize an AI system helpful to represent and control - visually and parametrically - pedestrian flows in a three-dimensional environment, either pre-existing or generated according to specific inputs. More generally, linking analysis and project, especially in more complex scenarios, it can serve as a tool for mapping and analyzing architectural contexts, as well as for implementing, verifying, and comparing design choices, that is, efficiently sustaining the whole chain of the architectural design process.

## Artificial Intelligence: NPC and Behaviour Tree

In order to develop the simulation mentioned above an AI process has been set and programmed. The simulation is mainly composed by three parts: the logic of how it works (Behaviour Tree or BT), a virtual actor (Non-Player Character or NPC) that can represent visually the result of the Ai logic process, and the basic physics (Collision Physics) of the digital environment of the scene (Map or Level). The First step has been about setting in the scene a NPC, shown in Fig. 4 and formed by the components appearing in the drop down menu placed on the top in the same figure.
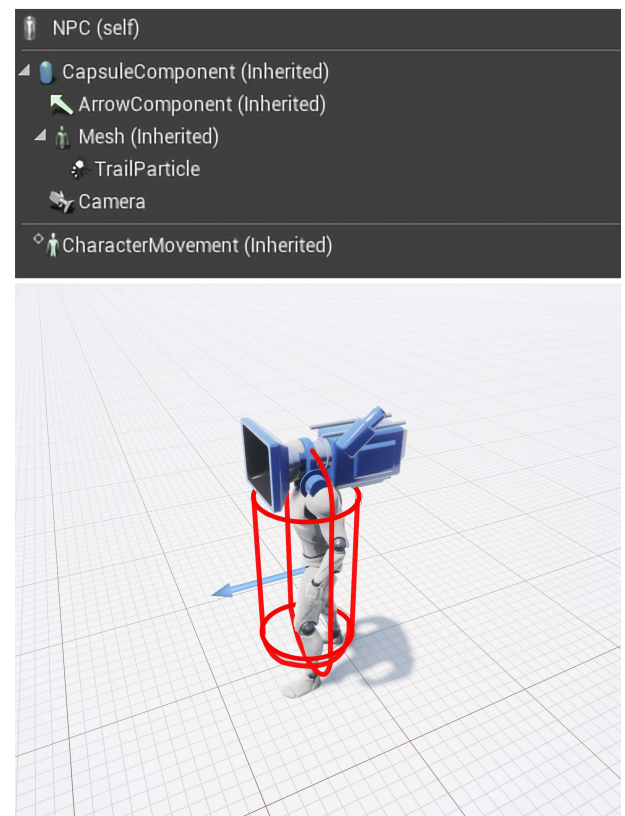


Figure 4: *[Above] NPC components list, [Below] NPC visual representation (Camera remain hidden during simulations)*

The mesh representing the body of the silhouette, embeds the physical information of the body including human joints and articulations and their possible movements in space. (Fig. 5)
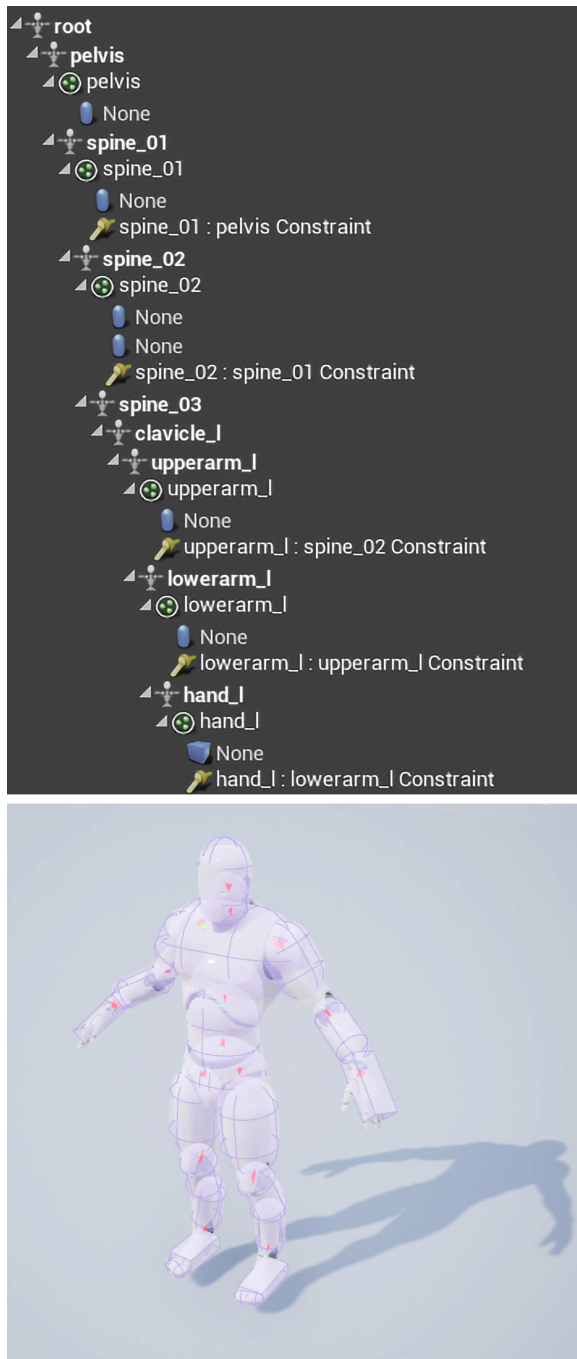


Figure 5: *[Above] NPC partial skeleton composition list, [Below] NPC with hidden overlapped collision physics*

The Arrow vector gives indication of the primary movement direction, and a capsule component is also used to trigger collision events or even understand where other NPCs are located in the scene. This function has not been used at the moment for the following tests, due to the particular induced behaviours when two or more NPC's path direction collide, and NPC simultaneously take the same decision to avoid the other(s). A video camera allows to record the AI movements, and finally a *trail particle* is set, which allows to trace the movements in the space basically linking the coding part with the representative graphic part. A *collision physics* useful to avoid overlapping geometries has been inserted in the scene by superimposing to all the solids a hidden simplified mesh of their geometry itself (see Fig. 5 in purple the simplified body mesh of the NPC)

Then, in order to represent flows in space, the first necessary step was to program an AI system which simulates a hypothetical logical process for which an individual tries to reach a point or an array of interesting locations by traveling in the fastest way and considering obstacles and areas where the passage is prevented for various reasons. In UE4 it is possible to obtain this result by using two integrated functions, the Bluprint Editor, that is, a visual scripting tool used to code functions, and the Behavior Tree (BT), which manages the programmed functions with a system of structural nodes. The Fig. 6 [Top] shows the BT system that simulates the user behavior, while in the Fig. 6 [Center and Down] some blueprints that manage specific behaviours.

In simplified terms the AI operation is based on the following logic: recalling by function the NPC; loading in memory the NPC location point and his destination point, previously set; imposing the creation of one or more vectors that connects the two points; making the NPC move towards the first point previously set, along the generated vector. Once at destination, a certain waiting time has been set (it can be avoided) before the following command is activated. At this point the AI must be activated to understand which is the next destination point, in order to repeat the process a number of times up to the end point of the array. Once it gets the last point, it would be possible to decide whether (or not) to reverse the preset points or make them repeat in loop. Another alternative is to randomize the system of the preset points, so that there is no predefined path by increasing the number of possible displacements, then without binding the movement to a predetermined sequence. This last option has been chosen in order to replicate a hypothetical not predetermined behaviour.

About the physics, it has been set what is called *collision physics* that gives to the elements in the scene the property

of "solidity" as in the real world, in order avoid geometries and element in the scene to interpenetrate, passing through each other. Also the *gravity force* has been set. Finally, closely linked to the *collisions*, and in order to be able to make the AI understand if there are obstacles along the path that the NPC will have to travel, a volume called "Nav Mesh Bounds Volume" has been added to the scene. It allows to create a mesh calculated on the basis of the objects to which a collisions physic was applied and which reside

within this volume. The generated mesh will be parallel to the surfaces of the scene, considering also the angles of the slopes. If they are slower than the established one it will be walkable. If higher it will be interpreted as obstacles. Therefore, this process will determine the space within which the AI can move, after eliminating the obstacles, and on which the AI logic will calculate the route towards the preset points.
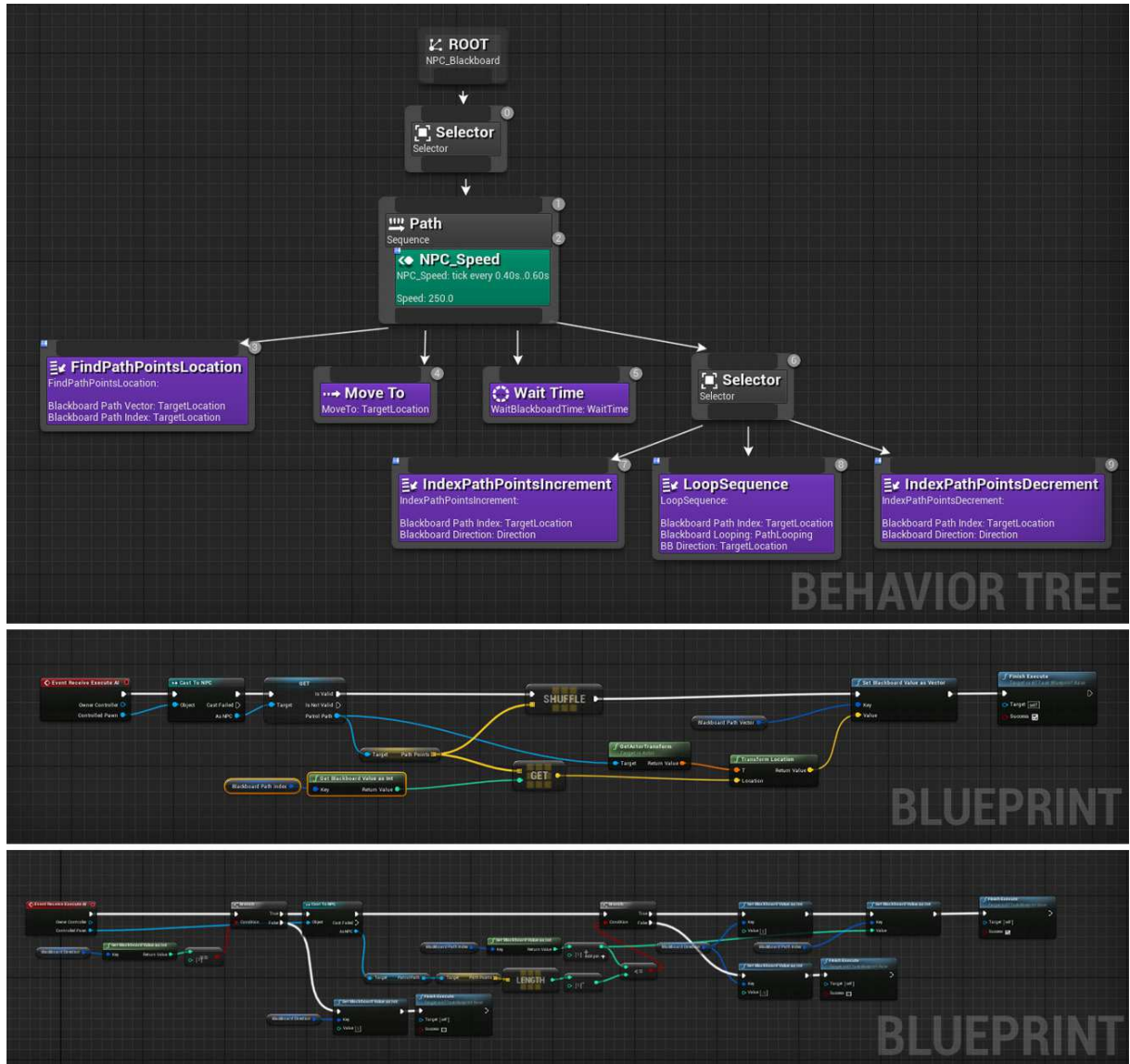


Figure 6: *[Above] Behavior Tree programmed to simulate user flows. [Center and Below] Examples of blueprints that manage some nodes of the BT.*
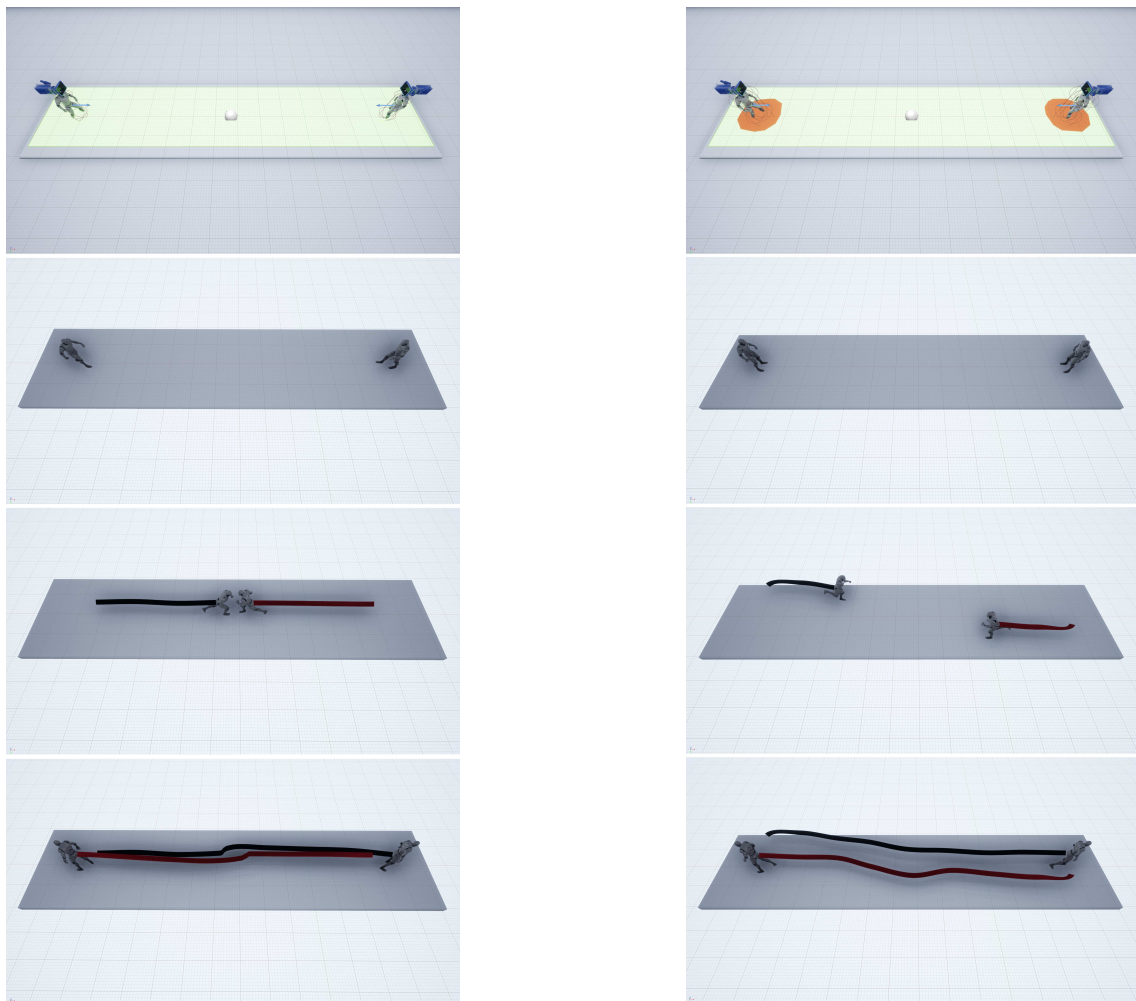
Figure 7: *[Sequence Left] Simulation with collision physics applied only to the body of the NPCs. If they collide they change their trajectory due only to physics. [Sequence Right] Collision physics applied to a larger area and calculated dynamically by the Nav Mesh Bounds Volume frame by frame. The AI that manages the NPC trying to find a way not to collide, since they see each other as obstacles.*

**Form to flows**

In order to test the AI programmed, a hypothetical residential interior space has been modeled, to which the volumes of some furnishings have been added. A series of points were subsequently assigned, within the housing hypothesis, in places of possible interesting areas. (Fig. 8)

The sequence of movement of the silhouette towards these points has been randomized so that it does not follow a predetermined sequence, but once the simulation has started it can move freely and randomly to any of the preset points inside the Nav Mesh Bound Volume. (Fig. 9)



Figure 8: *Hypothetical residential plan with the location of the 'PathPoints'*
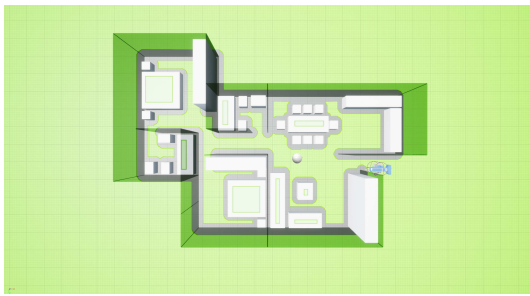
Figure 9: *Model with indicated in green the 'Nav Mesh Bounds Volume'*

Once the first point is reached, the sequence will be shuffled again so that from any point the silhouette can reach all the others, even the ones visited before. This prevents a previously reached point from being ignored at a later stage. It also prevents the same route from being traveled over time, and consequently allows to increase the number of possible routes that can be considered. Moreover, the choice to randomly determine the path of the NPC allows to evaluate the simulation from other points of view as a privileged point of view it is not predetermined. This choice, although it may seem simplistic, gives the AI a certain unpredictability that partly mimics human behavior. In order to be able to graphically represent the simulation, the silhouette has been equipped with a system that traces its movement during the displacement, and allows to visualize the flows in space for the time of the simulation. Since the simulation would go on to infinity, it was programmed to suspend it as soon as all the points in the scene were reached from each position. It should be noted that if the AI is set on the random proceeding of the points, each simulation is different from the other even though sharing similar patterns, while the most traveled areas, as well as those that are not, are graphically highlighted. In the residential housing hypothesized it can be seen that both in relation to the fastest routes and in relation to obstacles such as walls and furnishings, the corridor is one of the most crossed areas by the silhouette, as it is supposed to be in a real similar spatial situation. Fig. 10-13
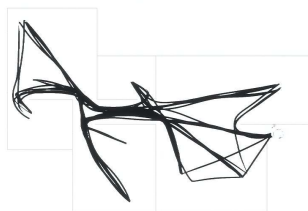


Figure 10: *AI calculated flows without considering furniture*
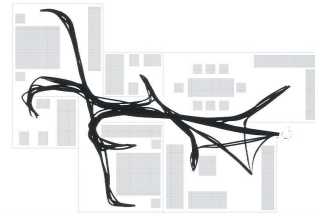


Figure 11: *AI calculated flows considering furniture*



Figure 12: *Perspective view of the AI calculated flows without considering furniture*



Figure 13: *Perspective view of the AI calculated flows considering furniture*

In another simulation, the AI was tested in a context with differences in heights reached through inclined corridors, or vertical lifts. Even in this case the movements' sequence was randomized for the same reasons as in the previous case. The representation of the flows appears here in three dimensions, according to the differences in high, then we have a properly said three-dimensional dynamic spatial scenario. The AI is able to calculate the hypothetical flows given any form of space. The (Fig. 14) show the model on which the test was carried out, (Fig. 15) the set of points that allowed the AI to address the Silhouette on the basis of the Nav Mesh Bounds Volume (Fig. 16) and finally the graphic representation of the resulting flows, represented both in perspective (Fig. 17) and in top view (Fig. 18).
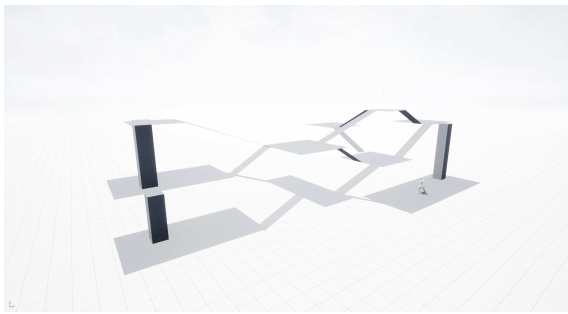
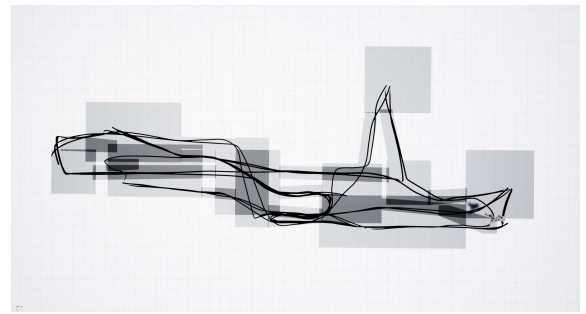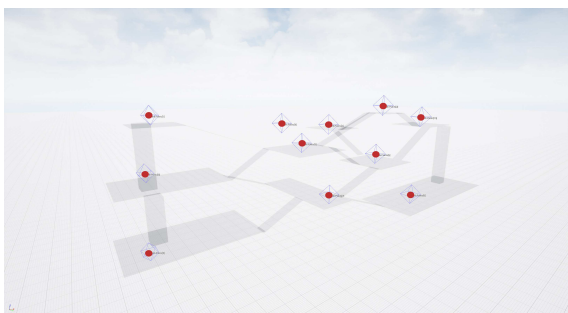Figure 14: *Hypothetical model designed with different levels*



Figure 15: *Model set with 'Path Points'*
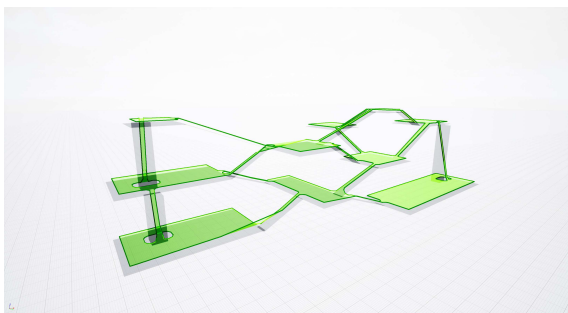


Figure 16: *Model with indicated in green the 'Nav Mesh Bounds Volume'*



Figure 17: *Model with the AI calculated flows represented*
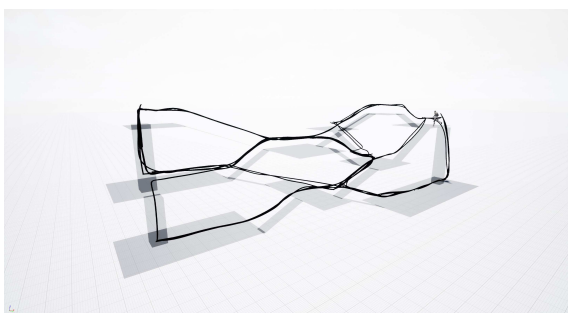


Figure 18: *Zenithal view of the model with the AI calculated flows represented*

**Flows to form**

Considering the inverse process that can be described as the determination of form given the flows, a generative system has been programmed to create, on the basis of various parameters (Fig. 19), a spatial system based on several floor levels, where some spaces are connected by ramps. The generation of spaces is based on a system of nodes (Fig. 20) which corresponds to hypothetical spaces of interest and which subsequently correspond to the points that the AI identifies as areas to be reached.
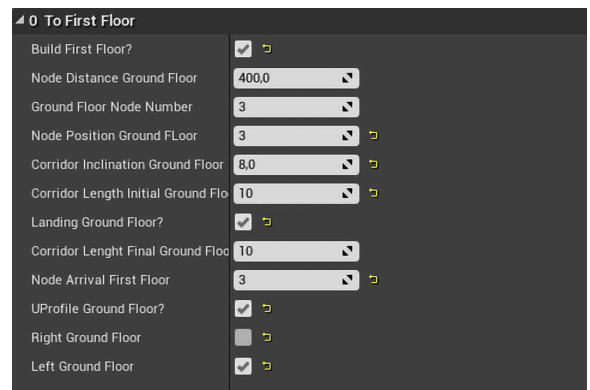


Figure 19: *Parameters: generation settings*
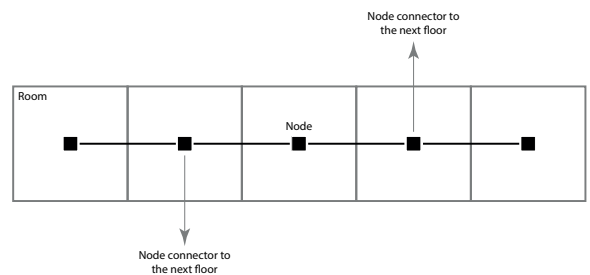


Figure 20: *Node based generation system*

The number of nodes also corresponds to the number of people who are supposed to reach a certain level or the probability of this happening. Knowing the points from where people start, up to where and in what number they have to arrive, is the information based on which the form of rooms and connections is generated and subsequently the AI is asked to determine the generation of the flows. Once the inputs have been set, we have to make sure that the generation will take place within the Nav Mesh Bounds Volume previously placed in the scene. Then, after starting the simulation, based on the parameters previously set the system calculates the forms, which automatically and dynamically will be read by the Nav Mesh Bounds Volume, that will adapt to the geometry of the spaces just created. This system, however abstract and partly limited, allows for the creation of forms and spaces in relation to the needs. The code that allowed the generation was programmed to create the various elements in sequence and then repeat the process on each floor but varying the generation points depending on what was previously created. Starting by the planes and volumes visible in Fig. 21 and on the basis of the number of nodes set the forms could be generated. (Fig. 22) The code (Fig. 23) that forms the basis for creating a floor is essentially the same as the one that generates the next floor, except for the variation of the generation coordinates, since also the elevation is considered.
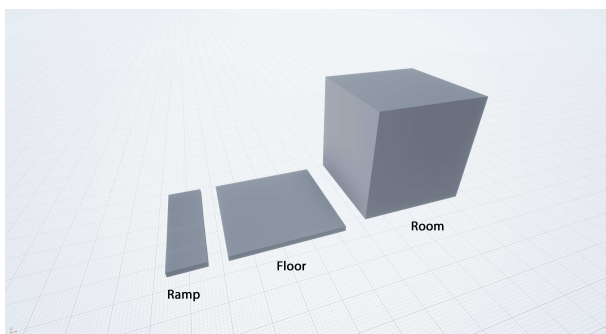


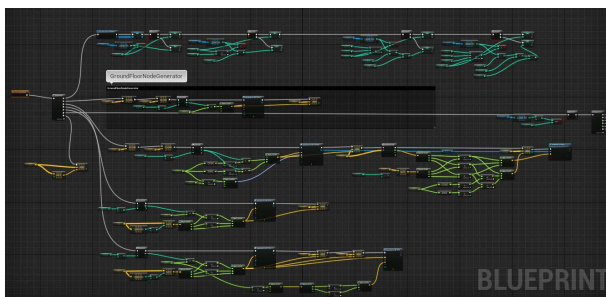Figure 21: *Basic geometric settings at the starting point*



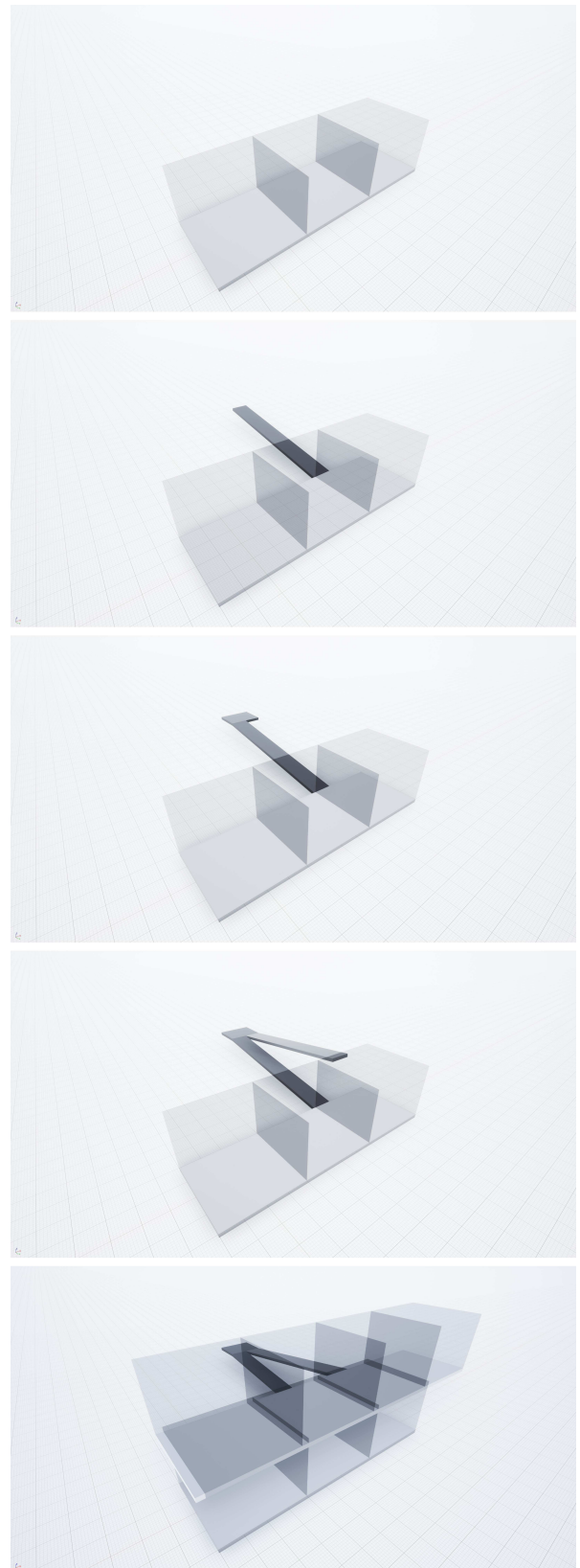Figure 23: *Code scheme for the generation process*



Figure 22: *Generation sequence*

So, each subsequent floors can be repeated and extended to the number of floors desired, which are placed as a series by adding the appropriate variables for each new floor. Fig. 24-25 show some generative examples obtained by varying the settings programmed, in synergy with the AI which automatically identifies the destination points generated.
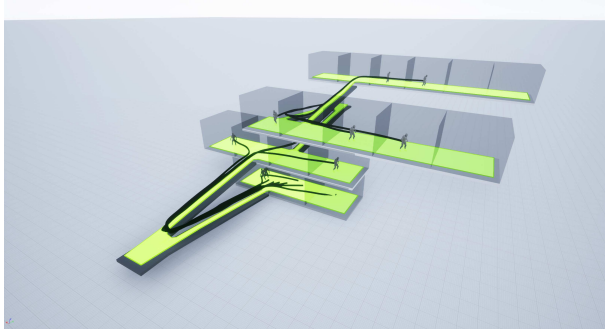


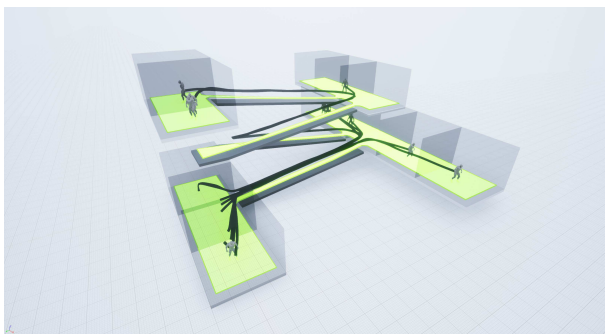Figure 24: *Forms generation with indicated the dynamic Nav Mesh Bounds Volume and AI flows calculation*



Figure 25: *Forms generation with indicated the dynamic Nav Mesh Bounds Volume and AI flows calculation*

A further development on the generative theme, based on linking users and flows, was in programming a system that is generated according to the number of people who are supposed to need space. In other words, space expands according to the number of users. The generative process that led to the realization of the architectural elements is based on the same script as in Fig. 23 placed in series but adding a piece of script that allows to indicate to the system if and when there is a need to add a new floor. In other words it activates (or not) the generation of new floors on the basis of an evaluation. This evaluation is managed by a function placed at the beginning of the entire generative process and which essentially sets the number of floors and the number of nodes desired for each floor based on the number of users. The generative sequence acts to always match the total number of nodes with a certain limit number of users preset. Fig. 26 shows in a graphic sequence the relation between users and the expansion of the space.
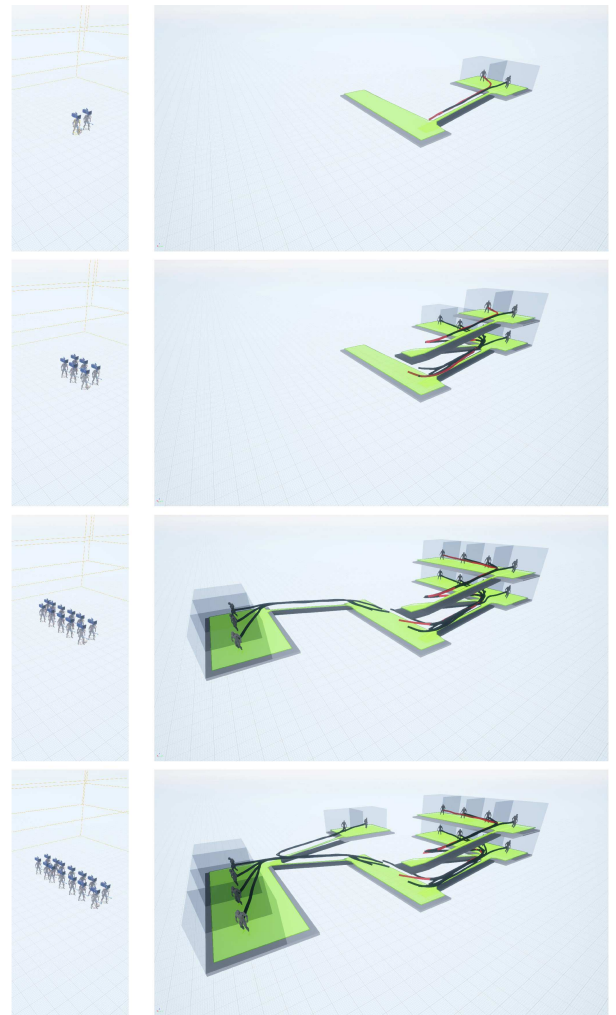


Figure 26: *Simulation of the sequences generating spaces in relation to the number of users added to the scene with subsequent simulation of flows through AI calculation*

### Campus Leonardo's main square at the Politecnico di Milano: flows simulation

The experimentations presented until now have been carried out either starting from pre-existing spatial situations or moving toward the hypothetical generation of new spaces, on a reduced scale. We present now a test of the AI system carried out on a real case and on a wider scale. Piazza Leonardo da Vinci, that is, the main square in front of the Campus Leonardo of the Politecnico di Milano (headquarter) is taken as a test area. Several simulations have been made to test the AI in this context. As in the previous cases, a series of points have been set which are visible in Fig. 27 which corresponds to the main access points of the Politecnico and to all the possible roads that can be followed to exit or enter the square. The digital model of the

space has been developed integrating data from the municipal vector maps, Google Maps and with a real life survey by photo modelling. The first simulation was done by controlling the flows, and directing them to predetermined points of interest without moving the silhouettes towards other points. Then a further simulation was done making people move from one point to another in Piazza Leonardo. In this case the NPC could reach a point and then randomly choose another one to go to, in this way the same NPC

could simulate a variety of user behaviours. Several situations were considered: first silhouettes moving from some designated points to other designated points, and finally towards any points at random. All the simulations were then repeated increasing the level of restrictions in the paths: considering green areas, benches, and driveways as obstacles. A summary of some results of these simulations can be seen in Fig. 28.
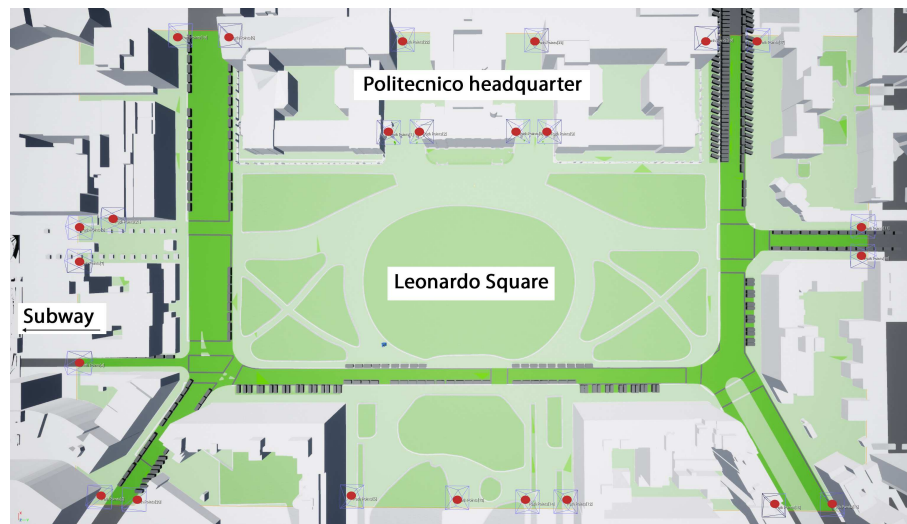


Figure 27: *Leonardo Square model with the set of 'Path Points' for the simulation flows through the AI*
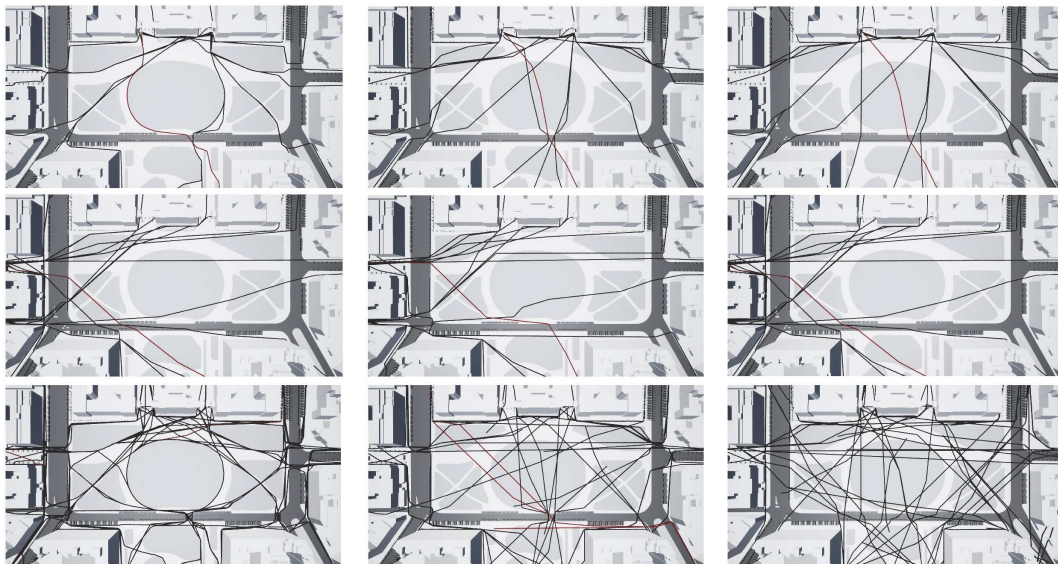


Figure 28: *[From Top to Down] Flows simulation on Leonardo Square: from the headquarter accesses to the access/exit points of the square, from the subway to the access/exit points and randomly. [From Left To right] Considering both the flower beds and the streets as not viable, considering only the roads as viable, completely free.*

Finally, a hypothetical movement of a NPC was reproduced by superimposing the virtual animated walk of the NPC and the corresponding graphic track of the path inside a video, previously recorded in the Piazza Leonardo da Vinci. To do this, additional software programs have been used, together with Unreal Engine. Once the video in the real place was made, the camera movement was traced through a software called Boujou (Fig. 29), which allows to track the movement performed by the operator and representing it three-dimensionally in a virtual space. Subsequently, the track made by the camera at the time of recording was exported in 3ds Max in which the viewpoint was positioned at the desired height and orientation (Fig 30). Finally the file was exported in .fbx format and imported into the UE4. In the UE4 a camera was set and it was given the same movement in the space traced by the Boujou software. Moreover, the parameters of light and sunshine were set on the basis of those detectable in the real space at the time of video recording. Subsequently, the desired movement of the silhouette was recorded on a green background (Fig. 31), and finally, the final sequence was composed using the software program After Effect, by combining the original video with the one created in the UE4, appropriately cropped to eliminate the green background (Fig. 32). The result can be seen in Fig. 33.
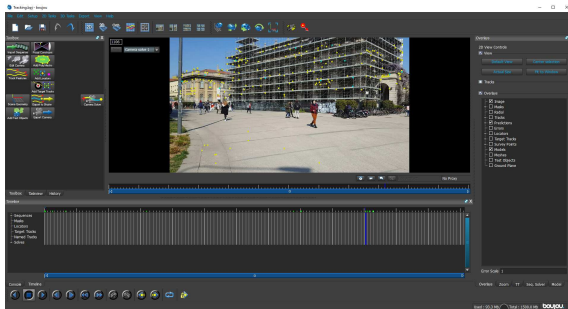


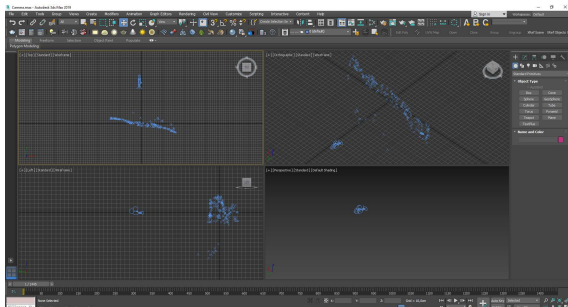Figure 29: *Boujou interface, used to track camera the movement of a video*



Figure 30: *Tracing camera movement exported in 3ds Max in order to set the right camera height, and for exporting the .fbx format loadable into Unreal Engine*
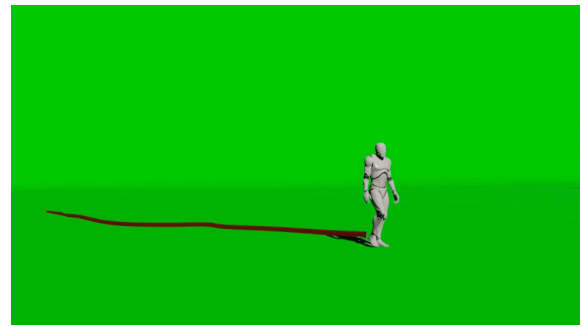


Figure 31: *Video screenshot with a green background rendered in Unreal Engine using the traced movement of the camera*
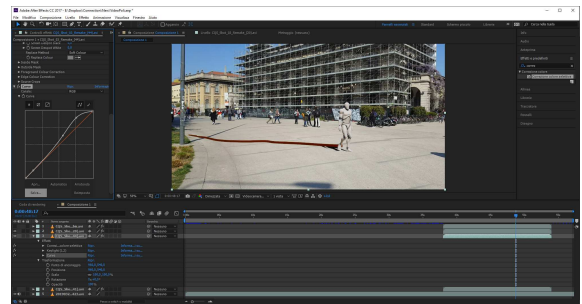


Figure 32: *Overlay of the original video and green screen video using After Effect*
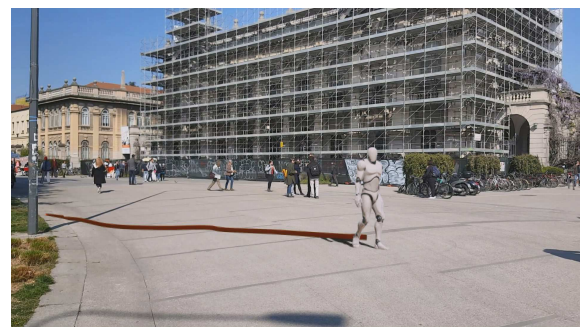


Figure 33: *Overlapping level and final result*

**Possible future developments**

In the area of AI research, further developments can be expected in different directions, either focusing on the simulation of contexts and their uses, either on types and behaviour of the users, as well as on the complexity of their interactions. Many of these are already at work in the world of Video Games. Concerning the path point they

could be set in a probability reach state, in other words each point would have a probability chance to be reached by the NPC, which could even change in relation to certain external factors. In the architectural field, a welcome development can of course deal with more advanced aspects, like patterns referring to perceptual senses (sight, hearing, or tactile, also including external events, and so on), and on their translation into the virtual environment, based on similar parametric operations. The integration of senses could suggest to the based subjects (NPC) changes of direction, path or any other behavioral reaction according to the context topic. Additional forms of AI can arise from the combination of more senses, as well as from other external factors generally attributable to virtual atmospheric events or other AI behaviours which could integrate the possibility for the AI to predict hypothetical future events and scenarios and take decision based on that. Strictly linked with this last topic is the psychological behavioral factor both related to the movement of the individuals in relation to the masses and vice versa. This point introduces a relevant and very actual subject linked to the "realism" of the context of the AI environment. In this case, given the difficulty of translating behavioral psychological aspects into

appropriate descriptive codes because of their probabilistic nature, it would be appropriate to introduce neural network technologies based on machine learning and deep learning systems, which we are aiming to do in the future.

**Conclusions**

What this study has brought to light is the possibility of using tools currently used in the video game world for architectural analysis, design or teaching purposes, bringing a series of potentials that are still almost rarely found among the tools currently used in the architectural design contexts. It has been shown how through the use of UE4 it was possible to realize an artificial intelligence-based process able to represent three-dimensional flows both in pre-existing and in generative models according to design needs, as well as to expand a space in relation to an increasing number of users. More extensively this system can be used for analyzing, comparing and even introducing new design choices, resulting very useful in contexts characterized by high levels of complexity and in the advanced stages of the design development.

## References

[1] E. AARSETH, Allegories of space. The Question of Spatiality in Computer Games. In: Von Borries, F. Walz P. S., Böttger, M., *Space time play, computer games, architecture and urbanism: The next level*, Basel: Birkhauser. p. 44, 2007.

[2] C. C. ABT, *Serious games*, University Press of America, 1987.

[3] A. BARICCO, *The Game*, Giulio Einaudi Editore, 2018.

[4] E. CHAMPION, *Critical Gaming: Interactive History and Virtual Heritage*, Routledge, 2015.

[5] G. FRASCA, *Play the message: Play, game and videogame rhetoric*, IT University of Copenhagen, Ph.D. Dissertation, 2007.

[6] M. GEROSA, *Second Life*, Meltemi Editore, 2007.

[7] M. HEMMERLING, L. COCCHIARELLA, *Informed Architecture. Computational Strategies in Architectural Design*, Springer, Cham, 2018.

[8] J. HUIZINGA, *A study of the play element in culture*, Switzerland, Routledge & Kegan Paul Lond, Boston and Henely, 1944.

[9] J. JUUL, The Game, the Player, the World: Looking for a Heart of Gameness. In Level Up: *Digital Games Research Conference Proceedings*, edited by Marinka Copier and Joost Raessens, 30–45. Utrecht, Utrecht University, 2003.

[10] D. G. LOBO, Playing with Urban Life, How SimCity Influences Planning Culture, In: Von Borries, F. Walz P. S., Böttger, M., *Space time play, computer games, architecture and urbanism: The next level*, Basel, Birkhauser, p. 206, 2007.

[11] W. MAAS, Spacefighter: A game for the evolutionary city. In: Von Borries, F. Walz P. S., Böttger, M., *Space time, play, computer games, architecture and urbanism: The next level*, Basel, Birkhauser, p. 362, 2007.

[12] MVRDV/DSD, *Spacefighter. The evolutionary city (game:)*, Actar-D, Barcelona, 2007.

[13] M. NOVAK, Liquid Architectures in Cyberspace, in Benedikt M. (ed.), *Cyberspace: First Steps*, MIT Press, Cambridge MA, 1991, 225–254.

[14] S. PORRO, *Playing Architecture. Using Real Time Engines as Operational Tools for Architectural Design*, (Master dissertation, tutor Prof. L. Cocchiarella), Politecnico di Milano, School of Architecture Urban Studies Construction Engineering (AUIC), 2019.

[15] J. SANCHEZ, *Block'Hood. Developping an architectural simulation video game*, 2015.

[16] J. SANCHEZ, *Gamescapes*, Studio Course Master, March Graduate Architectural Design, The Bartlett, UCL, London, 2013.

**Simone Porro**
e-mail: simone1.porro@mail.polimi.it
Politecnico di Milano, School of Architecture AUIC,
Via Golgi 42, 20133 Milano, Italy

**Luigi Cocchiarella**
orcid.org/0000-0002-3201-4189
email: luigi.cocchiarella@polimi.it
Politecnico di Milano, Department DASTU,
Via Bonardi 3, 20133 Milano, Italy

# INSTRUCTIONS FOR AUTHORS

**SCOPE.** "KoG" publishes scientific and professional papers from the fields of geometry, applied geometry and computer graphics.

**SUBMISSION.** Scientific papers submitted to this journal should be written in English, professional papers should be written in Croatian or English. The papers have not been published or submitted for publication elsewhere.
The manuscript should be sent in PDF format via e-mail to the editor:

Ema Jurkin
ema.jurkin@rgn.hr

The first page should contain the article title, author and coauthor names, affiliation, a short abstract in English, a list of keywords and the Mathematical subject classification.

**UPON ACCEPTANCE.** After the manuscript has been accepted for publication authors are requested to send its LaTex file via e-mail to the address:

ema.jurkin@rgn.hr

Figures should be titled by the figure number that match to the figure number in the text of the paper.

The corresponding author and coauthors will receive hard copies of the issue free of charge.

---

# How to get KoG?

The easiest way to get your copy of KoG is by contacting the editor's office:

Marija Šimić Horvath
msimic@arhitekt.hr
Faculty of Architecture
Kačićeva 26, 10 000 Zagreb, Croatia
Tel: (+385 1) 4639 176

The price of the issue is €15 + mailing expenses €5 for European countries and €10 for other parts of the world.

The amount is payable to:

| | |
|---|---|
| ACCOUNT NAME: | Hrvatsko društvo za geometriju i grafiku |
| | Kačićeva 26, 10000 Zagreb, Croatia |
| IBAN: | HR8623600001101517436 |